Bubble Formation and Bubble Rise Velocity in Gas−Liquid Systems: A Review

Amol A. Kulkarni and Jyeshtharaj B. Joshi*

Institute of Chemical Technology, University of Mumbai, Matunga, Mumbai-400 019, India

The formation of gas bubbles and their subsequent rise due to buoyancy are very important fundamental phenomena that contribute significantly to the hydrodynamics in gas−liquid reactors. The rise of a bubble in dispersion can be associated with possible coalescence and dispersion followed by its disengagement from the system. The phenomenon of bubble formation decides the primitive bubble size in the system (which latter attains an equilibrium size), whereas the rise velocity decides the characteristic contact time between the phases which governs the interfacial transport phenomena as well as mixing. In view of their importance, we herein present a comprehensive review of bubble formation and bubble rise velocity in gas−liquid systems. The emphasis of this review is to illustrate the present status of the subjects under consideration and to highlight the possible future directions for further understanding of the subject. The bubble formation at a single submerged orifice and on multipoint sieve trays in Newtonian as well as non-Newtonian stagnant and flowing liquids is discussed in detail, which includes its mechanism as well as the effect of several system and operating parameters on the bubble size. The comparison of results has shown that the formulation of Gaddis and Vogelpohl[22] is the most suitable for the estimation of bubble size in stagnant liquids. The special cases, such as bubble formation in reduced gravity conditions and weeping and in flowing liquids, are discussed in detail. The section on the rise of a gas bubble in liquid covers the various parameters governing bubble rise and their effect on the rise velocity. A comprehensive comparison of the various formulations is made by validating the predictions with experimental data for Newtonian as well as non-Newtonian liquids, published over last several decades. The results highlight that for the estimation of rise velocity in (i) pure Newtonian liquids, (ii) contaminated Newtonian liquids, and (iii) non-Newtonian liquids, the formulation based on the wave theory by Mendelson,[190] Nguyen's formulation,[155] and the formulation by Rodrigues,[153] (last two, based on the dimensional analysis), respectively are the most suitable. The motion of bubbles in non-Newtonian liquids and the reason behind the discontinuity in the velocity are also discussed in detail. The bubble rise is also analyzed in terms of the drag coefficient for different system parameters and bubble sizes.

10.1021/ie049131p CCC: $30.25
Published on Web 00/00/0000 **PAGE EST: 58.9**

1. Introduction

Gas−liquid contacting is one of the most important and very common operations in the chemical process industry, petrochemical industry, and mineral processing. Most commonly, it is achieved either by automation of liquid into gas in the form of drops or by bubbling (sparging) of gas into the liquid. In applications such as absorption, distillation, and froth flotation, the interaction of two phases occurs through bubbling of gas into the liquid pool and the equipment is designed based on the knowledge of the hydrodynamic parameters suitable for desired performance. In most of such equipment, the knowledge of the transport processes across the gas−liquid interface is useful for the estimation of transfer coefficients and requires the accurate prediction of volume of discrete phase, residence time of discrete phase, and its contribution to the mixing. Further, the physicochemical properties of liquid phase (viz. viscosity, surface tension, density, etc.) and few of the characteristics of the discrete phase (bubble size, bubble rise velocity, etc.) govern the hydrodynamics as well as flow pattern in the system. For example, for liquids with low surface tension, the sizes of bubbles that are formed for certain orifice diameters are always smaller. To withstand the drag induced by the liquid, they try to maintain spherical shape, which results in an enhancement of the gas hold-up in the system. Due to their smaller sizes, the rise velocities are slower, which results in larger residence time. In a bubble column reactor, at low gas flow rates, a homogeneous

* To whom correspondence should be addressed. Tel.: 00-91-22-24145616. Fax: 00-91-22-24145614. E-mail: jbj@udct.org.

regime prevails, whereas for the same gas flow rate in coalescence-inducing liquids either a transition or a heterogeneous regime is attained, which have totally different hydrodynamics than those of the homogeneous regime. One of the most important properties that helps in finding most of the design parameters (viz., effective interfacial area) is the bubble size or bubble size distribution. The average bubble size in a system is an effect of the size at bubble formation and the extent of coalescence and dispersion (break-up), of which the later two are governed by the local turbulence. The discussion so far strictly applies to the system where gas is in dispersed phase and volume fraction of liquid is substantially higher than gas phase (such systems can be considered as wet foams, where bubbles are separated by considerably thicker liquid films). At the disengagement zone of the column, where the bubbles leave the system, the energy dissipation is very high, and the liquid traps the fine bubbles, resulting in foam. In this zone, although the gas is in the discrete phase, if the volume of the gas is significantly higher than that of the liquid, i.e., gas bubbles are entrapped/separated by thin liquid films, and the phenomenon can be termed as foaming. In the majority of industrial equipment, where the discrete presence of gas in the form of bubbles exists in bulk, at the disengagement zone, where bubbles escape from liquid, the gas phase has significant fraction resulting in foaming. The extent of foaming is independent of the bubble size distribution in the system; however, it is a combined effect of the presence of gas bubbles and physical properties of liquid. Thus, for developing a better understanding about the role of gas bubbles in the hydrodynamics of a system, a good knowledge of the above-mentioned phenomena is required. The subject is vast and the large amount of literature published over last several decades is scattered in different journals, books, proceedings, and reports. In view of this, taking into account the amount of information available on these subjects individually, in this review we have decided to focus on the first two phenomena of bubble formation and bubble rise velocity. The remaining subjects of bubble coalescence, dispersion (bubble break-up) and foam break-up will be taken-up comprehensively and separately.

Basically, the remaining part of this review contains two sections, dedicated to the gas bubble formation at a submerged orifice/plate in liquid (Section 2) and bubble rise velocity (Section 3). In the second section of this review, we have discussed the bubble formation process over a wide range of issues, which include the effect of physicochemical properties of a gas−liquid system, orifice configuration, and various mechanisms of bubble formation in liquids and proposed models, a few of the recent developments, and finally, a few suggestions for the direction of further investigation in this field. In the third section, bubble rise velocity has been discussed in detail, which includes relationship between size, shape and rise velocity, dependence of rise velocity on system properties, various correlations for rise velocity and the drag coefficient. At the end of this section, a critical comparison of the different correlation is discussed for various liquids and suitable correlation, which is seen to be applicable for various system is recommended, followed by a brief review of the various available experimental methods for the bubble rise velocity measurements. We conclude this review with a few recommendations with regard to the use of proper experiments and generalized correlations, which can be used for design purpose.

2. Bubble Formation in Gas−Liquid Systems

In general, particulate systems are classified on the basis of the state of the particle present as gas bubbles, liquid drops, and solid particles/agglomerates. The gas bubbles exist in gas−liquid, gas−solid, and gas−liquid−solid systems. The system of gas−liquid contacting through bubbles is dynamically complex and needs attention. To pay attention to the concise field of gas bubbling in a liquid pool, it is desirable to understand the process of bubble formation, which can be considered as a static or quasi-static operation followed by the dynamic processes viz. coalescence, break-up, etc. Since the sizes of bubbles after its formation and its wake decide the rise velocity and also the direction of rise i.e., trajectory in the liquid, it even influences the above-mentioned dynamic processes, the overall turbulence in the system and hence the performance of the equipment to some extent.

The earliest studies on the formation of single bubble and drop can be seen in Tate[1] and Bashforth and Adams.[2] A significant amount of work in the area of bubble formation at submerged orifice(s) over a wide range of design and operation parameters has appeared in the literature in last few decades (Davidson and Schuler,[3,4] Tsuge et al.,[5−13] Kumar and co-workers,[14−17] Marmur et al.,[18,19] Vogelpohl and co-workers,[20−22] Tan and co-workers[23−27]) and the subject is interesting and important enough to fetch continuous attention even in the present decade.[28−41] Most of these studies can be grossly classified based on the operating conditions pertaining to the gas phase, such as the constant flow, constant pressure, and intermediate condition. In the late 1960s, Kumar and co-workers studied the mechanism of bubble formation for different conditions and also reviewed the earlier work very keenly,[17] specifically, the various methods of measuring bubble sizes experimentally. Later, Tsuge[6] reviewed the hydrodynamics of bubble formation from submerged orifices and discussed various proposed models for the mechanism of bubble formation, while Rabiger and Vogelpohl[20] have briefly discussed the various factors affecting bubble formation. Due to variation in the gas−liquid systems (properties), type of nozzles and operating parameters viz. gas velocity, system pressure, etc., the observations by many investigators are not concordant. This brings out a need to compare the individuals' approaches, observations and inference to develop a guideline for the forthcoming studies in this field. Additionally, many recent developments in the studies both in numerical methods used for the analysis of various stages in the growth process of bubble as well as the experiments conducted to investigate the contribution of individual forces on bubble formation need to be given attention. In view of this, we have reviewed the subject freshly, which includes most of the proposed models for bubble formation and the detailed discussion of the effect of various system properties on various growth phases in the process. This part of the review is organized as follows; the next section discusses the bubble formation at a single submerged orifice in Newtonian and non-Newtonian liquids and it gives a qualitative description about the various modes of bubbling and the subsequent effect on the liquid phase in its surrounding and also the effect of various governing parameters on the same.

Prior to the description of various models of bubble formation, since these models are based on visualization of the phenomenon, we have discussed the various observations in this regard. The third subsection discusses the phenomenon through force balance for the most suitable and realistically visualized bubble formation process. This is followed by a comprehensive discussion about the comparison of the experimental data with the predictions by various available correlations. We also review the multipoint bubble formation and also few subjective cases of this phenomenon (viz. reduced gravity analysis, bubble formation in the presence of weeping, etc.). Finally, a brief discussion appears on a few of the experimental techniques used for the analysis of the process of bubble formation. In the forthcoming subsections, under every parameter, the discussion is pertaining to (i) the Newtonian liquids, unless explicitly mentioned as being about the non-Newtonian liquids and (ii) bottom submerged orifices, unless explicitly mentioned about the other ways of submergence.

2.1. Bubble Formation at Single Submerged Orifice. Bubble formation at a single submerged orifice occurs in many modes viz. bubbling; chain bubbling, wobbling and jetting, which depends on the orifice configuration, the gas velocity, gas−liquid system properties, and finally magnitude of gravitational force acting on the system. Thus, it can be a periodic phenomenon over a wide range of frequency[42−44] or deterministic process with higher numbers of degrees of freedom as an effect of jet break-up at very high velocity[36,45] which depends mainly on the liquid properties. It is well-known that the modes of bubbling (mentioned above) in a given system are a strong function of the gas velocity and liquid depth. Muller and Prince[46] have shown a typically observed regime map for bubbling (Figure 1A). For very low gas flow rates and deep liquid (>100 mm), bubbling occurs singularly only till a certain value of gas flow rate where the mode changes from single bubbling to chain bubbling. In this case, the bubble size is primarily decided by the orifice diameter, surface tension and the density difference between two fluids. In the intermediate or chain bubbling mode, bubbles are larger than the earlier mode, bubbling becomes periodic and their production rate is proportional to gas flow rate. Further, at even higher gas flow rates, gas phase emerges as a continuous phase and maintains the continuity only for a certain distance from the orifice mouth. Bubble formation rate is more or less constant and bubble size increases with gas flow rate. In the jetting regime, bubble formation occurs mainly due to jet break-up resulting from the instability of jet. Typical dynamics associated with most of these bubbling regimes and the organized nature of flow in jetting regime can be seen in Tritton and Egdell[42] and Kulkarni,[45] respectively. Photographic images of four regimes of bubbling are shown in Figure 1B.[40] In the case of discrete single bubble formation, the main forces acting on a bubble in inviscid liquid are buoyancy, drag, surface tension, and gravity. In this case, the formation and detachment of bubble produces only local disturbance in the liquid and only a volume of the order of bubble is carried along with it as drift volume. In the case of chain bubbling, the continuous phenomena induces a driving force in liquid in the direction of bubble motion and in the vicinity of the trajectories of bubbles liquid has a positive upward velocity resulting into a weak circulation of which intensity of circulation is directly proportional to bubble size. In the jetting regime, the strong upward motion of the jet induces stronger recirculation in the liquid with upward motion along the jet and downward flow away from jet. However, in an infinite media, the downward velocities are distributed over a larger cross-section. It should also be noted that bubbling regimes are strongly affected by the liquid properties (Newtonian and non-Newtonian), where

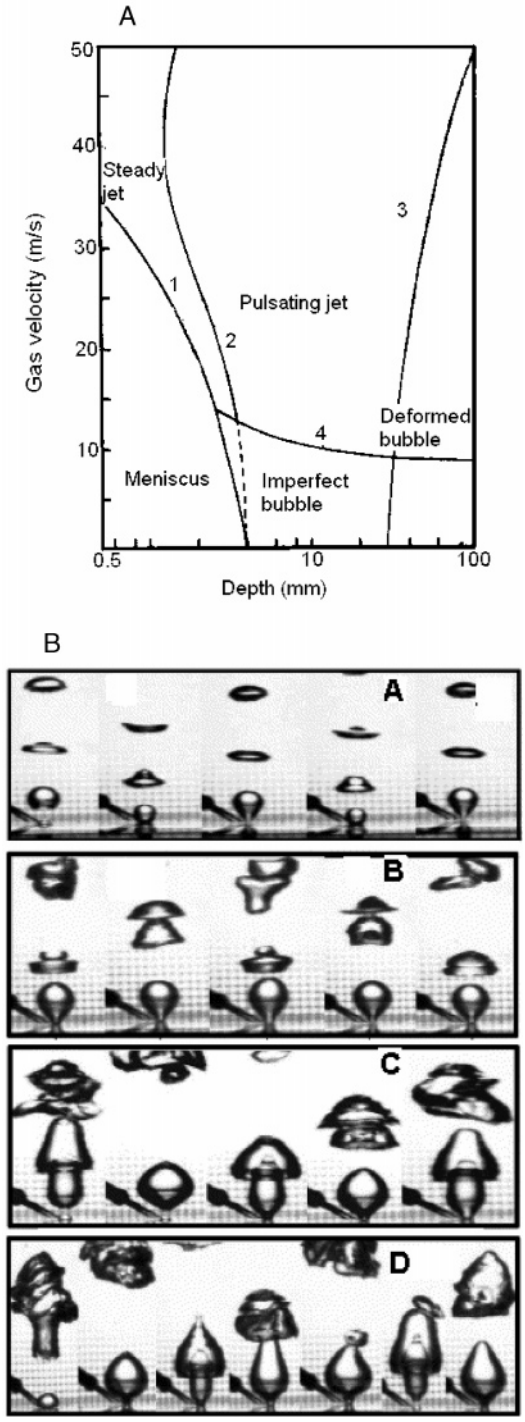

Figure 1. (A) Schematic representation of regimes of bubble generation (reproduced with permission of Elsevier from Muller & Prince[46]), (B) Modes of bubble formation at increasing gas flow rates (reproduced with permission of Elsevier from Zhang and Shoji,[40] Figure 2) (A) Single bubbling (q = 1.66 mL/s, Re_o = 68); (B) pairing (q = 5.83 mL/s, Re_o = 238); (C) double coalescence (q = 15 mL/s, Re_o = 612); and (D) triple bubble formation (q = 25 ml/s, Re_o = 1020).

liquid depth actually represents the static head, while bubble size/mechanism of formation is also decided by the orifice configuration. In view of this, we critically analyze the dependence of bubble size on various governing parameters.

2.1.1. Factors Affecting Bubble Formation. The process of bubble formation is governed by many operating parameters (i.e., gas flow rate through the orifice, mode of operation, flow/static condition of the liquid), system properties (viz. orifice dimensions, orifice chamber volume), and also the physicochemical properties, such as liquid viscosity, liquid density, and nature of liquid i.e., polar or nonpolar, etc., which decide the mode of bubble formation and subsequently reflects on bubble size. The main forces acting on a moving bubble are gravity, buoyancy, drag, viscous forces, added mass force, and the lift force. In many cases, the gas−liquid properties, orifice dimensions and the material of construction govern these forces. The flow rate of gas through the orifice and orifice dimensions mainly decides the bubble frequency and thus the detachment time, similarly orifice chamber volume decides the back-pressure on the bubble and hence bubble sizes in general. In this review, the effect of gas flow rate has not been discussed explicitly with regard to the effect of the other parameters. A chronological development in the understanding about this phenomenon and observations from a few significantly important studies that are helping in developing a basis for the recent studies in the subject are tabulated in Table 1. For further information about the recent analyses in this area, readers may read the introduction and literature review in Nahra and Kamotani.[55]

2.1.1.1. Effect of Liquid Properties. (a) Viscosity of the Liquid. With the variation in the viscosity of the liquid, the magnitude of viscous forces exerted during formation changes such that a stable bubble diameter is attained before its detachment. The experimental observations by various investigators have brought different views in this regard and are shown in Figure 2 and it has led us to analyze them in detail. The reported observations in such studies are contradicting viz. (i) the bubble sizes increase with liquid viscosity,[56,16] (ii) bubble sizes are independent of liquid viscosity,[57,50,51,17] and (iii) there is a very weak effect of viscosity on size.[58] In another totally different observation, Siemes and Kaufmann[59] have reported that for liquids of low viscosity, the bubble sizes are independent of the liquid viscosity while at higher viscosities an increase in liquid viscosity causes an increase in bubble size but at small flow rates. From Figure 2 and Figure 5A, it can be clearly seen that viscosity affects the bubble size however its evidence diminishes for large diameters and higher gas velocities. From the rigorous analysis of Jamialahmadi et al.[60] the size can be assigned a dependence on viscosity as $\sim\mu^{0.66}$.

(b) Surface Tension of the Liquid. In the case of bubble formation at a submerged orifice, for a growing bubble, its rear surface is dragged backward along with the liquid. In the front portion of the bubble, the surface is stretched and the new surface is constantly generated. In the portion close to the orifice, the bubble surface is compressed and the liquid is pushed toward the orifice edges. As an effect, the surface forces on a bubble arise out of the linear surface tension acting on it and it helps a bubble to adhere to the edge of orifice,[51] delaying the detachment process. Two types of surface tension forces

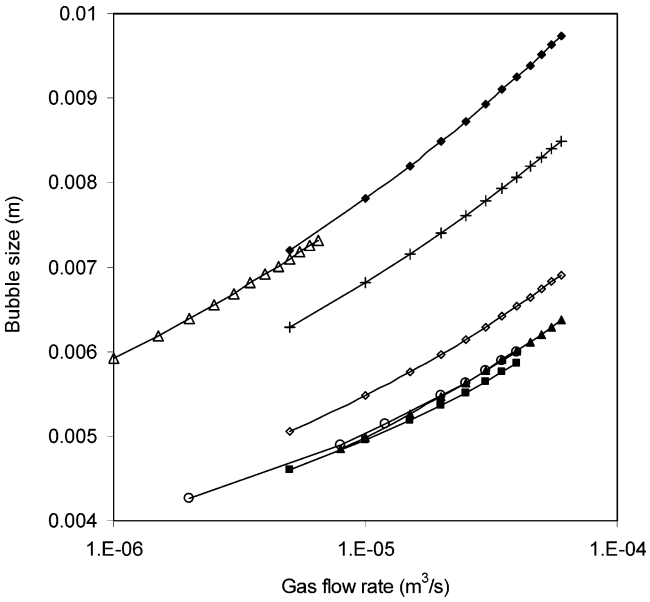

Figure 2. Effect of variation in liquid phase viscosity on bubble volume. The bubble sizes are estimated using the correlation by Jamailahmadi et al.[60] for the different liquids used by several investigators (Since these are predictions, symbols corresponding to different investigators are connected by lines) and $d_h = 1$ mm. (Ramkrishnan et al.[14]: ■ Water, $\mu = 0.001$, $\sigma = 0.072$, ◊ glycerol-aq $\mu = 0.0449$, $\sigma = 0.067$, ◆ glycerol-aq, $\mu = 0.552$, $\sigma = 0.063$), (Rabiger and Vogelpohl[20], ○ glycerol-aq, $\mu = 0.007$, $\sigma = 0.069$), (Davidson and Schuler[3], Δ glycerol-aq, $\mu = 0.515$, $\sigma = 0.063$), (Terasaka & Tsuge[11], ▲ water, $\mu = 0.012$, $\sigma = 0.053$, + Glucose, $\mu = 0.269$, $\sigma = 0.08$,)

act on a bubble, dynamic and static. During the initial part of growth phase, the surface tension is dynamic as its contact angle with the orifice changes continuously and in the later part, it reaches to a constant contact angle approaching to static surface tension, hence surface tension decides the orientation time/growth time for bubbles. Although the surface tension forces are small, they vary significantly with gas flow rate through the orifice[61,62,63] and these forces produce sudden motion resulting in a reduced pressure at the tip of the capillary initiating the next bubble. This occurs mainly because, the dynamic surface effect retards the stretching of the bubble surface and makes the detachment of the liquid film between the bubble and orifice, faster and consequently, it gives very fine bubbles. In a contradictory observation, Davidson and Schuler[4] have reported that surface tension affects the minimum value of absolute resultant pressure for bubbling to occur. For small diameter orifices, the effect of surface tension is negligible at high gas flow rates, hence at the constant gas flow rate, the surface tension loses its dominance. Also, there is a noticeable influence of surface tension on bubbles formed under constant pressure conditions, through an appreciable effect on the pressure in the bubble and also to some extent it governs the flow into the bubble. Surface tension force increases with diameter of the orifice and thus the orifice diameter affects the bubble contact/adherence time.[22] Figures 2 and 3 give some idea about the various experimental observations made in this direction. In a recent investigation, Liow[61] has reported that the surface tension forces in combination with the orifice diameter as well as thickness decide the bubble detachment time and hence bubble size. Also, Hsu et al.[62] has reported their observations about the mechanism in the presence of surfactants, where temporal variation of dynamic sur-

Table 1. Important Studies on the Bubble Formation at Single Submerged Orifice in Liquid. (This table covers the investigations that form the basis of the recent attempts. We confess our inability to include information from the entire published literature on this subject in this Table)

investigators	experimental system & observations	approach in the studies	parameters studied and conditions	limitations	conclusion & remarks
Schnurrmann[47]	Bubble formation through a porous diaphragm led to observation of one stage bubble formation.	Pressure variation over the diaphragm was modeled analytically.	r, μ, σ, g	Results were limited up to nonelectrolytic solutions. Formation of varying bubbles size due to diaphragm expansion was not taken in to account.	Size of bubble formed is independent of the viscosity of liquid.
Eversole et al.[48]	One stage bubble formation was observed for different orifice sizes.	Bubble volume was obtained by stroboscopic frequency measurements.	High gas flow rate, $\mu,\sigma\ \rho, P$	Conclusion is generalized assuming constant bubble frequency, contradictory to the experiments. Mechanism of static bubble formation is not applicable.	In pure liquids, bubble frequency is independent of the gas flow rate, liquid properties and the orifice diameter.
Krevelen and Hoftijzer[49]	Separate and chain bubble formation	Complete wetting of orifice was assumed with generation of spherical bubbles. Bubbles were classified as small, medium, and large. Ascending velocity was obtained from the gas flow rates.	Bubble diameter, gas hold-up, ascending velocity of bubbles, gas liquid interfacial area	Gas flow rate was not constant and hence frequency of bubble formation was not the same throughout. Theoretical results with frequency only less than one were in coordination with that of experimental.	For separate bubble formation d_B is independent of Q and proportional to cube root of orifice diameter. For chain bubbling d_B is independent of d_h.
Benzing and Mayers[50]		Dimensional analysis was used to correlate the experimental results.	Diameter of orifice (2.1−4.7 mm), g, μ, σ, ρ Liquids: Water, water-ethanol, sugar solution, Drene-water, ethylene glycol, Wesson oil.	Determined the data of drag coefficient for very small tips which does not match for the model by succeeding investigators though the method of approach seems to be same.	For low concentration of surfactants its effect on bubble size is negligible. Effect of orifice length is negligible only when gas flow rate is relatively small.
Hughes et al.[51]	Oscilloscope and stroboscope were used to count the bubble frequency. Process of bubble formation was assumed to have no stages.	Dimensional analysis was carried out for Re, N_C and virtual mass. Force balance was applied on a bubble. Pressure equations were considered and solved for C_D, V_T, frontal area of bubble, and V_B for different N_C.	$g, \mu_L, \sigma, \rho_L, \rho_G$, gas velocity, liquid velocity, vessel construction, gas inlet construction, pressure fluctuations (pulsation) at the tip of orifice.	It is doubtful whether the N_C has any independent effect on the bubble formation.	The chamber volume has strong effect on d_B. Tip length below 100 times tip diameter does not influence bubble size. Gas turbulence creates non-uniform size bubbles. V_B is independent of N_C for $N_C < 0.8$.
Leibson et al.[52]	Stroboscopic studies were performed.	The bubble sizes were found at various experimental conditions and empirical formulas were derived using formula for orifice discharge coefficient. The total number of bubbles was calculated from the frequency data for each size range.	Gas flow rate, ($0 < Re < 40000$) orifice diameter, and type of orifices	Method of normal distribution does not hold accurately for very high Re. Effect of liquid properties on bubble sizes has not been studied and hence results cannot be generalized.	Bubble size is relatively uniform at given Re and depends markedly on orifice diameter.

Davidson and Schuler[3] (Viscous liquids)	Stroboscobic method was used for the experiments.	Equation of motion and virtual mass of bubble was used to find out size of bubble theoretically.	g, μ, σ, ρ, gas flow rate, orifice dimensions.	Assumption that bubble always moves at its stokes velocity does not hold to reality and since surface tension forces are neglected, the model may not be valid for all sizes.	Bubble sizes were obtained theoretically match very well with those of experimentally.
Davidson and Schuler[4] (Inviscid liquids)	Stroboscobic method was used for the experimental observations.	Equation of upward motion is considered and solved under initial conditions to find out critical bubble volume.	μ, σ, ρ, gas flow rate, orifice dimensions	Drag coefficient is considered to be zero. In the virtual mass of bubble, the 11/16 term comes into play only for low viscosity liquids and this differs the values of bubble volume calculated from experiment.	As each bubble detach from the orifice it leaves behind a volume of gas which forms a nucleus for the next bubble. Drop weight method can be used for very low flow rates to determine the bubble volume.
Ramkrishnan et al.[14]	Stroboscobic method was used for the experimental observations.	Force balance was done and virtual mass concept was used in the first stage and for the second stage Newton's second law of motion was applied to get the bubble volume under constant flow condition.	g, μ (1−552cP), σ (41.4−71.7N/m), ρ (987−1257kg/m^3), gas flow rate (1−80 cm^3/s), time for bubble formation, contact angle, orifice diameter (1.3−7 mm).	The model can be applied only when the rising bubble is not caught up and coalesced with the next expanding bubble.	At extremely small flow rates only buoyancy and surface tension forces act on the bubble. The effect of different parameters on volume of bubble depends on the system under consideration and the experimental setup.
Satyanarayan et al.[15]	Stroboscobic method was used for the experimental observations.	Force balance was done without neglecting the effect of gas density for both stages at constant pressure condition.	g, μ (60−600cP), σ (35−72N/m), ρ_L (979−1246kg/m^3), gas flow rate (2−250 cm^3/s), orifice diameter (0.5−4.05 mm).	Model is complicated to be solved numerically and time-consuming since number of iterations to be carried out is large.	The volumes of bubbles obtained numerically matches with that of the experimental observation.
Khurana et al.[16]	Inlet pressure variation, average flow rate, weeping rate were measured and Stroboscobic method was used for estimating the bubble frequency.	Generalized equations of motion and force balance for unsteady state for bubble formation at intermediate conditions was studied.	g, μ, σ (40cp), ρ (960kg/m^3), gas flow rate (3 cm^3/s − 20 cm^3/s), orifice diameter (3 mm), orifice chamber volume (65 cm^3-600 cm^3), orifice submergence (0.156, 0.66, 1.28m).	In the iterative procedure for calculating the bubble volume instead of a linear, exponential discharge of gas from the chamber should be considered.	Concept of weeping time and formation time can be well applied to at intermediate condition to study bubble formation.
Kumar & Kuloor[17]	High-speed photography was used for experimental observations.	Force balance was done at negligible surface tension.	g, μ, σ, ρ_L, ρ_G, gas flow rate, orifice diameter, time of formation, expansion and detachment,	Surface tension forces are made negligible by using small diameter capillaries. Experimental observations were made only using smooth capillaries.	Two stage model with certain conditions decides the time dependent volume of the bubble.
Wraith[53]	High-speed photography was used for the experimental measurement of bubble sizes.	Concept of velocity potential was applied for an hemispherical expanding bubble to find its volume.	6.3 < d_h < 19.1 mm 30 < V_C < 45 cm^3. Gas kinetic energy, acoustic capacitance of the nozzle system, gas flow rate were varied	Surface tension forces are neglected. Model is applicable only abovecritical gas flow rate. At high gas injection rates this model fails because of coalescence.	Intrinsic coalescence is tendency of a two stage model for the flow rates other than immediately above critical flow rate.
Marmur & Rubin[18]	One stage slow bubble formation under quasi-static condition was observed visually and the observations are used for model formulation.	Theory of interfaces in equilibrium for a bubble was applied in the formation stage and its transition to a dynamic state of detachment was decided in gravity field using velocity potential.	Orifice dimensions, submergence, contact angle, chamber volume.	Effect of various parameters on dynamic nature of the detachment stage cannot be predicted by that on the quasi-static state of bubble formation.	Bubble sustains in equilibrium at maximum radius of the orifice and this radius depends on the liquid properties.

Table 1 (Continued)

investigators	experimental system & observations	approach in the studies	parameters studied and conditions	limitations	conclusion & remarks
Marmur & Rubin[19]		Equation of motion at the interface was developed and together with the thermodynamic equations for gas in the bubble and the chamber volume below it the instantaneous shape of bubble during formation was calculated.	Orifice submergence, g, μ, σ, ρ_L, ρ_G, gas flow rate.	Model is restricted to single bubble formation. Static or lift-off approach at the instant of equilibrium is inadequate. Gas momentum is taken negligible. Model is valid for only very small bubbles.	Instant of detachment i.e., the closure of neck can be determined theoretically.
Acharya et al.[54]	Single stage model	Wave theory was applied to determine the volume of the bubble in dynamic detaching condition.	Viscous, inertial, internal stresses, shear rate, gas flow rate, orifice diameter.	Surface tension forces are neglected. In case of highly viscous liquids since detachment of bubble is through neck formation observation of single stage bubble formation is unacceptable.	Only gas flow rate and acceleration due to gravity decide the volume of bubbles that are formed in non-Newtonian liquids.
Vogelpohl & Rabiger[21]	Multistage bubble formation	Formation of primary and secondary bubbles was modeled by force balance	g, μ, σ, ρ_L, ρ_G, gas flow rate, direction of flow, size of orifice, orifice submergence.	Model is applicable only in jetting regime. At higher μ_L neck motion is no longer sufficient to detach the primary bubble and bubble coalesces with secondary, which is not predicted from the model. Secondary bubble size cannot be calculated from the developed model as it is an induced process.	Suction effect of the primary bubble induces the formation of secondary bubble. Liquid motion has strong effect on the formation and detachment of primary bubble.

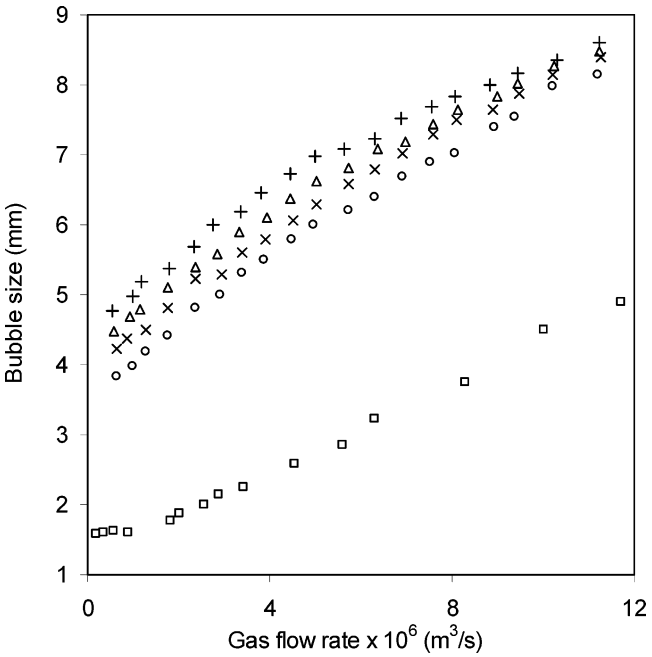

Figure 3. Effect of variation in surface tension of liquid on bubble volume. (+ water 0.073 N/m, Δ *n*-Propanol 0.0238N/m, × Ethanol 0.0228 N/m, ○ Methanol 0.0227 N/m, □ *i*-Propanol 0.0217 N/m).

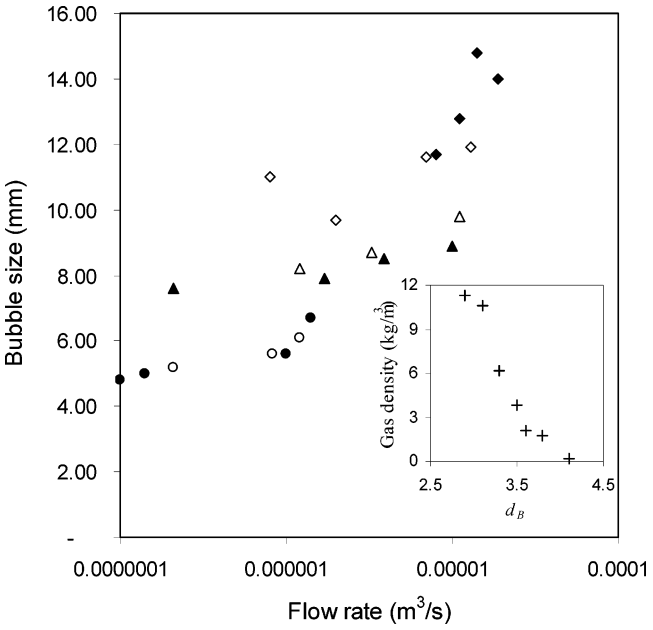

Figure 4. Effect of gas density on bubble size from single orifice. Helium: (◆ 0.1 Mpa, ▲ 0.6 MPa, ● 2.1 MPa), Nitrogen: (◇ 0.1 MPa, Δ 0.3 MPa, ○ 2.1 MPa). For the inset box, abscissa is the gas density in gm/cm^3 and ordinate is the bubble size in mm.

face tension is taken into account. The above interesting observations show that the phenomenon still needs understanding in terms of the concentration polarization at two opposite poles of the bubble, which will improve our knowledge in its contribution to the detachment stage and hence the actual time required for detachment. Interestingly, the effect of surface tension forces on a clean bubble and contaminated bubble are drastically different and needs analysis in terms of variation in the vorticity over different segments of surface during the growth and detachment.

(c) Liquid Density (ρ_L). To attain stability, a bubble attains a shape close to a sphere causing an early detachment. It is known that during the formation of a bubble, its pressure energy is equal to the static head above it, i.e., liquid density. The effect of density can be seen from the following two observations: (I) the bubble volume decreases with increase in liquid density and (II) it is independent of liquid density. Rise in the static head leads to the first observation, whereas the second observation should be true for very shallow liquid heads. Khurana and Kumar[16] have observed that (i) when the flow rate and viscosity are small, then the first result is obtained, (ii) when the flow rate is large and the viscosity is small, then for small orifice diameters, the second statement is true and finally, (iii) when the orifice diameter and viscosity are both small, again the second statement is found to be true.

2.1.1.2. Effect of Gas Density (ρ_G). The gas-phase density can be increased by increasing the pressure or even by using a higher molecular weight gas. As a result of increased gas density, the difference between the densities of two phases goes down resulting into the smaller sized bubbles and also reduction in the buoyancy force. The gas density comes into picture in terms of the added mass force. Interestingly, its contribution to the added mass coefficient is not very significant since the total density of the fluid which affects the motion of a single bubble can be given as $\rho = \rho_G + (11/16)\rho_L \approx (11/16)\rho_L$. For low gas density, at low gas flow rates, the surface tension force is dominant and the detachment is delayed. This reasoning is invalid for very small diameter orifices, as the drag force is the main resistance for bubble detachment and surface forces are negligible in comparison. Idogawa[63] (air, He and H_2) and Wilkinson[64] (He, N_2, Ar, CO_2, SF_6) have studied the effect of gas density on bubble sizes. They have reported that for a large diameter orifice, the detachment is faster in the case of higher density bubbles, whereas for very small diameter orifice, the gas density has negligible influence on the detachment. He has also shown that an increase in gas density for large chamber volumes results in an increase in gas momentum, a higher pressure drop at the orifice, and an increased rate of bubble necking, which finally lead to a smaller bubble at formation. Figure 4 depicts the quantitative analysis of these observations. This effect can also be seen by increasing system temperature, provided the difference between the molecular weights of gas and liquid are noticeable.

2.1.1.3. Effect of Orifice Configuration. The bubble formation in a pool of liquid takes place simply by injecting gas through the capillary or orifice or diaphragm or puncture in a membrane. Orifice submergence, orifice chamber volume, orifice diameter, type of the orifice, orifice material, etc. are important orifice-related parameters in the bubble formation process. Here, we have discussed their dependence in brief and have critically compared them for reaching an optimum configuration for the desired bubbling operation.

(a) Orifice Construction and Type of the Orifice. Many variations in the gas inlet design are possible, but the circular-cylindrical vertical tipped orifice is the most commonly used in these studies. In the case of a sharp-edged orifice operating in a gas−liquid system, the stream filaments of the orifice get converged to a minimum section downstream from the orifice and then diverge. An orifice of this type has a square cross-section toward upstream edge. The upstream edge of a round-edged orifice is bevelled to minimize the constriction of the stream filaments at the throat of the orifice. In a sharp-edged orifice, the pressure downstream is re-

duced, while a constant pressure is maintained upstream from the orifice. In the case of a long thin capillary, there is generally sufficiently high flow resistance in the tube such that the pressure gradient in the tube prevents events in the gas chamber upstream of the tube from interacting with the events at the bubble forming point. In this case, the size of the chamber has a negligible effect on the bubble formation mechanism and the bubble volume is a function of orifice radius given by $V_b = 2\pi R_o\sigma/(\Delta\rho g)$ known as Tate's law. Leibson et al.[52] have reported that the behavior of a thick plate orifice is similar to the sharp edged orifice.

(b) Orifice Diameter (d_h). Flow through an orifice is proportional to its cross-sectional area and the extent of growth of a bubble, i.e., its volume depends greatly on the orifice diameter (i.e., inner diameter, unless explicitly mentioned) as the surface tension varies continuously over the rim of orifice. Generally, it is assumed that the distance over which surface tension varies is $\sim O(d_h)$ and thus, depending upon the gas flow rate, the bubble volume increases until it is detached. It is always observed that the effect of diameter in small orifices is negligible, while for large diameter orifices, the bubble volume increases with flow rate.[5] For the smallest orifice diameter when the inverse of Weber number is equal to the sine of the angle between the interface the relation almost exactly represents the first stage of formation and the deviation occurs at larger orifice diameters. Further, the external diameter of the orifice also decides the maximum possible bubble volume as the contact angle of bubble varies with the thickness affecting the detachment period and hence the bubble sizes.[61] Figure 5 shows the experimental observations on effect of orifice diameter on bubble size under constant flow as well as constant pressure conditions.

In the case of PAA solutions (Figure 5C), the bubble volume has a very weak positive dependence on the orifice diameter for the gas flow rates ($Q_G < 2 \times 10^{-6}$ m^3/s) and above this value, the dependence is very strong. For small diameter orifice, the forces of attachment are very strong and also the contact angles have wide variation. At low gas flow rates where turbulence is lower, for smaller orifice diameters, the waiting time is longer, whereas for a high gas flow rate the detachment is faster.

(c) Orifice Chamber Volume (V_C). It is known that, the mechanism of bubble formation depends greatly on the mode of gas supply and hence on the chamber volume. Thus, for a very small chamber, the in-flowing gas to the chamber will be approximately equal to the gas flow into the bubble. This condition is known as the *constant flow* operation. On the other hand, for large chamber volumes, as a result of damped pressure fluctuations, the in-flowing gas to the bubble is not the same as into the chamber. Thus, the pressure forces through the chamber volume, which are dynamic in nature, affect the bubble formation in various ways. Satyanarayan[15] has observed that the bubble volume increases with chamber volume by almost the same amount at all flow rates. However, at low orifice submergence, the effect becomes more pronounced. The *constant pressure conditions* can be said to exist when a further increase in chamber volume does not vary the bubble volume where the discharge resistance is small. Thus, in smaller chambers, initially, the pressure in the bubble and in the chamber will increase beyond the initial pressure as an effect of the inflow of gas and the

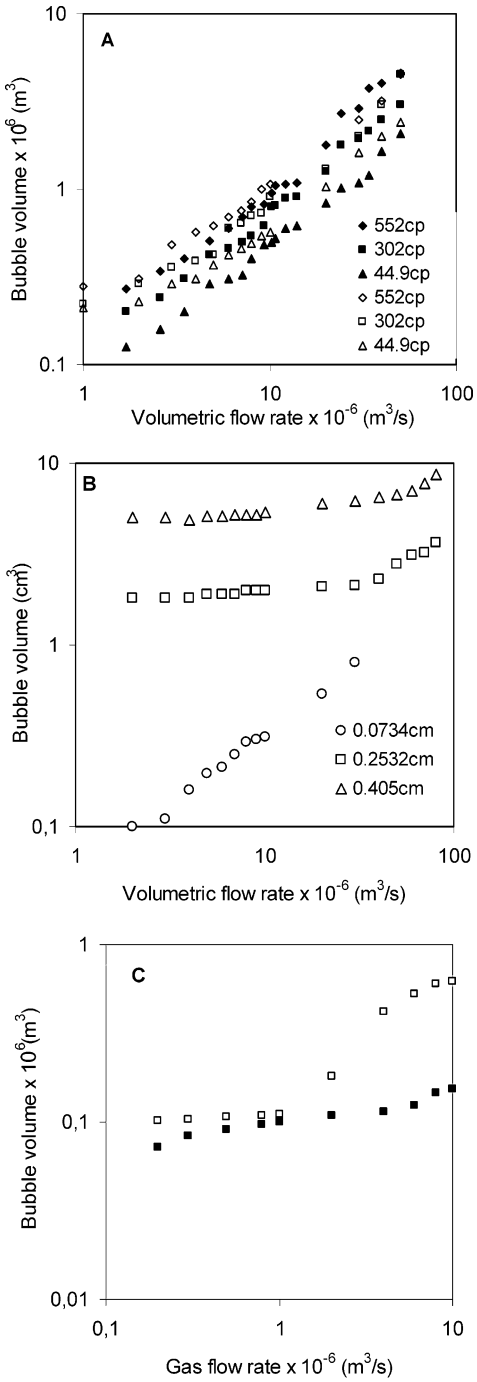

Figure 5. Effect of orifice diameter on bubble volume. (A) Filled symbols correspond to the bubble sizes obtained for orifice of diameter 3.67 mm and empty symbols correspond to the bubbles from orifice of diameter 5.94 mm, for different liquid viscosities, (B) effect of orifice diameter on bubble size in water, (C) effect of orifice diameter on bubble size in different viscous liquids (PAA) ■ μ = 1.09 cP, □ μ = 6.19 cP.

inertia of liquid. This results in the growth of the bubble and thus suppresses the effect of surface tension forces, which tends the bubble to grow faster than the rate at which gas is being supplied to the chamber volume developing a negative pressure gradient. As a result of this, the chamber pressure $P_C(t)$ decreases while, the bubble pressure $P_B(t)$ would decrease further. From a thermodynamic viewpoint, the rate at which these two pressures decrease (as a result of velocity fluctuations) depends on the system pressure, chamber volume and heat capacity ratio.[62] In the case of a larger chamber, the pressure in the orifice $P_O(t)$ will remain virtually

equal to the initial pressure $P_C(t)$. Thus, the inflow of gas to the bubble (Q_C) during bubble formation can be larger than the gas flow rate to the chamber and will be independent of the flow to chamber but will depend on the value of the initial pressure and the pressure drop across the orifice.[65,16,5,66] In the case of larger orifice diameters at higher flow rates, an increase in chamber volume decreases the bubble frequency as a result of large bubbles generated at the orifice. However, for lower gas flow rates with the same orifice-chamber configuration, bubble frequency is always lower and is independent of orifice diameter. In the case of the top submerged orifices, the bubble size is almost independent of the chamber volume since the back pressure effect is nominal. In air−water system, using sharp edged square shaped orifice and over a wide range of chamber volume, Antoniadis et al.[66] observed that, even at low gas flow rates, the number of bubbles in a group and their volume increased with an increase in chamber volume, whereas at higher gas flow rates, single bubbles were generated with the same effect of increased V_C. For small orifices, an increase in V_C causes a much smaller pressure drop in the chamber and as a result, at higher volumes, the bubble detachment becomes unstable, producing many bubbles rapidly in succession. Also, for the same V_C but with varied chamber diameter, the number of bubbles formed in groups is the same. In the case of larger orifice diameters at higher flow rates, increase in chamber volume decreases the bubble formation frequency as a result of large bubbles generated at the orifice. These results are certainly helpful in deciding the range of flow rates to be maintained for getting desired bubble sizes for a given orifice diameter and V_C; however, it would be helpful to understand the effect of chamber geometry on bubble size. A detailed account of the efforts in this direction are given in Hughes et al.,[51] Antoniadis et al.,[66] McCann & Prince,[67] Marmur & Rubin,[18,19] Kumar & Kuloor,[17] Park et al.,[68] and Wilkinson.[64]

A typical pressure variation cycle in a gas chamber during bubble formation is studied by Kupferberg and Jameson,[65] Khurana and Kumar,[16] Hsu et al.[62] Their analysis supports the observations by Tsuge and Hibino[5] where, in a system with wide variation in the gas−liquid properties, the bubble volume was found to increase with chamber volume and gas flow rate only for certain capacitance number $N_C \approx (4V_C g\rho_L)/(\pi d_h{}^2 P_h)$, however, bubble volume was found to be independent of gas flow rate beyond ($N_C > 25$). In another studies, Davidson and Amick[69] have observed that, the bubble volume was independent of N_C for $N_C < 0.8$, while at higher gas flow rates, critical value of N_C drops down to ($0.2 \times V_C$), which supported the results by Hughes et al.[51] and is contradictory to the above results. In the case of the top submerged orifices, the bubble size is almost independent of the chamber volume since the back-pressure effect is nominal.[70]

In non-Newtonian liquids at large flow rates, bubble volume increases with increasing chamber volume, mainly due to the fact that accumulation of the gas fed into the gas chamber results in a higher chamber pressure (than the hydrostatic pressure) at the orifice and helps to increase the volume of the bubble. However, at low gas flow rates and large chamber volumes, the time period without bubble growth (waiting time) is required so that the bubble volume depends on chamber volume. On the other hand, for the case of high gas flow rates the waiting time is short enough so that the effect of the chamber volume on bubble volume is low.

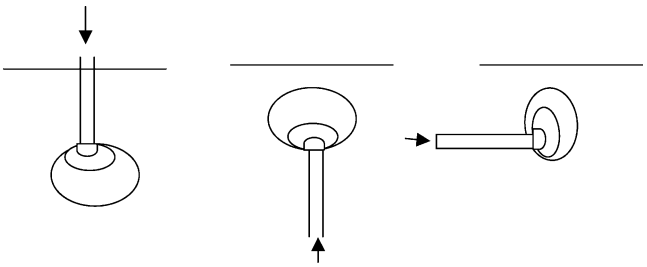

Figure 6. Schematics of various ways of orifice submergence. (A) top submergence, (B) bottom submergence, (C) side submergence.

(d) Orifice Submergence. An orifice can be submerged in three ways: top submergence, bottom submergence, and side submergence (Figure 6). The first kind of submergence is very common in the metallurgical industry, while the later two are usually found in the chemical process industry where the aim is uniform dispersion of gas. In the case of bottom submergence, the viscous forces, surface tension forces, pressure, gravitational forces, and inertia are counter-balanced by the buoyancy and gas flow rate through the orifice. Kumar and co-workers[16,14,15] have shown that the bubble volume reduces exponentially with increase in orifice submergence. This rate of reduction of bubble volume is higher for larger chamber in the wide range of orifice submergence. Under constant flow and constant pressure conditions, submergence has a negligible effect on bubble volume. For the top submerged orifice, the pressure required to initiate bubble formation is higher and once the bubble goes past its maximum bubble pressure, the chamber volume rapidly depressurizes leading to rapid growth and detachment. In comparison with the bottom submerged orifices, here, the surface tension forces and viscous forces are of less importance and friction in the capillary is dominant. It has been reported that the growth rate of bubbles in this case is comparably small, and bubble sizes (traverse diameter) are larger than the earlier case,[57,71] and bubble size depends up on the thickness of the orifice[61] as many stable contact angles exist for the same orifice. Thus, depending up on the thickness of the orifice, the number of stable contact angles changes and gives a range of possible bubble sizes. The detachment stage is better controlled by the orifice diameter. Finally, side submergence is very rare, but many times it is used in the air-loop lift reactors and small bubbles are formed as liquid is in cross-flow mode resulting in an early detachment. Recently, Iliadis et al.[72] have studied the effect of orifice submergence on bubble formation experimentally, using four orifices (of diameters 1.15, 2.1, 3.25, and 4.35 mm). Experiments were conducted in the range of gas flaw rates 0.75−56.7 mL/s, chamber volumes 150−7000 mL and orifice submergence 0.1−1.5 m. Results show that in the region of single bubble formation the bubble size increases with the orifice submergence. In the region of group formation of bubbles, the individual bubble size is reported to be independent of the orifice submergence, ranging from 0.1 to 0.5 mL for the smallest orifice and from 0.2 to 1 mL for the other ones. No effect of orifice submergence was observed on weeping.

(e) Orifice Contact Angle. It is known that, the surface tension force affects even the bubble shapes and

the effect of surface tension can be taken into account by including the angle of inclination of the interface at the triple point of solid−liquid−gas while estimating the surface forces. This inclination angle depends on the contact angle and type of orifice (sharp-edged or curved). For a sharp-edged orifice, the angle of contact is approximately the same as the angle of inclination, whereas for a curved orifice, there is a large difference between the two because of the local conditions i.e., radius of bubble curvature, thickness of the orifice, the gas pressure inside the bubble neck and the local contamination. Details of the effect of contact angle on bubble size can be found in Marmur and Rubin.[18]

(f) Orifice Orientation. In the cases where the axis of the orifice is inclined with respect to the vertical, the formation, growth, and expansion of a bubble takes place in vertical direction. Hence, during force balance, the vertical component of the surface tension force is always considered. Kumar and Kuloor[17] have discussed this aspect in detail. This particular aspect is important for modeling the bubble formation over the holes in blades of a gas inducing impeller system.

(g) Material of Construction of the Orifice. Surface forces depend on the material of construction of orifice and hence decide bubble size. As discussed earlier, the contact angle between the gas−liquid and solid is one of the parameters determining the detachment time, which mainly depends on the wetting properties of material of construction. Ponter and Surati[73] have reviewed the effect of material of construction and have recommended the suitable material based on the hydrophilic/hydrophobic nature of liquid (wettability) and polarity. In another investigation under constant gas flow conditions, Sada[74] has reported that, when water is in the liquid phase, for carbon nozzles, bubbles contact the inner surface while, for Teflon nozzle, bubbles were formed at the outside surface of the nozzle owing to nonwettability of the surface. Thus, the bubble size changes depending upon the wettability property of the nozzle, for the same inner diameter and varied outer diameter of the orifice. Hence, for obtaining smaller size bubbles, the orifice material should be wettable for the liquid under consideration. Hughes et al.[51] have shown that for the case of glass and brass orifices of the same diameter, the variation in bubble sizes with respect to gas flow rate is negligible. Wraith[53] has given the variation in the hemispherical radius of a bubble versus gas flow rate from orifice of different materials of construction, where it is shown that for the same gas flow rate, the bubble radius is always greater in Perspex orifice than in brass orifice.

The most important messages from the above discussion are the very diverse experimental observations by various investigators, which have appeared in the respective correlation for bubble size. Hence, it is of utmost importance to identify a correlation, which would be more generalized (i.e., it should show a good agreement with the experimental observations over wide range of parameters).

2.2. Mechanisms of Bubble Formation in Newtonian Liquids. Bubble formation in a gas−liquid system is a sequential process, and several approaches have been followed to understand the mechanism of bubble formation. In general, we know that when gas is passed through the capillary or porous material, as an effect of certain forces acting on the system the gas phase cannot come as a continuous stream up to a finite Reynolds number, whereas only at very high gas flow rates continuous gas jet may impinge from the orifice/pores. The discontinuity in the streamlined gas results into the formation of small packets of fluid, which we term, bubbles. The models proposed for understanding the mechanism of bubble formation can be grossly classified based on the number of stages considered i.e., one stage model, two-stage model, and multistage model. Although the modes of bubble formation totally depend on the system properties described earlier, the number of stages is a function of the gas flow rate and the orifice dimensions. When gas starts flowing through the capillary, initially for a while, it passes at constant flow condition raising the pressure inside the bubble linearly. The rapidly varying volume of the bubble at the tip induces oscillations in the liquid in the immediate vicinity of orifice at a frequency equal to that of bubble formation. The sudden motion resulting from the detachment of a bubble may produce a reduced pressure at the tip of the capillary and help to initiate formation of the next bubble. The length of neck varies with the gas flow rate. Rabiger and Vogelpohl[21] have discussed the variation in neck length in detail. In the majority of studies, various assumptions are made for convenience as well as for simplicity in the model. A list of assumptions made for the development of these models is given in Table 2. A summary of the models considered, correlation developed along with the limitations of each model and formulation for bubble size/volume are given in Table 3. These correlations are either complicated, require iterative procedure for solving or very simple but applicable for only a narrow range of conditions. On the gross level, the approaches for all these studies can be classified as (i) basic force balance, (ii) dimensional analysis, and finally (iii) use of finite difference or finite element methods. The details of models based on force balance (as a simple case) and the comparison of its predictions with experimental data over a wide range of parameters are discussed below.

2.2.1. Force Balance Approach in Bottom Submerged Orifice in Stagnant Liquid. The expansion of bubble followed by its detachment is governed by the dominance of different forces at different instants clearly indicates that the process of bubble formation is not a single stage process and hence, Davidson's one stage model cannot be accepted as universal, and it is required to analyze the two stages, i.e., expansion and the detachment of bubble separately. In view of this, Satyanarayan and Kumar[15] proposed the concept of two-stage bubble formation for the first time. During the first stage, the bubble expands while its base remains attached to the tip of the orifice whereas in the detachment stage the bubble base moves away from the tip, while bubble itself would be in contact with the orifice through a neck. According to Siemes and Kaufmann,[59] for the inviscid liquids, in the two-stage mechanism, the process is divided in the following two stages: (i) the first stage is presumed to be exactly analogous to the formation of a bubble when gas flow rate approaches zero and (ii) the second stage begins when the buoyancy forces exactly balance the surface tension forces and the bubble proceeds to detach itself. However, in the case of viscous liquids, it has been assumed that the volume of bubble does not depend on the gas flow rate. This approach has resulted in faulty estimation of detachment time during which, the bubble even gets inflated. In two-stage mechanism, the effect of drag force during

Table 2. List of Assumptions Made for Modeling the Process of Bubble Formation

1.	The bubble is spherical throughout.
2.	The drag coefficient is inversely proportional to the instantaneous Reynolds number of the bubble.
3.	The bubble velocity is proportional to the flow rate with no allowance for change in bubble cross-section during growth.
4.	The frontal area for the drag term is constant at its final value.
5.	The carried mass of liquid is constant during bubble growth.
6.	Diameter of liquid column is so large that the wall does not influence ascending bubbles.
7.	Liquid column does not contain any obstacles.
8.	Liquid in the column is not circulated except by the action of the bubbles themselves or circulation of liquid is negligible.
9.	a) Complete wetting of orifice, b) incomplete wetting of orifice.
10.	The motion of the bubble is not affected by the presence of another bubble immediately above it.
11.	The momentum of the in-flowing gas is negligible.
12.	The bubble is at all instants moving at the Stokes velocity appropriate to its size.
13.	Liquid is infinite in comparison to bubble volume.
14.	The liquid is inviscid.
15.	The gas injection rate is constant and the gas incompressible.
16.	Gas density is neglected.
17.	The bubble is a volume of revolution around the axis of the orifice.
18.	The interface is acted upon by pressure difference between gas and liquid and surface forces.
19.	Added mass coefficient of inviscid fluid is taken constant.
20.	The gas is ideal.
21.	The gas in the bubble, as well as the gas in the chamber flows and expands adiabatically.
22.	Pressure difference exists across the orifice, which determines the rate of gas flow into the bubble.
23.	The pressure within the bubble is uniform and the same holds for the pressure in the chamber underneath the orifice.
24.	Bubble detachment occurs when the neck that forms narrows to zero at one of its points.
25.	Volumetric gas flow is constant
26.	The flow rate of gas flowing into the bubble through the nozzle is constant during bubble formation,
27.	The bubble formation is a a) one, b) two and b) three stage process.
28.	The pressure in the bubble is uniform as that in the chamber.
29.	A pressure difference exists across the orifice and it determines the rate of gas flow into the bubble.
30.	Flow of gas in the chamber is an adiabatic process. In the orifice and bubble it is isothermal.
31.	The gas liquid interface is acted on by a pressure difference between the gas and the liquid and by surface tension forces.
32.	The interfacial surface tension is constant and uniform.
33.	In the case of the liquid cross-flow, the flow is isothermal, uniform, inviscid and irrotational.
34.	There is no energy exchange or mass transfer across the interface.
35.	At reduced gravity condition, buoyancy forces are negligible when compared with liquid drag.
36.	The volume contribution by neck is negligible as compared to the spherical portion of the bubble.
37.	Completion of the growth cycle occurs when the gas neck severs.
38.	For constant flow condition, the bubble growth rate is equal to the gas flow rate entering the system.
39.	Formation frequency is constant.
40.	Bubble growth occurs at constant rate.
41.	Flow around a bubble is irrotational and unseparated.
42.	First stage in the formation process ends when the upward and downward forces equate.
43.	Surface tension has not effect on bubble size.
44.	Liquid viscosity has not effect on bubble size.
45.	Bubble is symmetric about the axis.
46.	Liquid is stationary.

initial expansion (growth) has been neglected and in no way, the reliable detachment time could be estimated. Hence, Satyanarayan and Kumar[15] came out of a reasonably acceptable model, which can be used for explaining the process of bubble formation. According to them, the final volume is the sum of the volumes pertaining to two stages. Here, we discuss some of the models based on this approach.

2.2.1.1. Kumar and Co-workers.[14,15.] At finite gas flow rate Q, the bubble expands at a definite rate giving rise to inertial and viscous drag, which adds to surface tension. The first stage is assumed to end when the forces in opposite direction become equal. The forces considered in this approach are as follows

$$\text{buoyancy force} = V(\rho_L - \rho_G)g, \qquad \text{viscous drag} = 6\pi\mu v_e r_e$$

$$\text{surface tension forces} = \pi D\gamma\cos\theta,$$

$$\text{inertial force} = Q^2\left(\rho_G + \frac{11}{16}\rho_L\right)\frac{V^{-0.66}}{12}\pi\left(\frac{3}{4\pi^{0.66}}\right) \quad (1)$$

and virtual mass of the bubble is given as $M = (11/16\ \rho_L)Q\ t_e$.

The uppermost point of the bubble is assumed to move with a velocity equal to the rate of change of the bubble diameter and hence the average bubble growth velocity is the velocity of its center, which is equal to the rate of change of bubble radius, i.e.

$$v_e = (dr_e/dt_e) = Q/4\pi r_e^{\ 2} \quad (2)$$

and balancing the corresponding momentum gives

$$\frac{dMv_e}{dt_e} = M\frac{dv_e}{dt_e} + v_e\frac{dM}{dt_e}$$

where

$$\frac{dv_e}{dt_e} = -\left[\frac{Q^2}{6}\pi\left(\frac{3}{4\pi^{2/3}}\right)\right]V^{-5/3}, \frac{dM}{dt_e} = \left(\frac{11}{16}\rho_1\right)Q \quad (3)$$

The values of dv_e/dt_e and dM/dt_e are obtained on differentiating two Equations in Davidson & Schuler[4] and on simplification gives

$$\frac{d(Mv_e)}{dt_e} = Q^2\left(\frac{11}{16}\rho_1\right)V^{-2/3}/12\pi\left(\frac{3}{4\pi}\right)^{2/3} \quad (4)$$

Table 3. Various Correlations for Bubble Sizes

investigators	model proposed through experimental observations	method of approach	assumptions used in formulation[a]	diameter/volume of bubble
Eversole et al.[48]	One stage model was observed for different size orifices.	Bubble volume was obtained by stroboscopic frequency measurements.	1,2,3, 4, 5, 6, 7, 20, 27a, 9a 10, 39, 40, 48	$d_B = 81.18\frac{\sigma}{P_o g}$
Krevelen and Hoftijzer[49]	Separate and chain bubble formation	Bubbles were classified as small, medium, and large. Ascending velocity was obtained from flow rate of gas. The same was studied for three different regimes of gas flow.	1, 9a, 6, 7, 8, 32, 13, 27a, 31, 48	$d_B = \frac{6d_h}{g\Delta\rho}$
Benzing and Mayers[50]	Static and dynamic region of bubble formation process were considered.	Dimensional analysis was used to correlate results.	1, 5, 6, 7, 8, 9a, 10, 11, 13, 16, 20, 46	$d_B = 1.82\frac{d\sigma^{0.25}}{g d_h^2 \rho_L}$
Hughes et al.[51]	Process of bubble formation was considered to be a continuous one without any stages in it.	Dimensional analysis was carried out for Re, Nσ, virtual mass. Force balance was applied on a bubble. Pressure equations were considered and solved for drag coefficient, bubble velocity, frontal area of bubble, and bubble volume this was verified for different NC.	1, 5, 6, 7, 8, 9a, 10, 11, 13, 20, 46	$V_B = 1.82\frac{\pi g d_p \sigma}{g\Delta\rho}$
Leibson et al.[52]	Standard deviation and probability methods were used to find the range of sizes of bubbles. Effect of orifices dimensions and gas flow rate on dB was studied using stroboscopy.	The bubble diameters were found at various experimental conditions and empirical formulas were derived using formula for orifice discharge coefficient.	1,5,6,7,8,9a, 20, 39,	$d_B = 0.19 D_o^{0.48} N_{Re}^{0.32}$
Davidson and Schuler[3] (Viscous liquids)	Single stage model was studied for constant flow and constant pressure conditions.	Equation of motion and virtual mass of bubble was used to find out size of bubble theoretically.	27a, 1, 8, 10, 11, 12, 13, 20, 32, 19, 48	$V = 1.772\frac{G^{6/5}}{g^{3/5}}$
Davidson and Schuler[4] (Inviscid liquids)	Single stage model in unsteady state was studied for constant flow and constant pressure was considered.	Equation for upward motion is considered and solved under initial conditions to find out critical bubble volume. Assumptions used for model formulation are different with respect to gas flow rates.	27a, 1, 8, 10, 11, 12, 13, 20, 32, 19, 42, 2, 48	$R = \frac{16g}{11}\left[\frac{t^2}{4} + \frac{V_o t}{2Q} - \frac{V_0^2}{2Q^2}\ln\left(\frac{Qt + V_0}{V_0}\right)\right]$ $V_0 = 4\pi r_0^2/3$
Kumar & co-workers[14−17]	Two-stage model.	Force balance was carried out assuming negligible surface force.	27b, 1, 5, 19, 10, 48, 43, 32, 34, 20,	$V_F = \left(\frac{4\pi}{2}\right)^{0.25}\left(\frac{15\mu Q}{2\rho_1 g}\right)^{0.75}$
Wraith[53]	Two-stage model.	Concept of velocity potential was applied for a hemispherical expanding bubble to find its volume.	6, 7, 8, 27b, 13, 44, 5, 16, 45, 48	$V = 1.09 Q^{6/5} g^{-3/5}$
Park et al.[68]		Model is based on the material balance and force balance using Tate's law.	1, 6, 7, 8, 46, 48	$V_b = \frac{2\pi R_o \sigma}{\Delta\rho g}$
Acharya et al.[54]	Single stage model	Wave theory was applied to determine the volume of the bubble in dynamic detaching condition.	1,5,6,7,8,9a, 27a, 46, 44	$V_b = 0.976\left(\frac{Q^2}{g}\right)^{3/5}$

Rabiger and Vogelpohl [20]	Multistage bubble formation	Formation of primary and secondary bubbles was modeled by force balance	45, 20, 15, 11, 27c, 6, 7, 8, 18, 40, 32, 34, 22, 23, 48	$d_B = \sqrt[3]{\frac{3\sigma d_h}{\rho_L} + \sqrt{\left(\frac{3\sigma d_h}{\rho_L}\right)^2 + \frac{KV_G^2 d_h}{g}}}$
Rice & Lakhani[75]	Two-stage model	For an elastic hole from rubber sheet bubble volume of bubble was found out applying small and large deflection theories	27a, 1, 8, 10, 11, 12, 13, 20, 32, 19, 42, 2, 48	$V_b = \frac{8\pi\sigma r_H}{\rho_1 g} + 2\frac{G^2}{g}\left(\frac{3}{4\pi V_f^2}\right)^{0.33}$
Tsuge and Hibino[5]	Two-stage model	Bubble volume is obtained by force balance including virtual mass of bubble. It is given in terms of dimensionless groups.	27b, 1, 5, 6, 7, 8, 9a, 16, 19, 20, 25, 28, 32, 34, 37, 21, 23, 48	$V_b = \frac{M'X - \left[\frac{4\rho_g Q^2 t^2}{\pi D_o^2} - 0.5 C_D \rho_1 \left(\frac{dX}{dt}\right)^2 \pi r^2 t^2\right]}{(\rho_1 - \rho_g) V_b g t}$
Gaddis and Vogelpohl[22]	Multistage model	Bubble detachment diameter is developed by force balance in terms of a few dimensionless numbers.	27b, 5,6,7, 8, 20, 15, 1, 45, 28, 32, 34, 42, 48	$d_B = \left[\left(\frac{6D_o\sigma}{\rho g}\right) + \frac{81\nu V}{\pi g} + \left(\frac{135V^2}{4\pi^2 g}\right)^{5/3}\right]^{0.25}$
Tsuge et al.[7]	Two-stage model for bubble formed at downward facing orifice submerged in liquid.	Model is obtained by force balance, equation of motion of bubble for both wetted as well as nonwetted orifices for constant flow condition	26, 1, 10, 42, 14, 27b, 5, 19, 40, 24, 20, 5, 6, 7, 9a, 9b, 48	$d_B = 6.9\left(\frac{\sigma}{\rho_1}\right)^{0.5} u_g^{0.44}$
Sada[74]	Single stage model	Model is entirely based on the experimentally observed bubble dimansions.	27c, 9, 14, 17, 20, 23, 34, 48	$d_B = (a^2\, b)^{1/3}$ a: maximum bubble diameter b: minimum bubble diameter
Tsuge et al.[8]	Continuous bubble growth model at high system pressure	Bubble surface is divided into a number of axisymmetric elements which are characterized radii of curvature. Under polytropic high-pressure system Modified Rayleigh equation and equation of motion are solved by finite differences.	15, 20, 25, 6, 7, 8, 9, 34, 17, 47, 10, 48	$V_B = \frac{\pi d_h \sigma}{\Delta\rho g}$
Marshall et al.[76]	Two-stage model	Potential flow theory was applied with Bernoulli's equation and equation of continuity to get volume of bubble formed under cross-flowing liquid.	23, 22, 21, 20, 11, 32, 33, 34, 35, 1, 27b, 36, 37, 19	$R_b = 0.48\, R_o^{0.286}\left(\frac{Q_1/\pi R_o^2}{U_1}\right)^{0.36}$
Wilkinson & van Dierendonck[77]	Nonspherical two-stage bubble formation model	Thermodynamic equation of gas flow along with the equation of motion was solved.	20, 21, 27b, 44, 46, 25	$V_B = \pi d_0^3/12$
Pamperin & Rath[78]	Two-stage quasi-static unsteady shape bubble formation under reduced gravity.	Force balance including virtual mass was used to find the detachment stage	27a, 27b, 35, 34, 37, 25, 38, 20, 9a	$d_B = D_0 A \sqrt{(\rho_L - \rho_G)(We/(We-8))}$ $A = \sqrt{\frac{4}{Re} + \frac{0.124}{\sqrt{Re}}}$ $Re = \frac{2v_B D_0}{\nu_f}$
Buyevich et al.[79]	Two-stage spherical bubble model	Force balance neglecting the gravitational force was carried out for getting bubble size	5,6,7,8,9a, 35, 36, 46, 44	$R_B = \frac{4}{11} g t^2 + \frac{8}{11}\frac{kQ}{\pi r_o^2} t$
Tsuge et al.[10]	Two-stage nonspherical bubble formation in quiescent liquid.	Equation of motion and modified Rayleigh equation were used to simplify the formula for bubble volume at reduced gravity.	2, 4, 5, 6, 7, 8, 9a, 27b, 46	$V_B = \frac{\pi d_0 \sigma}{\rho_L g}$

Table 3 (Continued)

investigators	model proposed through experimental observations	method of approach	assumptions used in formulation[a]	diameter/volume of bubble
Tsuge et al.[9]	Microgravity conditions for top submerged nozzle.	Bubble volume of is proportional to the inverse of gravitational acceleration for small gas flow rates. Growth rate increases with the gas flow rate. For $g/g_t \sim 0.001$ no detachment takes place under constant flow conditions	33, 34, 35, 36, 46,	$V_B = \frac{\pi d_0 \sigma}{\rho_L g}$
Rielly et al.[80]	Two-stage hemispherical bubble formation.	Behavior of buble during formation under liquid cross-flow is analyzed experimentally.	5,6,7,8, 20, 16, 46, 27b	$d_B = \left(\frac{8' d_n \sigma}{C_D V_o^2 \rho_L}\right)^{0.5}$
Forrester and Rielly[81]	Liquid cross-flow condition over impeller blades.		33, 46, 44, 34, 27a, 20	$d_B = 2.4\left(\frac{Q_0}{U_0}\right)^{0.5}$
Jamailamhadi et al.[60]	Neural network approach has been adopted to handle the nonlinear dependence of the various parameters on bubble size.	The results from the model are found to give an excellent agreement with the experimental results.		$d_B = d_O = \left[\frac{5}{Bd_O^{1.08}} + \frac{9.26Fr^{0.36}}{Ga^{0.39}} + 2.147Fr^{0.51}\right]^{0.33}$

[a] Numbered with reference to Table 2.

Making a force balance and letting $V = V_E$ at the end of the first stage yields

$$V_E^{5/3} = \frac{11}{192\pi(3/4\pi)^{2/3} g} Q^2 + \frac{3}{2(3/4\pi)^{1/3} g} \times \frac{\mu}{\rho_1} Q V_E^{1/3} + \frac{\pi D \sigma}{g \rho_1} V_E^{2/3} \quad (5)$$

When the first two terms on the right side are neglected the equation reduces to the one used for evaluating static bubble volume.

In the second stage of detachment, since upward forces are dominant than the downward forces, the bubble accelerates. The bubble is assumed to detach when its base has covered a distance equal to the radius of the force balanced bubble. It is assumed that, the rising bubble is not caught up and coalesced with the next expanding bubble. Further, the bubble motion can be given by Newton's second law of motion along with force balance as

$$M\frac{dv'}{dt} + v'\frac{dM}{dt} = \left[(V_E + Q_t)\rho_L g - 6\pi\mu r(v + v_e) - \frac{Q_t^2(11/16\rho_L)}{12\pi[3(V_E + Q_t)/4\pi]^{2/3}} - \pi D\gamma\cos\theta\right] \quad (6)$$

where v' is the velocity of the center of the bubble i.e., $v' = v + (dr/dt)$.

Above expression in terms of two velocity components v and dr/dt divides the drag into two terms and on dividing the simplified equation by $(11\rho_1/16)$ $(V_E + Q_t)$ we yield

$$(Dv/dT) + A(v/T) = B - GT^{-4/3} - ET^{-5/3} - CT^{-1} \quad (7)$$

where

$$A = 1 + \frac{6\pi(3/4\pi)^{0.33}(1.25)V_E^{0.33}\mu}{Q(11/16\rho_L)}, B = \frac{16g}{11Q}, C = \frac{16\pi D\gamma\cos\theta}{11Q\rho_L} \quad (8)$$

$$E = \frac{Q}{12\pi(3/4\pi)^{0.66}}, \text{ and } G = \frac{24\mu}{11(3/4\pi)^{0.33}\rho_L}$$

for boundary condition of at $x = r_E$, $T = V_F$, it gives

$$r_E = \frac{B}{2Q(A+1)}(V_F^2 - V_E^2) - \left(\frac{C}{AQ}\right)(V_F - V_E) - \frac{3G}{2Q\,A^{-1/3}}(V_F^{2/3} - V_E^{2/3}) \quad (9)$$

Thus, the radius of a force-balanced bubble can be easily obtained using the two-stage model. Though the formulation of model is simple, information about the contact angle (θ) is required.

For the case of intermediate region between constant pressure and constant flow rate, Khurana and Kumar[16] have formulated a two-stage model. Considering the bubble formation at constant flow rate, a two-stage

model can be generalized and the resulting force balance yields.

$$V_t(\rho_L - \rho_G)g = \frac{(\rho_G + 11/16\rho_L)}{12\pi(3/4\pi)^{2/3}V_t^{2/3}}\left[3V_t\frac{Q_t}{dt_e} + Q_t^2\right] + \pi D\gamma\cos\theta + 3\mu\frac{Q_t}{2(3/4\pi)^{0.33}}V_t^{1/3} \quad (10)$$

The first term on right-hand side of (eq 10) is the expansion force $d(Mv_e)/dt_e$, which on substitution in the force balance equation gives the generalized equation for the first stage. For the second stage of the detachment, inertial force is obtained by equating the inertial force to the net upward force acting on the bubble. Velocity of the bubble center can be given as ($v' = v + v_e$) and the force balance can be given as

$$\frac{d(Mv')}{dt} = V_t\Delta\rho g - 6\mu\pi r'v - \pi D\gamma\cos\theta \quad (11)$$

substitution for v' in above equation gives

$$M\frac{dv}{dt} + v\frac{dM}{dt} = V_t\Delta\rho g - 6\pi\mu r(v + v_e) - \pi\gamma D\cos\theta - \frac{\left(\rho_g + \frac{11}{16}\rho_l\right)\left(3V_t\frac{dQ_t}{dt} + Q_t^2\right)}{12\pi(3/4\pi)^{2/3}V_t^{2/3}} \quad (12)$$

$$M\frac{dv}{dt} + v\frac{dM}{dt} + M\frac{dv_e}{dt} + v_e\frac{dM}{dt} = V_t\Delta\rho g - 6\pi\mu r(v + v_e) - \pi\gamma D\cos\theta \quad (13)$$

where

$$M = V_t\left(\rho_g + \frac{11}{16}\rho_l\right) \text{ and } \frac{dM}{dt} = Q_t\left(\rho_g + \frac{11}{16}\rho_l\right) \quad (14)$$

substituting for $M(dv_e/dt) + v_e(dM/dt)$ in above equation yields

$$\frac{d}{dt}(Mv') = V_t\Delta\rho g - 6\mu\pi rv' - \pi D\gamma\cos\theta \quad (15)$$

But for using these general equations it is necessary to express flow rate as a function of time and also the change in radius in the second stage was also included to yield

$$V_t\chi\frac{dv}{dt} + Q_t\chi v = rV_t\Delta\rho g - 6\pi\mu(v + v_e) - \pi\gamma d_h\cos\theta - \frac{\chi\left(3V_t\frac{dQ_t}{dt} + Q_t^2\right)}{12\pi(3/4\pi)^{0.66}V_t^{2/3}} \quad (16)$$

where

$$\chi = \left(\rho_G + \frac{11}{16}\rho_L\right)$$

This model takes into account the detachment stage, all the viscous forces and the pressure gradient in the orifice-chamber as an effect of submergence and the weeping time as an effect of transient pressure variation in the chamber volume at the stage of bubble detachment. This helps in correcting the chamber pressure term and increases the accuracy in predicting the bubble size. Additionally, the model can also be used for finding the bubble sizes in extreme conditions of constant flow or pressure. However, the number of parameters considered for calculations are more as compared to the earlier models. Since the calculation procedure for the size is tedious, here we have discussed another simpler model which can be used for the estimation of bubble size and comparison with experiments.

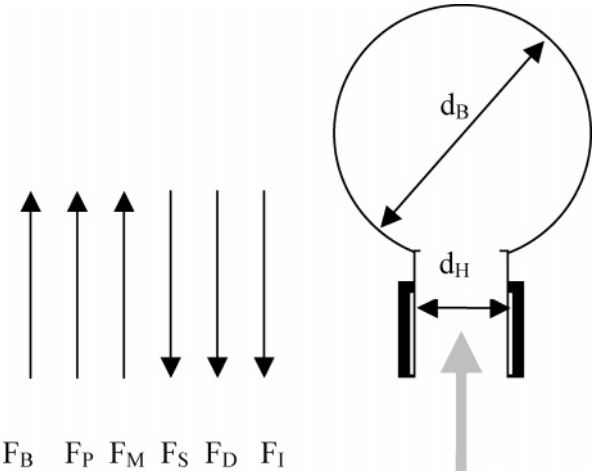

Figure 7. Model for spherical bubble formation at constant flow conditions (reproduced with permission of Elsevier from Gaddis and Vogelpohl[22]).

2.2.1.2. Gaddis and Vogelpohl Model.[22] A simple model for bubble formation in quiescent liquids under constant flow condition was proposed by Gaddis and Vogelpohl.[22] Comparison between theoretical predictions and experimental measurements made by large number of investigators has shown that the model is, valid over a wide range of viscosity and gas flow rates, and hence highly reliable. The prediction of the detachment volume is complicated, but it was obtained by releasing the constraints of spherical bubble shape and cylindrical neck. Further, equation of motion was applied for the resulting geometries of hemisphere and the conical neck, which were not taken into consideration by earlier investigators (Davidson,[3,4] Kumar and coworkers,[14–17] Marmur and Rubin[18,19]), etc. But the approach to solve the equations in this way is lengthy and rarely used in practice. In view of this, the model under discussion[22] suggested two different approaches; (i) the equation of motion was applied to the neck at the moment of detachment and then with the help of a few assumptions simplified equations were obtained, which were later solved analytically, and (ii) in the second approach total volume of the bubble just before detachment was calculated as the sum of the volume of the bubble at the end of detachment stage and the volume of gas in the neck during detachment. The volume of the bubble at the end of the detachment stage was found out by force balance. Since the second approach carries a number of errors in including the neck volume correctly the first is always used in the investigation for the dynamics of bubble formation. Considering the following conditions again (i) constant volumetric gas flow, (ii) Liquid is quiescent and has infinite intensity in every direction, and (iii) Bubble is spherical in geometry and various forces (with reference to Figure 7) can be defined as

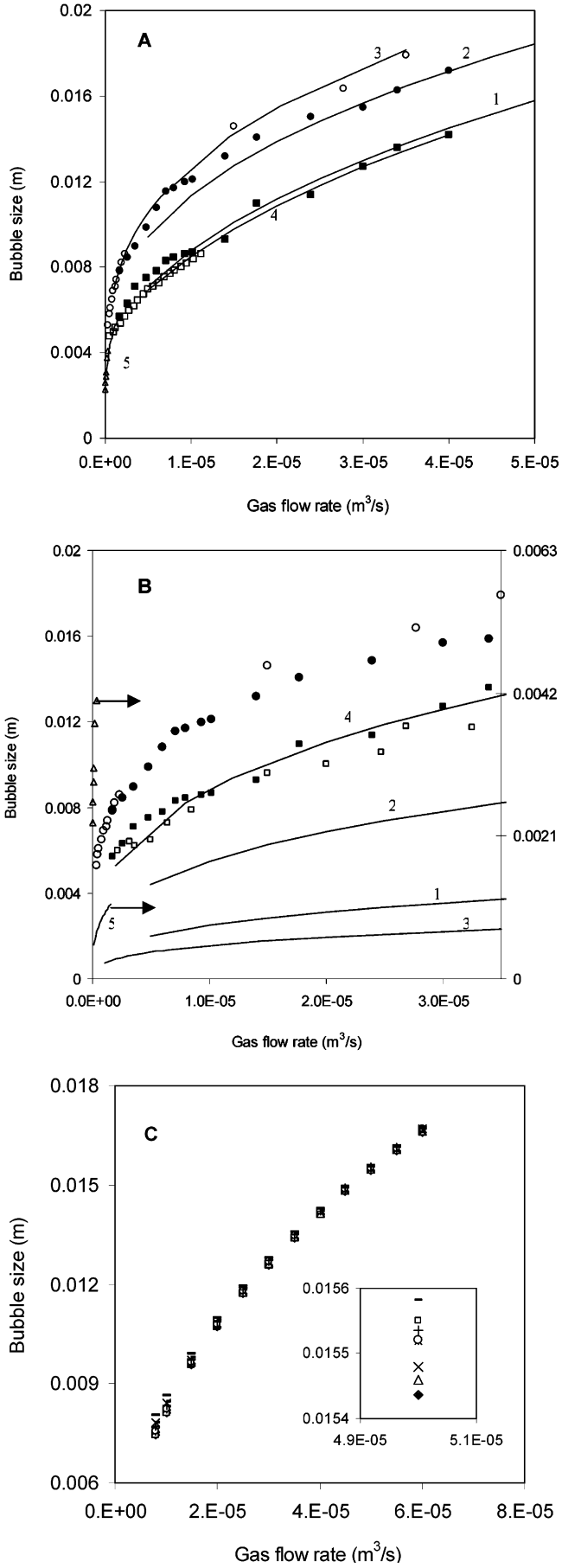

Figure 8. Comparison of the predictions with experiments for various liquids. See details at right.

$$F_b = \frac{\pi}{6} d^3(\rho_L - \rho_G)g,\ F_p = \frac{\pi}{4} d_h^2(p_G - p_L),$$

$$F_m = \frac{\pi}{4} d_h^2 \rho_G w_G{}^2$$

$$F_s = \pi d_h \sigma,\ F_d = \frac{\pi}{4} d^2 C_D \frac{\rho_L w_L{}^2}{2},\ \text{and}\ F_i = (\rho_G V - \rho_L V_1)a \quad (17)$$

Different investigators have tried to solve the equations resulting from the force balance using wide range of drag coefficient values for different systems. The results showed that the maximum neck length is always 1/4th of 'd' and displacement of the bubble center from the nozzle at the moment of detachment is 3/4th of 'd'. Balancing these forces as

$$F_b + F_m = F_s + F_d + F_i \quad (18)$$

Can be given entirely in terms of bubble size (d) as

$$d^3 = S + L/d + T/d^2 \quad (19)$$

where

$$S = \frac{6 d_h \sigma(4 - We)}{4\Delta\rho g},\ L = \frac{81\eta V}{\pi \Delta\rho g},$$

$$T = \left(\frac{135}{4\pi^2} + \frac{27\rho_G}{\pi^2 \rho_L}\right)\frac{\rho_L V^2}{\Delta\rho g},\ We = \frac{16\rho_G V^2}{\pi^2 d_h{}^3 \sigma} \quad (20)$$

Then three different conditions can be applied to control the detachment diameter to yield a generalized equation for d_B as

$$d_B = \left[\left(\frac{6 d_h \sigma}{\rho_L g}\right)^{4/3} + \left(\frac{81\nu V}{\pi g}\right) + \left(\frac{135 V^2}{4\pi^2 g}\right)^{5/3}\right]^{1/4} \quad (21)$$

Since in the transition to the jetting regime, drag and the inertial force due to liquid acceleration differ greatly compared with those calculated by the given formulas, the validity of above equation can be considered only up to the point of transition to the jetting regime. A jet is formed only when (i) the force due to gas momentum exceeds the surface tension force and (ii) surface tension is not capable of forming the spherical or quasi-spherical bubble. This occurs at a critical Weber number which is equal to 4, and thus the force balance changes to $F_m + F_p = F_s$. Having an inverse dependence of *We* on hole diameter, the results clearly show that for achieving a critical *We*, the nozzle velocities should increase with increasing hole diameter. The predictions from this

Figure 8 (continued). In A and B, symbols indicate the experimental data of (1) Ramkrishnan et al.[14]: ● $d_h = 0.00367$ m, $\mu = 0.552$ cP, (2) Ramkrishnan et al.[14]: ■ $d_h = 0.00367$ m, $\mu = 0.045$ cP, (3) Davidson and Schuler[4]: ○ aq. glycerol $d_h = 0.00067$m, $\mu = 1.05$cP, (4) Rabiger[270]: water □ $d_h = 0.002$ m, $\mu = 0.001$ cP, (5) Morgenstern and Mersmann[93]: Glucose, Δ $d_h = 0.0002$ m, $\mu = 0.268$ cP. (A) *Predictions based on Gaddis and Vogelpohl[22] force balance based model:* The line numbers correspond to the predictions for individual data sets as numbered above. (B) *Predictions based on Leibson's formulation:* The line numbers correspond to the predictions for individual data sets as numbered above. (C) Effect of orifice diameter on bubble size (Terasaka & Tsuge[11]) bubbles generated in water (◆ $d_h = 0.0003$ m, ◇ $d_h = 0.0004$ m, Δ $d_h = 0.00198$ m, × $d_h = 0.003$ m) and in 68% glycerol solution (*$d_h = 0.0003$ m, ◇ $d_h = 0.0004$ m, Δ $d_h = 0.00198$ m, × $d_h = 0.003$ m).

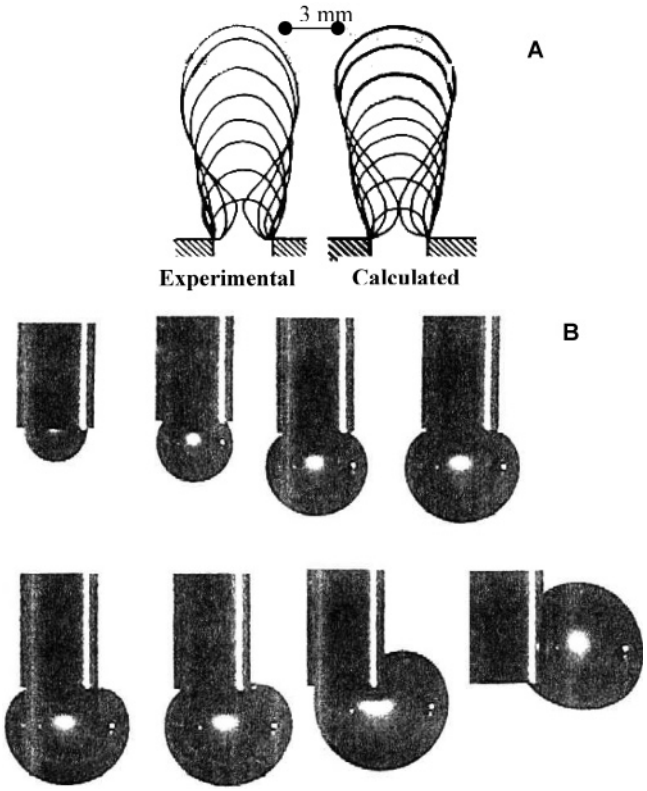

Figure 9. (A) Sequence of simulated bubble shapes during its growth at constant gas flow from a bottom submerged orifice (R_h = 1.52 mm, $G = 1.74 \times 10^{-6}$ m^3/s) (reproduced with permission of Elsevier from Terasaka and Tsuge[11]). (B) Sequence of bubble formation from a top submerged orifice (reproduced with permission of Elsevier from Liow[61]).

correlation show a very good match with the experimental data (Figure 8A), whereas the same data it can be seen to have less agreement for Leibson's correlation, indicating the importance of surface tension in the formulation of d_B. Typical simulation result for the sequence of bubble formation in bottom submerged orifice can be seen in Figure 9A.[11]

In addition to the above two simple ways, several other methods of bubble formation analysis exist. These include the analysis based on finite elements methods, the boundary integral methods and the use of Laplace integral equations. Here we discuss a few other investigations which are important in the process of understanding the subject of bubble formation.

2.2.2. Application of Potential Flow Theory. 2.2.2.1. Wraith Model (1971).[53] For the first time, Wraith[53] showed that the velocity potential can be successfully used in developing a two stage mechanism for bubble formation and it could be used to calculate the volume of the bubble. Here, two-stage model has been considered with an additional concept of the expanding envelope. The model is based on the following assumptions: (i) The liquid is inviscid and of large extent, (ii) Surface tension may be neglected, (iii) The gas injection rate is constant and the gas incompressible, (iv) Gas density is negligible, and (v) the bubble surface is spherical.

Initially applying the pressure equation to a gas bubble formed in the liquid

$$\frac{P}{\rho_L} + 0.5q^2 - \frac{\partial \Phi}{\partial t} = F(t) \tag{22}$$

which for a stationary expanding sphere of radius 'r' takes form as

$$\frac{P}{\rho_L} + 0.5\frac{r^4}{R^4}\left(\frac{dr}{dt}\right)^2 = F(t) \tag{23}$$

at constant flow rate, the growth rate can be given as $\phi = Q/(4\pi r^2)$, which on substitution in the pressure equation at $R > r$ yields

$$\Phi = \frac{r^2}{R}\frac{dr}{dt},\ q = \frac{r^2}{R^2}\frac{dr}{dt} \tag{24}$$

Assuming that the pressure at infinity is negligible, in the above equation, we have $F(t) = 0$. The visual observations can be used to take into account the 'hemispherical bubble' growth with 'a' as the radius of sphere.

$$\frac{d\Phi}{dt} = \frac{r^2}{R}\left(\frac{d^2r}{dt^2}\right) + 2\frac{r}{R}\left(\frac{dr}{dt}\right)^2 = 0 \tag{25}$$

Then

$$da/dt = Q/(2\pi a^2)$$

Again using the pressure equation for the hemispherical surface at $R = a$.

$$P_\theta = \frac{\rho_L Q^2}{8\pi^2 a^4} + P_o - (\rho_L g a)\cos\theta \tag{26}$$

Equating the surface forces and the reactive forces in the liquid gives

$$\frac{P_e}{\rho_L} + \frac{Q^2}{8\pi^2 a^4} = 0 \tag{27}$$

P_θ has two components as the hydrostatic pressure and the pressure due to expansion. Since there is no expansion at the plate surface

$$F_R - \frac{\rho_L Q^2}{8\pi a^2} - \pi a P_o + \frac{2}{3}\pi a^3 \rho_L g = 0 \tag{28}$$

Substituting in the force balance equation and integrating over the hemispherical solid angle

$$F_R - 2\pi a^2 \int_0^{\pi/2} P_\theta \cos\theta \sin\theta d\theta = 0 \tag{29}$$

if $F_R \gg \pi a^2 P_o$, the bubble is in equilibrium, and it remains in contact with the plate. This gives the maximum radius attainable by the bubble and the maximum hemispherical bubble volume as

$$a_h = 0.453\, Q^{2/3} g^{-1/5} \text{ and } V_h = 0.194 Q^{6/5} g^{-3/5} \tag{30}$$

respectively. In comparison to the earlier attempts, this model is distinct as it takes into account the growth of bubble accompanied with the change in shape from spherical to hemispherical during expansion before detachment. The resulting bubble volume is given as

$$V_B = 1.09\, Q^{6/5} g^{-3/5} \tag{31}$$

Interestingly, the bubble volume is shown to have no effect of gas−liquid system's physicochemical properties as well as the orifice properties, which reduces its possible use for realistic estimations of bubble volumes for a wide range of gas−liquid systems.

2.2.2.2. Marmur and Rubin[18] Approach based on Equilibrium Shape of Bubble. Equilibrium shape of a bubble generated at a submerged orifice, detachment, delayed release of bubbles and finally multiple bubble formation can be studied based on the Laplace equation and its further simplification. Marmur and Rubin[18] studied the effect of chamber volume on bubble formation by taking into account the detailed force balance across the interface, where the interface was discretized in several elements. Their approach for understanding the effect of chamber volume on bubble size assumes that the gas flow rate is maintained such that the bubble remains attached to the orifice and the bubble formation process is quasi-static.

2.2.2.3. Marmur and Rubin.[19] In bubble formation process, the second stage of detachment is a result of the dominance of the buoyancy over the other forces, which was considered in all previous models. Buoyancy is dominant if the bubbles are of large sizes. The bubbles' lift-off process from the orifice due to buoyancy was put as a misleading approach by Marmur and Rubin[19] who proposed the process of detachment as a dynamic process caused by the inward radial motion of the liquid at the orifice. This motion, which narrows the neck of the bubble up to detachment, takes finite time, during which the bubble continues to grow. Hence, according to them the static approach to lift-off at the instant of equilibrium is inadequate. Since the whole analysis is highly involved, here we have restricted ourselves to explain the approach and important findings in a qualitative manner. To solve the underlying problem, they have solved the equation of motion numerically under the following assumptions: (i) The bubble is a volume of revolution around the axis of the orifice. (ii) The gas liquid interface is acted upon by pressure difference between the gas and the liquid and by surface tension forces. (iii) Inertial mass is assigned to the bubble interface, which equals the instantaneous mass of liquid being accelerated. Added mass of inviscid fluid exists for every bubble. (iv) The volume of liquid around the bubble is very large as compared to the bubble volume. (v) The gas in the bubble, as well as the gas in the chamber flows and expands adiabatically. (vi) Pressure differences across the orifice determine the gas flow rate into the bubble. (vii) The pressure within the bubble is uniform and the same holds for the pressure in the chamber underneath the orifice. (viii) The momentum of the gas is negligible. (ix) The formation of the bubble is unaffected by the presence of the other bubbles. (x) Bubble detachment occurs when the neck narrows to zero at one of its points.

Approximate equation of motion for the gas−liquid interface was used. It was considered that the surface force is due to pressure differences between the gas in the bubble and the liquid and the line forces are due to surface tension. In the dynamic process of bubble formation the resultant of these forces is equal to the rate of change in the liquid momentum, assuming that the gas momentum is negligible. In the analysis of growing bubble surface, a systematic approach was developed for taking into account the position of each surface element so that a converging solution of equations was achieved. Under the assumption that the motion of interface was transient with respect to any point on the bubble surface, concept of added mass was used to solve the Navier−Stokes equation by the Lagrangian approach. The equations were solved using the boundary conditions of symmetry at the top and that at the three-phase point at the edge of the orifice. In addition, two more boundary conditions of restricting the bubble growth with respect to orifice and no slip were used. To neglect the effect of buoyancy, bubbles were assumed to be of small size. To correlate the solution of equation of motion and bubble volume, an approach through thermodynamic equation of gas phase was used.

A set of 11 equations was solved using finite difference. It was observed that the solution could converge very well for values of added mass coefficient of 0.85 and orifice coefficient 0.65. To maintain the force balance across the interface, the computations were subjected to adoption of bubble shape during its growth. The model was found to be sensitive to orifice diameter at higher flow rates, as it resulted in deviating bubble sizes. Their results were found to support the conclusion as deduced by Davidson and Schuler[4] in the case of inviscid fluid.

2.2.3. Approach based on Boundary Integral Method. In general, boundary value problems with interfaces exhibit relatively large surface-to-volume ratio, and in this case, the boundary element method is expensive compared to domain techniques such as the finite element method. Boundary element methods are very important for solving boundary value problems in the PDEs. Many boundary value problems of PDEs can be reduced into boundary integral equations by the natural boundary reduction. The boundary integral method is based on Greens's formula, which on reformulation of the potential problem as the solution of a Fredholm integral equation helps in reducing the dimension of the problem by one. Although the method has been used in several different areas of research, very few investigators have used this approach to evaluate the problem of bubble formation. Below, we discuss the two important contributions made in the subject under consideration.

2.2.3.1. Hooper's Approach of Potential Flow.[82] The boundary element method has been applied for the study of the bubble formation, which also helps in mathematically understanding the mechanism of detachment of the bubble using the equations of motion for the liquid. It has been assumed that volume of liquid is large so that the effect of side walls is negligible and the depth is much greater than the largest size of the bubble. Hooper[82] applied this technique assuming the surrounding liquid to be inviscid. The velocity was related with the gradient of stream function as $u = \Delta\phi$ and

$$\frac{\partial \Phi}{\partial t} + \frac{1}{2}|u^2| + \frac{(P_1 + \rho_L g z)}{\rho_L} = C(t) \qquad (32)$$

Bernoulli's equation was applied for the liquid in motion in terms of velocity potential.

As

$$z \rightarrow \infty, P_1 + \rho_L g z \rightarrow 0$$

hence

$$C = 0$$

Writing the equation in Lagrangian form for convenience yields

$$\frac{D\Phi}{Dt} = \frac{1}{2}|u^2| - \frac{1}{\rho_L}(P_1 + \rho_L g z) \tag{33}$$

For the compressible fluid the continuity equation can be written in Laplace form as $\Lambda^2 \phi = 0$

Since there is no flow through the orifice pate at $z = 0$, $d\phi/dz = 0$.

At the interface the normal velocity of the liquid and of the bubble are equal and surface tension results in the pressure jump. Hence on S, $d\phi/dn = v_s$ and $P_1 = P_b - \sigma k$.

For a closed system with radius r_O the orifice coefficient was given as

$$H = k(\pi r_o^2)\sqrt{(P_C - P_b)/\rho_C}$$

Above equations were solved simultaneously to take into account the pressure correction at each time step. The following assumptions were made while solving the equations:

(i) For very small chamber volume, the gas flows directly into bubble at the entrance pressure,

(ii) When chamber volume is very large, P_C and ρ_C are approximately constant and equals P_E and ρ_E.

(ii) Expansion of bubble is isothermal.

The equations were solved under the boundary conditions, which relate P_1 to P_b and the gas equations from which P_b can be calculated are substituted into equations of motion. Initial conditions for the values of P_b and P_C and the initial position of bubble surface and the value of ϕ on bubble surface are needed. A systematic approach has been used for analyzing the bubble growth in time, and the results are validated with the published literature. However, the processing time for the calculations greatly depends on the initial conditions and boundary conditions. Second, since the model does not take into account the effect of wake pressure, the effect of the primary bubble on the secondary bubble is neglected. Pinczewski[83] has also followed a similar approach for describing bubble formation at a single submerged orifice.

2.2.3.2. Xiao and Tan's Boundary Integral Method.[28] In a very recent attempt, Xiao and Tan[28] have proposed an improved boundary integral method which is an extension to the above-discussed analysis by Hooper.[82] Under the assumption of constant flow rate condition, the viscosity of liquid is considered to be negligible and the flow is irrotational. They have used Laplace's equation to describe the velocity potential and Bernaulli integral is applied between the liquid side of the bubble surface and a point in the liquid. Their systematic approach includes the following steps and equations: (i) Laplace's equation, (ii) thermodynamic equations for the gas flow, (iii) curvature of bubble surface from the analytical planar geometry, (iv) volumetric growth rate of bubble, (v) estimation of the normal velocity through Green's integral formula for a piecewise smooth surface, (vi) reduction of dimension by assuming axisymmetry of bubbles, where the surface is divided in several elements and an isoparametric linear approximation is used for the surfaces and functions through proper discretization, and (vii) system of images used for satisfying the zero-normal-velocity condition at the rigid boundary. (vii) The surface velocity specifications are completed by defining the tangential velocity over the surface through cubic spline interpolation over the surface, and finally, (viii) solution of these set of equations is carried out in time domain while an iterative trapezium rule with Euler's method is used for updating the time and space coordinates of a growing bubble. The approach is systematic and has a few important advantages over the method by Hooper,[82] however the estimated bubble sizes are noticeably higher when compared with the experimentally obtained bubble sizes of Kupferberg and Jameson[65] (Figure 4 from Xiao and Tan[28]). Also, the simulated bubble sequences do not show the existence of bubble neck, which in reality is known to exist from several experimental observations in the literature.

Importantly, these approaches based on detailed modeling of the development of bubble surface form an important direction for further research in systems where the experimental analysis is always not feasible (viz. bubbling in plasma, reduced gravity conditions, bubbling in opaque liquids such as mercury, etc.). The most important component is the validity of the approach through comparison with the cold flow experiments, which should be satisfied to optimize the use of available computational power.

2.3. Mechanism of Bubble Formation in Top Submerged Orifice in Stagnant Liquids. The advantages of quick withdrawal of orifice in the event of failure of gas supply and less clogging of the orifice facilitates easy control of operation and hence makes the top submerged orifice very commonly used in the metallurgical industry. In earlier studies, Datta et al.[42] have shown that the diameter of a bubble formed at the tip of the top submerged orifice is larger than that of the bottom submerged orifice of the same diameter. However, the diameter of the bubble is not a strong function of the way of submergence but of the diameter of the orifice. In this subsection, we discuss the models explaining the mechanism of bubble formation at the top submerged orifice in brief.

2.3.1. Tsuge Model[6]. The two-stage model for bubble formation under constant flow condition was used for the prediction of the size of the bubbles formed. The mathematical model that was used to validate the experimental data was based on the following assumptions: (i) The flow rate of gas into the bubble through the nozzle is constant during bubble formation. (ii) The bubble maintains spherical shape during its growth. (iii) Bubble motion is not affected by the presence of other bubbles. (iv) The bubble formation consists of two stages.

In this case, the first step is similar to earlier described expansion stages while during the detachment stage the buoyancy force is balanced by the other forces and the bubble continues to grow while lifting up vertically but the gas is still fed through the nozzle. The detachment stage comes to an end when the base of the bubble detaches from the nozzle tip and the bubble separates. According to their approach, wettability of the nozzle can be considered as the basic criteria for study and thus the wetted and nonwetted nozzles were considered.

(A) Wetted Nozzle Condition. Bubble formation process in the case of liquids such as water and organic liquids (in a wetted nozzle) takes place in two stages. In the expansion stage constant flow condition is written as

$$Q = \frac{dV_B}{dt} = \frac{d(4\pi r^3/3)}{dt} = \text{constant} \quad (34)$$

where the initial conditions are $r = d_i/2$ and $dr/dt = Q_g/\pi d_i^2$. The detachment stage then begins when the force balance is hold vertically.

$$\rho_L V_{B2} g = 0.5 C_D \rho_L \pi r^2 \left(\frac{dr}{dt}\right)^2 + \frac{d(M_1' dr/dt)}{dt} + \frac{4\rho_G Q_G^2}{\pi D_i^2} + \pi D_i \sigma \quad (35)$$

where V_{B2} is the volume of the bubble less hatched by that of orifice which gives the virtual mass (M_1') was assumed for an ascending spherical bubble parallel to the wall as $0.5\rho_L V_{B1}$. In this case, every time as the volume of the bubble increases, the volume hatched along with it also increases, and thus the virtual mass of the bubble changes with time toward the detachment stage. Now from the balance of forces the earlier equation to the equation of motion in the detachment stage gets modified and in the same way M_2' also changes. This equation can be solved for initial conditions to get the volume V_B and d_B at detachment stage as

$$V_B = 4\pi \frac{r^3}{3} - \pi \frac{d_h^2 r}{2} \quad (36)$$

(B) Nonwetted Nozzles. This condition has been observed in the molten liquids and the equations resulting from the force balance and equation of motion are same as the earlier case except the initial conditions. Hence, the equations for calculating volume and the diameter remain same, but in both the cases a discrepancy remains between the calculated and the experimentally observed values of diameter of the bubble. This was because (i) Fractional gas hold up affects the overall liquid density if liquid is a molten metal. (ii) As the heat transfer between gas bubble and the liquid metal was not considered in this model, the bubble size will be predicted to be smaller by this model than by the approach which considers the interfacial heat transfer. (iii) Constant flow condition is not actually fulfilled. Thus, balancing the forces is of much reliability as compared to the other methods to calculate the volume of the bubble.

2.3.2. Liow Model. The mechanism of the bubble formation at a top submerged orifice having a length longer than that of the normal orifices was experimentally studied and modeled by Liow.[61] In the case of top submerged orifice, the orifice contact angle varies while the bubble grows, but the bubble size mainly depends on the orifice diameter rather than the contact angle. In view of this, Liow[61] has taken the Laplace equation of the interface in equilibrium with gravity as

$$\frac{d^2z/dr^2}{[1 + (dz/dr)^2]^{3/2}} + \frac{dz/dr}{r[1 + (dz/dr)^2]^{1/2}} - \frac{\rho^* g z}{\gamma} = \frac{-P^*}{\gamma} \quad (37)$$

using few dimensionless parameters, the bubble volume was obtained by solving

$$\frac{dV^*}{ds^*} = r^{*2} \frac{dz^*}{ds^*} \quad (38)$$

where

$$\frac{dr^*}{ds^*} = \cos\phi, \frac{dz^*}{ds^*} = \sin\phi \text{ and } \frac{d\phi}{ds^*} = \text{La} + \text{Bo } z^* - \frac{\sin\phi}{r^*}$$

by subjecting it to initial conditions: $\phi = 0$, $z^* = 0$, $R^* = 0$, $d\phi/ds^* - \text{La}/2$ at $s^* = 0$ using MATHEMATICA. The variation in the maximum bubble pressure for a range of Laplace number (La) and Bond number (Bo) was obtained which showed that although the dimensionless pressure increases with Bo, the actual values of the pressure for a given system fall with increasing lance diameter. As mentioned by many investigators, the maximum bubble size occurs when $\phi = P$ at the lance. The bubble maximum diameter is shown to increase faster than the bubble heights with increasing lance diameter leading to flatter bubbles.

His analysis shows that the mechanism of bubble formation in the case of top submerged orifice is a three step process. In the first step, a spherical cap is formed at the lance opening which reaches to a hemispherical shape and the point of attachment moves away from the orifice diameter. Thus, the bubble size is governed by the lance inner diameter. Further, due to local imbalance, bubble prefers to grow outward at one side of the lance and begins to slip past the outer diameter. It clings to the lance before it becomes unstable leading to detachment. Here the intermediate portion between the inner and outer diameters of the lance governs the maximum stable bubble size. This is because, for a given system, there are many stable contact angles and the larger the thickness, the more time is taken to achieve the maximum bubble size. Once the maximum bubble pressure is attained, the bubble formation process is controlled by the outer diameter of the lance. Thus, the larger the lance diameter, the better is the control on the detachment stage. The typical sequence of bubble formation at top submerged orifice is shown in Figure 9B. The entire process of detachment is dynamic since once the maximum pressure of the bubble at the inner diameter has been reached, the bubble is in a quasi-steady state, which continually moves toward a new equilibrium position until outer lance diameter is unable to keep the growing bubble stable. When compared with the experimental data, the model showed a slight difference in the predictions because the increase in bubble volume due to excess chamber pressure adds to the volume of the bubble at the detachment stage, which was not taken into account in the model.

2.4. Model for Formation of Non-spherical Bubbles. In most of the realistic cases, the bubbles that are formed at the orifice are nonspherical. The reasons are mainly the surrounding flows. A few attempts appear in the literature[11,19,23,84] to understand the mechanism of nonspherical bubble formation. In this subsection, we have discussed the model by Terasaka and Tsuge,[11] while the other attempts are discussed elsewhere in appropriate subsections.

Nonspherical Bubble formation under constant flow conditions is studied by Terasaka and Tsuge,[11] and a model based on the following assumptions was developed: (i) The gas flow rate into the bubble through an orifice or a nozzle is constant. (ii) Liquid surrounding the bubble is at rest. (iii) Bubble shape is symmetrical about the vertical axis. (iv) Bubble motion is not affected by the presence of other bubbles.

The bubble surface was divided into '*n*' elements, and for every element, two equations of motion, in radial and vertical directions, are solved to give its radial and axial velocities. Then, the positions of the elements are determined. Pressure change in the bubble can be obtained by the application of energy balance and the ideal gas law for adiabatic expansion of gas bubble as

$$\frac{dP_B}{dt} = \frac{P_B}{V_B}\left(Q_G - \frac{dV_B}{dt}\right) \tag{39}$$

Further, equivalent radii (R_E) are found out using two-dimensional symmetric elements, and R' is the radius of the elemental circle, then

$$\frac{1}{R_E} = \frac{1}{2}\left(\frac{1}{R} + \frac{1}{R'}\right) \tag{40}$$

Pressure balance on the gas liquid interface is taken on any element 'j' at which bubble radius is R, then a modified Rayleigh equation (the force balance) was used as

$$P_B - P_H = \rho_L\left[R\frac{d^2R^2}{dt^2} + \frac{3}{2}\left(\frac{dR}{dt}\right)^2\right] + 2\frac{\sigma}{RE} + \frac{4\mu_L dR}{R}dt - \frac{1}{2}\rho_G\left(\frac{4Q_G\cos\theta}{\pi {d_i}^2}\right) \tag{41}$$

Now, introducing the equation of motion of a rising bubble, which is again a force balance, we get

$$\frac{d}{dt}\left(M'\frac{dz}{dt}\right) = (\rho_L - \rho_G)V_B g - \frac{1}{2}C_D\rho_L\left(\frac{dz}{dt}\right)^2\frac{\pi d_M^2}{4} + 4\rho_G\frac{Q_G^2}{\pi}d_i^2 \tag{42}$$

To solve these two differential equations, a procedure was followed to get the volume of the bubble in both the stages of bubble formation as follows: (i) Determine the initial bubble pressure. (ii) Calculate P_B at any time '*t*' using the first equation. (iii) At any element on the bubble surface, evaluate R and R' from the geometry and calculate R_E by the second equation. (iv) Evaluate the radial acceleration and velocity of the bubble surface by solving the equation of pressure balance between the inside and the outside the bubble surface using third equation. (v) Evaluate the vertical acceleration and velocity of the bubble by solving the equation of motion of the rising bubble by fourth equation. (vi) Convergence of these calculations occurs on closing of the calculated bubble neck. This novel procedure to evaluate non-spherical bubble formation deals with the sequence right from the beginning up to the detachment. As mentioned previously, other attempts in this direction are explained elsewhere in this Review.

2.5. Mechanism of Bubble Formation in Flowing Liquids. Sieve plates in distillation columns, orifices on the moving blades of gas inducing impellers, spargers in up-flow and down flow bubble columns, air-lift reactors, fermentation systems and the ring sparger in the stirred tank are a few examples of the bubble formation where liquid is also in motion. In general, these situations are complicated, and the mechanism of the bubble formation is slightly different than in the stagnant liquid. The motion of liquid phase has an important effect on bubble formation. In the co-current and the cross-current flows, the drag force developed by the liquid flow results in an early detachment of the bubble, and hence, the bubble sizes are smaller. As an effect, these small-sized bubbles, being more in number, result in a dispersion with narrow bubble size distribution and high void fraction. Hence, in addition to the parameters, which affect the bubble sizes in stagnant liquid, here, the liquid velocity and direction of flow are also important. In this section, we have critically discussed the effect of liquid flow on mechanisms of bubble formation, various existing models and a comparison in their approaches toward development of a model has been given based on their results. On the basis of the direction of the flow with respect to the gas flow, this subsection is divided into three parts as co-current flow, counter current flow, and cross-flow.

2.5.1. Co-Current Flow. In co-current flow for the bottom submerged orifice or the sieve plates, the detachment of the bubble occurs at an earlier stage as compared to the other two flows because, the resultant force due to liquid flow and the buoyancy is more dominant. Many investigators have modeled this phenomenon by force balance at the orifice, and here, we briefly discuss a few of these models. Chuang and Goldschmidt[85] have developed one stage model based on the force balance at the orifice (0.0136 and 0.0481 mm i.d.) under constant gas flow conditions. Their experimental observations show that the bubble volumes do not depend on the gas flow rate for liquid flow velocities higher than 0.303 m/s in the experimental conditions. Considering all the forces explained in the model by Kumar[86] and also the momentum applied due to the liquid motion, the force balance can be given as

$$0.5\frac{d}{dt}\left(\bar{m}\frac{ds}{dt}\right) = \frac{\pi\rho_L {d_B}^3}{6} + \frac{C_D\pi\rho_L({d_B}^2 - {d_i}^2)}{4}\left(\frac{\rho_L}{2}\left(V_L - \frac{d_B f_B}{6}\right) - \pi d_i\sigma\right) \tag{43}$$

where V_L and f_B are the liquid flow velocity and the bubble formation frequency. This equation can be solved with suitable boundary condition at the orifice to get the final bubble volume. The predictions from this model deviate from the experimental observations mainly due to the fact that, for such small sized orifices, the bubble sizes are also small and hence the buoyancy has negligible contribution, while inertial forces and the liquid flow were dominant. Hence to overcome this difference, later, few investigators have introduced the two-stage model in bubble formation for the same situation. Sada et al.[87] studied the phenomenon using stroboscopic methods and observed that, at any gas flow rate, the bubble size decreased with increasing superficial liquid velocity. A simple force balance approach was followed to develop a relationship between bubble volume and flow regimes using Froude number. This model was further modified by Takahashi et al.[88] by considering the process to be of two stages and all equations are solved using boundary conditions depending upon the liquid flow direction. Since the contribution during detachment was also taken into account the results obtained after modification were found to match very well with the experimental bubble sizes.

Since the experimental observations clearly indicate that the bubble shapes under the liquid flow condition

deviated from the spherical ones, Terasaka et al.[13] developed a model for *nonspherical bubble formation in co-currently upward flowing liquid*. Initially, equivalent radius of bubble is obtained by dividing the surface of nonspherical bubble in various elements. Further, pressure balance is taken over the surface by applying Bernoulli's equation as

$$P_B - P_H = \rho_L\left[R\frac{d^2R}{dt^2} + \frac{3}{2}\left(\frac{dR}{dt}\right)^2 + \frac{V_L^2}{2}\right] + \frac{2\sigma}{R} + \frac{4\mu_L}{R}\frac{dR}{dt} \quad (44)$$

where P_B, P_H, ρ, σ, μ, and V_L are the pressure in bubble, static liquid pressure at any element, liquid density, surface tension, viscosity, and liquid velocity, respectively. In the second stage, when the growth of the bubble is included and the center of the bubble is considered to go away from the orifice surface in the form of equation of motion as

$$\frac{d}{dt}\left[\bar{m}\frac{dz}{dt}\right] = (\rho_L - \rho_G)V_B - \pi d_i\sigma - \frac{1}{2}C_D\rho_L\left[\frac{dz}{dt}\right]^2\frac{\pi d_M^2}{4} + \frac{4\rho_G Q_o^2}{\pi {d_i}^2} \quad (45)$$

where $\bar{m}$, V_B, D_M, D_i, Q_O are virtual mass, bubble volume, maximum horizontal bubble diameter, orifice inner diameter, and gas flow rate through an orifice respectively and C_D is the drag coefficient. Further, since the elements on the bubble surface undergo motion to follow the changes in shape of bubble, under the assumption of axisymmetric expansion, the mean expansion velocity of each element was defined in terms of the reference angle between the normal axis to bubble surface at the edge of the nozzle and bubble volume. This expansion velocity along with the liquid velocity and the apparent rise velocity together give the absolute rise velocity. Since V_C and P_C fluctuations have noticeable effects on the bubble size, the pressure fluctuations in chamber are taken into account along with the pressure drop across the nozzle (which depends on the type of nozzle) to obtain an overall pressure balance in the system. The volume of the bubble was obtained by solving all the pressure balance equations simultaneously using finite difference method. The results from numerical solution for the effect of the liquid velocity, gas velocity on bubble volume and shape were compared with the experimental observations and the model was found to give excellent match for both the spherical as well as the nonspherical bubbles.

2.5.2. Counter-Current Flow. The bubble formation at an orifice in counter current flow of the liquid is a common phenomenon in distillation operations and also in the counter current bubble column operations. In this case, for a bubble to form, the pressure drop across the orifice should be much larger to overcome the hydrostatic pressure force and the liquid force acting downward together. Also the shape of the bubble no longer remains spherical, as it expands against the liquid force and it starts to be an ellipsoid so that the resistance to the opposing forces is minimized. The theoretical model for this type of bubble formation is similar to that of the co-current except that sign of forces will change since the direction of liquid flow acting on bubble surface is changed. For the quantified difference in various liquid flow conditions, readers may refer to Takahashi et al.[88]

2.5.3. Cross-Flow. As mentioned previously, the motion of liquid in the traverse horizontal direction is very common in the case of flow-over sieve plates, distillation trays, air-loop reactor and in a sparged stirred tank where the liquid flow is largely due to impeller motion. In the case of relative liquid motion, two effects are observed prominently. (i) The drag force by the liquid flow results in early bubble detachment and hence smaller bubbles resulting into the enhancement of gas−liquid interfacial area and improved boundary layer transport causing higher k_La. (ii) Bubble coalescence is prevented because of liquid motion, and thus bubble sizes are controlled. Maier[89] was among the first to demonstrate that the shear force experienced by a growing bubble in a flowing liquids causes its early detachment and it is at a maximum when the liquid has an exact cross-flow with respect to the nozzle axis. Stich and Barr[90] studied this phenomenon experimentally and proposed an empirical correlation for the final bubble size. Sullivan and Hardy,[91] systematically analyzed the phenomena through a semiempirical model based on expansion, vertical displacement, horizontal displacement of the spherical shaped bubbles and finally correlated the bubble volumes to *Re* and *Fr*. Other studies in this most realistic case are by Kawase and Ulbrecht,[92] Morgenstern and Mersmann,[93] Wace et al.,[94] Marshall et al.,[76] Forrester and Rielly[81] and the most recent being Zhang and Tan.[27] Most of these studies are based on the spherical shapes of bubbles, whereas a recent analysis by Tan et al.[23] discusses the complex case of the nonspherical bubble formation in liquid cross-flow. Here we discuss a few of these models developed specifically for the case of liquid cross-flow.

Model by Marshall et al.[76] for bubble formation in the cross-flow is based on many assumptions. Although these assumptions are far from reality, they may be accepted for gross simplification of physical reality to develop a relevant model. The actual assumptions can be seen from the assumption numbers given in Table 3 as listed in Table 2. In the studies, they tried to transform the experimental results into the model by potential flow theory. In the case of the uniform stream condition, bubble slides over the orifice plate and it resembles the situation like a flow past sphere in the liquid. Since the knowledge of the velocity potential enables the liquid pressure on the surface of the sphere to be determined from the unsteady form of Bernoulli's equation, we get

$$\frac{\Delta P}{\rho} = \frac{P - P_\infty}{\rho} = \frac{\partial\Phi}{\partial t} - 0.5|V_L|^2 \quad (46)$$

where P is the pressure on the sphere surface and P_∞ is the hydrostatic pressure of the undisturbed liquid. Since by the first assumption liquid pressure on the bubble surface is uniform, it can be given as

$$\frac{\Delta p}{\rho} = \frac{P - P_\infty}{\rho} = \frac{1}{4\pi R^2} \times \int_0^{2x}\int_0^{x}\frac{\Delta P}{\rho}R^2 \sin\alpha\, d\alpha\, d\psi \quad (47)$$

The radius of the bubble can be calculated using the normal procedure of applying the equation of motion for the system under consideration and considering the virtual mass of the system. The virtual mass coefficient was obtained from the potential flow solution by considering the kinetic energy of the liquid and then the Lagrangian equation of motion was considered. To get

the Reynolds number for the system, the drag coefficient was calculated. Knowing the liquid and bubble velocities and the orifice radius, bubble radius can be easily calculated.

$$R_B = 0.48 R_o^{0.826} (V_G/V_L)^{0.36} \quad (48)$$

where V_G is the superficial gas velocity given by $V_G = Q_i/\pi R_o^2$. Further modification yields

$$U_B = 0.375 \frac{C_D (V_L - U_b)^2}{\bar{m} R} \quad (49)$$

Thus, knowing the average bubble rise velocity and other parameters, bubble size can be estimated. These investigators have reported that the chamber pressure fluctuations do not significantly affect the bubble size in cross-flow situation. Although the authors could observe that the initial stages of bubble formation and also the detachment by neck closure both are dynamical, it was not considered while formulating the model.

Sullivan and Hardy[68] assumed that bubble formation has three sequential steps and the first two steps are the expansion and translation of bubble along the liquid flow while the third is that of detachment from the position of adherence. To model this condition (i) the force balance was taken in the vertical direction, (ii) Newton's law of motion was applied assuming the forces to be in horizontal direction, and finally, (iii) the equations are solved at specific boundary conditions to get the volume of the bubble. Further, Takahashi et al.[88] modified the two-stage model by considering that the formation occurs at an inclination of angle θ to the vertical line. Their force balance gave the bubble volume in terms of very low and very high velocities as

$$V_B = V_1(1 - e^{\zeta}) + V_2 e^{\zeta}, \text{ where } \zeta = -a'/U_1^b \quad (50)$$

and $a' = 1$, $b = 0.242$ are obtained experimentally.

Tsuge et al.[95] studied this phenomenon under the varying gas pressure conditions in the chamber using generalized Bernoulli's equation in terms of velocity potential. The pressure equation was solved numerically to get a simplified inequality

$$S \geq [R + (1 - 0.02U_1)D_i]\,[1 - (C_D \rho_1 U_i^2 R^2/2d_i\sigma)]^{0.5} \quad (51)$$

which gives the minimum distance (S) between the center of the bubble and orifice at the final condition of detachment. U_i is the velocity of the growing surface at time t.

Recently, Tan et al.[23] proposed a model for nonspherical bubble formation in cross-flow condition by interfacial element approach. Initially, force balance is taken over each surface element to obtain a set of differential equations of motion in cylindrical coordinates as

$$r\Delta P \mathrm{d}r - \sigma \mathrm{d}(r \sin\beta) = \frac{\mathrm{d}}{\mathrm{d}t}(U_z \bar{m})$$

$$r\Delta P \mathrm{d}z + \sigma\left[\mathrm{d}(r\cos\beta) - \frac{\mathrm{d}z}{\sin\beta}\right] = \frac{\mathrm{d}}{\mathrm{d}t}(U_r \bar{m}) \quad (52)$$

where r and z are the radial coordinate from the axis of the bubble and the axial coordinate from the orifice horizontal level, respectively, ΔP is the pressure difference between the bubble and the liquid pressure at each element, β is the angle defined as $\beta = \tan^{-1}(\partial z/\partial r)$and $\bar{m} = (0.6875\rho_L + \rho_G)V_B$ is the virtual mass. For the solution of this problem, equations of mass balance at bubble, chamber and the orifice are required.

(i) The equation for the mass balance on the chamber is given as

$$V_C \frac{\mathrm{d}\rho_C}{\mathrm{d}t} = \rho_a Q - \rho_C q \quad (53)$$

(ii) The pressure equation on the chamber is given as

$$V_C \frac{\mathrm{d}P_C}{\mathrm{d}t} = \gamma(P_a Q - P_C q) \quad (54)$$

(iii) The equation for gas in the bubble and the chamber is given as

$$V_B \frac{\mathrm{d}P_B}{\mathrm{d}t} + \gamma P_b \frac{\mathrm{d}V_B}{\mathrm{d}t} = \gamma P_C q + (\gamma - 1)\frac{\rho_C q^3}{2a_O^2} \quad (55)$$

where, V_B is the bubble volume, γ is the adiabatic gas constant, and a_O is the cross-sectional area of the orifice.

(iv) Finally, the orifice equation is given as follows

$$q = C\pi R_O^2 \left[\frac{P_C - P_B}{\rho_C}\right]^{0.5} \quad (56)$$

where C is the orifice constant. The inclination in the angle of a growing bubble due to liquid cross-flow (V_L) was obtained as $\omega = \tan^{-1}(V_L V_B/QR_B)$, where R_B is the equivalent radius of nonspherical bubble. Virtual bubble coordinate system along with the stationary axisymmetry was used to find the stagnation point θ, which indicates the outermost point of attack. Equations 53–56 were solved simultaneously for discerning the development of bubble growth in liquid cross-flow condition. The results from the simulations showed that the bubble growth begins immediately in a flowing liquid when compared with the stagnant liquid, and they are smaller. The comparison of the predictions with the experiments by Marshall[96] showed a reasonable match. The simulations showed a difference in the mechanism at higher flow rates where the bubbles stick to the plate of orifice during its growth and thus delay the detachment of simulated bubbles.

In a different situation of bubble formation accompanied with weeping at the submerged orifice with a liquid cross-flow, Zhang and Tan[27] have used potential theory to describe the pressure field around a bubble. The bubble growth is assumed to be the same as in the case of stagnant liquid followed by a displacement and rotation before it gets detached. The liquid head is assumed to be high and has no effect on weeping and bubbling, which are supposed to be occurring alternately. Their differential equation for the camber fluctuations is same as in the quiescent liquid, while the orifice equation is given in terms of the growth rate and pressure difference (Miyahara and Takahashi[97]) as

$$\frac{\mathrm{d}V_B}{\mathrm{d}t} = \pi R_o^2 \sqrt{2/\rho_G C_G}(P_C - P_a)^{0.5} \quad (57)$$

The generalized Bernoulli equation is used for the determination of liquid pressure at different positions (r, θ) and procedure from Tsuge et al.[98] is followed to derive the velocity potential, which can be used for the

estimation of local absolute velocity. The forces acting on a bubble in the vertical and transverse directions are modeled separately under the assumption of no slip. The bubble detachment criteria is based on the angle achieved during rotation of bubble such that if the distance from the bubble center to the orifice center is x, then a bubble would detach if $x \geq R + (1-0.02V_L)d_h$. In addition to this, the condition of weeping is dependent on the instantaneous pressure fluctuations in the chamber and hence the dynamics of this pressure fluctuation can be modeled from the gas flow equation in terms of differential pressure followed by the integration over the weeping period. Their results are seen to match very well with their own experiments and the pressure cycles are analogous to the published literature. An interesting observation is the adaptation of sequential process of growth, displacement and rotation, which may not be realistic, as in reality, these processes overlap to some extent.

More recently, Loubière et al.[32] studied the impact of the liquid cross-flow on the bubble generation at the flexible orifice made out of a rubber membrane through force balance in two different directions and also by stroboscopic method. Their observations have clearly proved that the liquid velocity has a strong impact on bubble formation such that (i) the bubbles of significantly smaller sizes are generated at higher formation frequencies and (ii) the bubble coalescence and the likelihood of breakage during their ascent in the system. The following important observations are reported: (i) during its growth, the bubble moves downstream and is flattened due to effect of the liquid motion; (ii) except for the first moments, the bubble inclination angle remains roughly constant during the bubble growth; it depends only on the liquid velocity and can be calculated, (iii) as under quiescent liquid conditions, the bubble volume varies linearly with the growth time, (iv) the bubble formation at a flexible orifice is a continuous phenomenon, (v) as under quiescent liquid conditions, the bubble spreads over the orifice surface during its growth; the bubble advancing contact angle is larger than the receding one, (vi) drag force due to the liquid cross-flow is responsible for the bubble detachment and not the buoyancy force.

The above discussion and force balance based models clearly indicate that, although this approach is simple, it is not very easy to incorporate all of the dynamical features of the phenomenon for the accurate prediction of bubble size. However, the use of surface disintegration followed by the application of finite elements or potential flow based approaches seems to be robust even for the case of nonspherical bubbles.

2.6. Bubble Formation under Reduced Gravity Condition. During the process of bubble formation, the surface forces due to pressure difference between the gas in the bubble and the liquid and the line forces are due to surface tension. For a static interface, these forces are in equilibrium but in the process of dynamic formation, the resultant of these forces is equal to the rate of change in the liquid momentum assuming the gas phase momentum is negligible. As it can be clearly seen from the earlier discussion in this review, the process of bubble formation is grossly made up of two stages, the expansion/growth of bubble (when surface forces are dominant) and the detachment (when buoyancy force is dominant and hence important). For very small bubbles, buoyancy is very small and the larger the bubble, the greater is the buoyancy resulting in nonideal liquid flow in its vicinity, which even induces a liquid motion in its vicinity and thus helps in severance of the neck. Hence, in order to understand the exact contribution of the buoyant forces in the process of bubble formation, it is required to physically eliminate the forces acting in the downward direction. In view of this, recently, many studies are being carried out[55,78,79,99−103] under the condition of reduced gravity. Additionally, the effect of individual component forces in the force balance equations by changing either viscosity or surface tension or flow rate of gas or liquid individually can also be seen when gravity has no role to play in the overall mechanism. These types of analyses are important since the gas liquid systems are commonly observed in propulsion, power generation, storage and life supporting systems in the space.

To understand the bubble formation in the reduced gravity condition, in one of the first attempts, Pamperin and Rath[78] observed only two regimes of bubble formation i.e., with and without bubble detachment. They defined the detachment criteria on the basis of value of *We*. Their stroboscopic observations showed that the bubbles formed at all the gas flow rates were spherical in shape. Their force balance was based on the assumption of immediate detachment of bubble from the orifice. Their observations showed that the bubble sizes in the absence of buoyancy are directly proportional to the orifice diameter to the power S, such that $0.33 < S < 1$. Also, the bubble that already detached least affects the bubbles getting formed at the orifice due to the small level of turbulence developed in the liquid due to small sizes of bubbles, thus eliminating the idea of primary and secondary bubbles.

2.6.1. Models for Bubble Formation. 2.6.1.1. Nonspherical Bubble Formation Model (Tsuge et al.[10]). The phenomenon of bubble formation, where the liquid flow was considered as an external force was carefully analyzed by Tsuge et al.[9,10] under the hypothesis that the liquid flow causes the bubbles to take a definite shape. The procedure followed for the theoretical development of model was based on the concept of nonspherical bubble formation model by dividing the bubble surface into several elements. The force balance in the reduced gravity condition can be given as

$$\frac{\mathrm{d}}{\mathrm{d}t}\left(\bar{m}\frac{\mathrm{d}z}{\mathrm{d}t}\right) = \Delta\rho V_B - 0.5C_D\rho_L\left(\frac{\mathrm{d}z}{\mathrm{d}t}\right)^2 \times \frac{\pi(d_M^2 - d_h^2)}{4} + \frac{4\rho_G Q_o|Q_o|}{\pi d_h^2} \quad (58)$$

where $\bar{m}$ is the virtual mass of the bubble, and d_M is the maximum vertical bubble diameter of the bubble. Using Reynolds number it is easy to obtain the velocity of the element on bubble surface which gives the horizontal distance covered by the bubble in certain time and this in turn gives the radius of the bubble at any time if the bubble contact angle with the orifice is known. This can be solved numerically only if initial conditions are known. They observed that when the liquid flow was co-current the bubble growth rate increases with an increase in the gas flow rate. Under constant flow condition the bubble volume increases in proportion to the bubble growth time. In the case of counter current flow the bubble growth rate increases with increasing gas flow rate and the bubble grows

under constant flow conditions. During the experiments, it was observed that the bubble did not grow symmetrically about the horizontal axis so that the bubbles turn away and detach from the nozzle earlier. In cross current flow, bubbles are formed at regular intervals. Bubble shape changes from spherical to nonspherical due to the bubble movement and expansion by the flowing liquid. But the model developed by them could not give results in coordination with that of the experimental results. It was also observed that bubble volume was the smallest among all due to regular detachment of bubbles from the nozzle.

2.6.1.2. Two Stage Bubble Formation Model. Buyevich and Webbon[79] have discussed the effect of gravity on bubble detachment through a two stage bubble formation model. The model assumes the bubble to maintain spherical shape throughout the process. The simulations from their model showed that the duration of expansion in normal gravity condition is independent of the gas flow rate whereas, the final bubble volume is roughly proportional to it. However, in reduced gravity conditions, expansion time is inversely proportional to the gas flow rate and expansion volume is independent of it indicating the static regime of bubble formation, where the bubble size is only a function of orifice radius and the density difference. In the case of constant pressure condition, the authors have reported a different kind of mechanism of bubble formation with modifications in the dependencies of bubble size on orifice radius and gas density. Their results to understand the effect of higher and lower gravity have shown that the bubble volume continuously increases at low gravity with slow lengthening in the neck. This happens mainly because at low gravity, the force due to injection of gas into bubble is the only force which pushes the bubble upward and the momentum arising out of it is weak and compensated by the inertial forces arising out of increasing bubble volumes. At high gravity, the bubble volume increases with very rapid lengthening of neck leading to instant detachment. The most important feature of this work is a careful, universal analysis of forces experienced by the growing bubble. Since there is a discrepancy in the conditions at which the model is formulated and analysis of experimental results, the model is still not validated by experimental results but the interpretations from the results are physically relevant to the process of bubble formation. Although the model seems to have taken care of all the possible conditions, the classification of gravity level is not clear as they mention low, reduced and high gravity in the paper and in the absence of experimental data at reduced gravity, the comparison was done only under normal gravity.

2.6.1.3. Mechanism of Bubble Formation in Quiescent Liquids. In another similar investigation, Tsuge et al.[9] analyzed the bubble formation mechanism under microgravity conditions. Similar to the earlier model developed by Terasaka and Tsuge[104] for nonspherical bubbles assuming the behavior of gas in the chamber is to be polytropic and the formulation and solution procedures are similar to their earlier work. The experimental system, which was used for the validation of model consisted of three liquids of different properties, and the nozzle was top submerged. They found out that volume of bubble is proportional to the inverse of gravitational acceleration for a small gas flow rate when other conditions are the same. The experimental observations showed that the bubble growth rate increase with the gas flow rate and the bubbles do not detach from the nozzles during the 10 s under low gravity in low gas flow rates. They estimated bubble volume as

$$V_B = \frac{\pi d_h \sigma}{\rho_L g} \tag{59}$$

Bubble formation time increases with a decrease in the gas flow rate and gravity level resulting in increase in bubble volume when bubble detaches from the nozzle. Similarly, when the ratio of gravitational acceleration to the terrestrial gravitational acceleration is equal to 0.001, bubbles do not detach from the nozzle under constant flow conditions. The predictions from their model are seen to be very good on comparison with their experimental results and that by Pamperin and Rath.[78]

To adequately disperse bubbles in liquids for mass transfer or chemical reaction processes at relatively low gas flow rates under reduced gravity, it becomes necessary to force bubbles to get detached from nozzles by external forces such as liquid flows. Such an analysis has been carried out by Tsuge et al.[10] The same model as above was also used for external forces acting on bubble in the form of liquid flow in reduced gravity condition. The investigators studied the variation in bubble formation mechanism under the conditions of co-current, counter-current and cross-current flow of liquid. In the co-current flow situation, the predicted bubble detachment volumes were found to increase with the gas flow rate. They observed that in the case of constant flow conditions, in the counter-current liquid flow situation the bubble growth rate increased with liquid flow rate and the growth was asymmetric. In crosscurrent flows, bubbles were formed regularly with irregular shapes, and bubble volumes were the smallest among all the flow conditions due to early detachment of the same.

Similar analysis was done by Nahara and Kamotami[103] who observed that the effect of liquid flow is more when the experiments are carried out in reduced gravity conditions. Their investigation involved the analysis based on force balance, where the main forces that were taken into account were the buoyancy, surface tension, momentum flux of the gas, liquid drag in two orthogonal directions, liquid inertia in two orthogonal directions, and shear-induced lift force due to the liquid cross-flow. At normal gravity conditions, the bubble formation was seen to follow a two stage mechanism, and the liquid velocity was seen to have a low effect on the detachment. Under reduced gravity conditions, in the absence of any neck the formation mechanism is reported to have a single stage with relatively higher bubble sizes even in the presence of liquid cross-flow. In a recent comprehensive attempt by these authors,[103] a two-dimensional model was developed on the basis of global force balance on bubbles evolving from a wall orifice with liquid cross-flow. The analysis is complete in many respects and shows a good comparison match with the experimental data at reduced gravity conditions.

2.7. Bubble Formation in Non-Newtonian Liquid. Similar to the case of bubble formation in Newtonian liquids, bubbles formed in the non-Newtonian liquids follow certain mechanism before they actually detach from the source of generation. The mechanism of generation of a bubble is almost the same until the stage of expansion, but during its detachment, the neck

motion is mainly governed by the rheology of the liquid and the effect of the neck formation induced on the liquid motion. Non-Newtonian liquids that are considered here are structurally viscous liquids[105] and viscoelastic liquids. The characteristic feature of bubbles in non-Newtonian liquids is their larger size than in a Newtonian liquid having the same apparent viscosity[3]. The factors that govern the phenomenon are viscosity, viscoelasticity, gas flow rate, surface tension, chamber volume, the orifice diameter and the complex hydrodynamics of these fluids.

Apart from the parameters discussed in Section (2.1.2) of Newtonian liquids, two more parameters: concentration of liquid and viscous stresses are very much important in non-Newtonian liquids and are interrelated. If the concentration of the viscoelastic liquid increases, then the viscoelastic stresses become large and affect the bubble growth time (defined as the time from the beginning of bubble formation to the detachment of the bubble) by elongating it, and thus the volume of the detached bubble increases. The contribution of the viscous stresses and extensional stresses comes into picture when a bubble undergoes deformation due to the internal stresses. These stresses also affect the growth of the bubble through the characteristic stretch time, which is much smaller than the relaxation time for viscous liquids. At very high concentrations of the viscoelastic liquid the rheological behavior makes the system complicated to predict the bubble behavior during its formation.

2.7.1. Structurally Viscous Liquids. The bubble formation in these liquids is a multistage process and the diameter of the primary bubble steadily increases with augmenting flow rate of gas. The rheological behavior of the liquid exerts a decisive influence on the secondary bubble formation, and thus, the dispersion of the primary bubble is favored by the induced liquid motion and non-Newtonian flow behavior. Thus, more thorough dispersion of the primary bubbles and earlier inception of the jet regime are the two characteristic features of the process of bubble formation in non-Newtonian liquids. Coalescence of two successive bubbles during/immediately after the detachment limited by higher value of viscosity is reached. During the formation of primary bubbles, vigorous motion of the liquid causes deformation of the upper contour of the bubble since stronger inertial forces act on the bubble during the first stage of formation, consequently larger bubbles are formed.

In the case of bubble formation in moving non-Newtonian liquid, the main effect is on the detachment stage. For structurally viscous liquids at low gas velocities the primary bubble diameter does not show any noticeable effect on the change in gas velocities, while the formation of the secondary bubbles is mainly due to the rearrangement of the flow profile at low velocity as an effect of the primary bubble. The neck formed in the second stage is longer than that in the Newtonian liquids and it induces a more pronounced motion of the liquid after severance of the bubble than would be the case in a liquid at rest. Consequently, primary bubbles are more effectively dispersed. As the liquid velocity increases the forced motion of the liquid dominates over the rearrangement of the flow profile, and the neck becomes shorter. Because of the altered rheological behavior in the viscous liquids very high velocities of gas are needed for introducing in jetting regime.

If the motion of the liquid is counter-current to the bubble motion, then the most noticeable effects are on the detachment motion of the bubble and on the liquid motion induced by neck. Slower detachment of the bubble is observed along with a longer neck as compared to that of in the stagnant liquids. Severance of the bubble results in the more vigorous liquid motion induced by neck causing more effective disintegration of the primary bubbles and decrease in the secondary bubble diameter at low liquid velocities. Further, the associated increase in the gas content in the channel no longer permits direct action of the liquid flow on the process of the primary bubble formation, and hence, the primary bubbles again become smaller while the disintegrating effect of the induced liquid motion becomes less pronounced. Many times at higher viscosity of the liquid maximum of the primary bubble diameter and minimum of the secondary bubble diameter are not observed but the diameter of the previous one remains constant with augmenting liquid velocity and disintegrating action of the induced liquid motion steadily decreases.

2.7.2. Viscoelastic Liquids. The flow media, possessing time dependent flow behavior are termed as the viscoelastic liquids and are characterized by viscous behavior and the deformational elasticity. The stress state of the viscoelastic liquid at a given time depends on the previously observed deformation in it. The effect of the formation of the primary bubble is similar to that in the case of the viscous liquids. After the severance of the neck from the capillary orifice, the elements of the liquid are strongly deformed in the direction of motion as a result of the subsequent acceleration of the neck end. This causes a pronounced increase in the elongation viscosity and results into elongational flow in the liquid in the wake. The resistance due to deformation of the liquid elements dominates over the shear viscosity and is perpendicular to the direction of the motion. This rheological behavior causes the subsequent bubble to be elongated as a result of the stronger suction, and even the detachment process is decisively affected. At the start of the secondary bubble formation the effect of the primary bubble still continues. After the induction of liquid motion by the neck, liquid penetrates into the primary bubble and draws a second, which is smaller in size. With increase in the pressure in the primary bubble the neck decelerates and the liquid tends to recover the energy expended resulting in dispersion of the liquid elements. Consequently, the bubbles coalesce because of the increase in the pressure predetermined by the bubble shape, since this pressure cannot be overcome. The decreasing deformation in the neck is compensated by the augmenting deformation of the liquid elements in the annular flow. As compared to the viscous liquids here, no deviation in diameter of the primary bubbles takes place. Much longer bubbles are created in the viscoelastic liquids at equilibrium and this bubble shape persists after their detachment because of the properties of the liquid.

Ghosh and Ulbrecht[106] introduced a three-stage bubble formation model with bubble growth, elongation and a waiting stage. The first two stages correspond to the total formation time of a gas bubble and the last stage is responsible for the lapse time during which pressure builds up in the chamber to form an interface at the orifice. The elongation stage ends when the neck of the bubble breaks off and the bubble detaches. The system

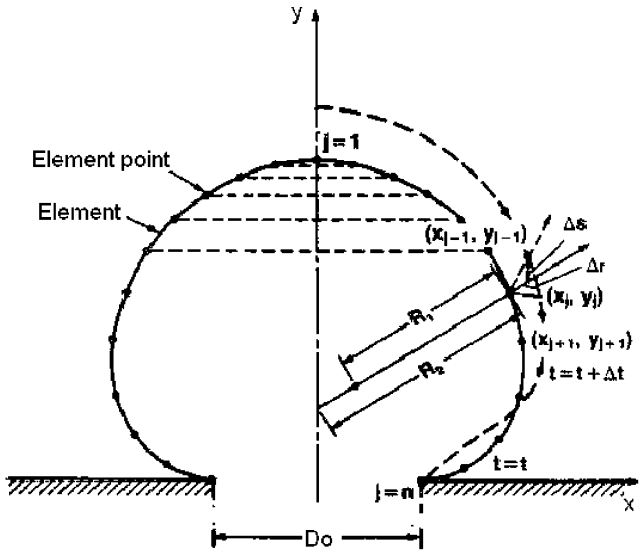

Figure 10. Bubble surface divided in '*N*' grid points at gas-liquid interface. (reproduced with permission of Elsevier from Ghosh and Ulbrecht[106]).

was studied under constant gas flow condition. The theoretical analysis was based on a few assumptions and force balance was taken including terms expressed by L'ecuyer and Murthy[107] for pseudoplastic and viscoelastic liquid

$$P_B + P_G - P_L = \Delta p_\sigma + \Delta p_\mu \qquad (60)$$

The effect of gas motion is found out from stream function corresponding to the circulatory motion of gas inside the bubble, and the pressure distribution due to the gas momentum at the interface. The velocity potential around the bubble is obtained from the summation of different potentials as mentioned in the case of the Newtonian liquids. Since besides the radial expansion of the bubble, vertical translation also occurs, the net upward force due to the vertical component of the liquid pressure becomes positive. To find out the dimensions of bubble its surface is divided in '*N*' grid points (Figure 10). As the bubble starts growing, the new coordinate positions of the grid points on the bubble surface are computed by employing a finite difference procedure for moving boundary. The integral method and truncated cone method are used to estimate the bubble volume, which yielded a good comparison with the experimental results. Also in the case of polymeric liquids, the bubble shape is elongated to its vertical axis even at lower gas flow rates due to complicated stress field around the axisymmetric body in a viscoelastic liquid.

Terasaka and Tsuge[12] studied the formation of bubbles at single orifice in viscoelastic liquid viz. PAA and proposed a model for nonspherical bubble formation. In the model, the bubble surface is divided into a number of elements as in the earlier case, and the flow of gas is considered to be constant. Two equations of motion in the radial and vertical directions are simultaneously solved to calculate the radial and vertical velocities for each element on the bubble surface and the positions of elements are estimated. The convergence was subjected toward the detachment of the bubble. The model is based on the assumptions that the strain in a liquid does not exist at all before bubble growth and bubble grows symmetrically about the vertical axis on the center of orifice. The concept of relaxation time of the bubble was used and it was found out that at high gas flow rates the relaxation time was smaller than the growth time except for the initial period of bubble formation. But in the case of low flow rates, the elasticity influences the bubble growth as well as the initial period because of the temporary decreasing bubble volume at that point. Ghosh and Ulbrecht[106] followed the two-parameter version of the Oldroyd model for bubble formation in viscoelastic liquids, which is convenient to measure the dynamic elasticity and viscosity. From their observations, Terasaka and Tsuge[12] have suggested that for polymeric liquids other than PAA, it is better to follow Maxwell's rheological model rather than Oldroyd's model. For the details about bubble growth in viscous Newtonian and non-Newtonian liquids, readers may refer to Favelukis and Albalak.[108]

2.8. Bubble Formation Accompanied with Weeping at the Submerged Orifice. In the operation of distillation and absorption using sieve trays, weeping through the holes is a significant and most commonly observed problem affecting the performance of the overall operation of the process equipment. In view of this, it is required to understand the mechanism of bubble formation while weeping occurs. Weeping rate can be measured either physically by collecting samples of liquid accumulated in the chamber from time to time or by measuring the pressure fluctuations in the chamber, which represents the transient pressure difference between the liquid at the orifice and the gas chamber. McCann and Prince[109] were the first to study this problem systematically, by following a potential theory based approach to predict the liquid pressure distribution in the wake of bubbles. The understanding developed by these investigators based on the experimental observations is generally used as a basis for developing weeping models; however, the two main assumptions of sphericity and negligible effect of the external orifice diameter on bubble volume deviate the predictions. Kupferberg and Jameson[65] observed that at low gas flow rates, the process of bubble formation follows dumping in the orifice-chamber region and dumping occurs just before the weep point is reached. In the process of dumping, the pressure drop across the liquid above and the orifice chamber is just sufficient to maintain a liquid level above the sparger and thus, any value below it starts weeping. During weeping bubbles are generated very discretely and only large bubbles are formed. Recently, Zhang and Tan[24] have studied this problem very carefully using the first law of thermodynamics and the Bernoulli's equation across the orifice mouth and the potential theory for understanding the surrounding liquid flow. Their predictions showed that wake pressure exerts a back-pressure on the orifice such that while it goes away from the orifice, chamber pressure goes down. The predicted weeping velocity for various gas flow rates show small deviation from the experiments mainly because; the model assumes that the bubble attains its terminal rise velocity immediately after its detachment. Also, the weeping rate is greatly affected by the orifice diameter as well as the chamber volume and hence an optimum combination of the two should be reached to eliminate the weeping condition. Miyahara et al.[110] have also studied the phenomena in greater detail. Byakova et al.[33] have reported experimental results of the surface phenomena effect on bubble formation from a single orifice (1 mm diameter)

submerged in water with extremely small gas flow rate (2 cm^3/min). Bubble formation was studied for a wide range of contact angles (68°−110°) at liquid-orifice plate-gas interface using key geometrical parameters of a bubble: volume (V_B), surface area (S), radius at the tip (R_0) and the dimension of bubble periphery at the base (d_h). The formation was observed to occur in four stages: (1) nucleation period, (2) under critical growth, (3) critical growth, and (4) necking. It was determined that bubble volume essentially depends on wettability. With severing wetting conditions (e.g., equilibrium contact angle increases from 68° to 110°) the bubble size was reported to increase at the same gas flow rate.

2.9. Bubble Formation at Perforated Plates and Sieve Trays Submerged in Liquid. In the case of bubble formation under submerged multi-orifice systems such as sieve plates and perforated plates although the applicability is wide, very less attention has been given mainly because, a number of bubbles are generated simultaneously and the system is much more complex than the single submerged orifice. In such a case, bubbles are not spherical because (i) the pressure drop across each hole is not the same resulting in the stratification of the liquid in its vicinity causing distortion of shapes, and (ii) during its expansion, bubble adheres to the plate surface deviating its shape from the spherical ones. Also the formation of a bubble is a hindered process and the hindrance needs to be included in the models in terms of number of bubbles formed simultaneously, pitch of holes and distance between sieve plates and the hole-gas velocity.

Mechanism of bubble formation is same as that from single orifice but the bubble generation from each orifice or perforation occurs at different time and also its mode of detachment, and hence, the overall mechanism of bubble formation on sieve trays is different from a single orifice. Generally, bubble formation under sieve plates is considered to have two different mechanisms. In the first mechanism, as in the case of single orifice, bubbles are generated under low gas velocities such that every single bubble is detached individually while in the second, bubbles are formed as a consequence of jet break-up, where a fine dispersion is seen. Most of the time, in operating bubble columns, the gas is supplied for achieving jetting regime, which leads to bubble formation due to jet break-up. In such a case instead of the bubble sizes, the bubble size distributions are predicted and used in design of the system. As mentioned previously, at low gas velocities, individual bubbles are formed at each orifice on a sieve plate sparger. Most of the bubbles are of the same size. With increase in the superficial gas velocity, depending upon the chamber volume, a pressure drop profile is generated inside the chamber, and it achieves a dynamic nature. As a result, the formation of bubbles at the sieve plate occurs dynamically and varies in space. This leads to turbulence in the sparger zone. At even higher gas velocities, each hole acts as an independent orifice and leads to jetting. The state of the different holes on the sparger at any instant can be in the range of blocked orifice (time gap between two bubbling/jetting cycles) to completely open orifice (jetting). However, depending upon the chamber volume, static liquid height above the sparger and the gas velocity, the duration for this phenomena and its dynamics can vary. On the other hand, with a porous plate with very fine holes ($20\ \mu < d_h < 200\ \mu$), the pressure drop across the sparger is extremely high and this leads to equal bubbling from all the orifices in time. Subsequently, continuous production of the tiny bubbles results in froth formation above the sparger with very narrow bubble size distribution in the sparger region. This happens at relatively higher gas velocities, while at lower gas velocities, depending upon the properties of the liquid, bubbles coalesce right above the sparger and thus result in normal bubbly flow. The important difference between the two spargers is the formation of froth (porous sparger) and jetting (sieve plate). Here, we have compiled the significant observations of many investigators.

2.9.1. Observations of Bubble Formation at Multi-Point Sparger. Houghton et al.[111] were the first to estimate the bubble sizes produced from porous plates in different liquids using the hold-up and gas flow rate. Mersmann[112] was among the first few investigators to experimentally study the bubble formation on sieve plates and perforated plates and outline the difference from the single orifice mechanism. Later in due course many investigators (Kumar and Kuloor,[17] Miyahara and co-workers,[113−115] Koide,[116,117] and Schwarzer et al.[118]) made attempts to propose various mechanisms of bubble formation under submerged sieve trays and perforated plates including the effect of various physical parameters that affect the bubble formation. Until now, all of them have tried to validate their theoretical model with experimental observations, and thus, we have a number of correlations, which give bubble diameter or volume with certain limitations.

As we shift from single orifice to multi-orifice condition the complexity in the system increases and the experimentally observed bubble dimensions deviate from that of theoretical. McCann and Prince[119] developed a bubble interaction model to predict bubble frequencies placed in a line of five orifices with 2.3 cm spacing. They have reported that bubble frequency depends on the total chamber volume however; the interaction model did not appear to be applicable to other orifice configurations. As discussed previously, for the case of a single orifice bubbling, the effect of chamber volume pressure fluctuations is significant on deciding the bubbling frequency as well as the bubble volume to some extent, with an increase in orifice number this effect decreases and finally vanishes when the orifice number is more than 15.[120] Many authors have tried to calculate the bubble diameter in terms of Sauter mean diameter, equivalent spherical diameter and volumetric mean diameter. Mersmann[120] has recommended that for bubble formation at sieve plates for a complete flow, Weber number $We > 2$. Miyahara and Hayashino[115] analyzed the process considering nonspherical shape of bubble and volumetric mean diameter was found out theoretically assuming logarithmic bubble size distribution. Li et al.[121] studied the same phenomenon using a narrow slot by producing bubbles simultaneously from the closely spaced slots. Southern and Wraith[122] and Li and Harris[123] have shown that bubbles are formed continuously at a series of spontaneous sources distributed on a slot length and each source acts like a self-contained, self-regulating nozzle. The number of sources on slot and size of bubbles they produce vary with gas flow rate and the width of the slot opening and many small bubbles are generated at low flow rate. Ruzicka et al.[124,125] investigated bubble formation at two orifices and identified two types of bubbling modes through the analysis of pressure fluctuations in the gas

chamber. On increasing the orifice number to 13, more types of bubbling modes were identified based on various plate configurations.

Since the forces acting on a bubble in multipoint spargers or a multi-orifice configuration are slightly different from the single orifice, to understand this complex phenomenon, it is required to compare the available theoretical models for its mechanism.

2.9.2. Mechanism of Bubble Formation on Multi-Orifice Systems. As mentioned previously, bubble formation on multi-orifice systems takes place in two modes, chain bubbling and the dispersion due to jet breakage. The geometry of the hole affects the shape of resulting bubble by virtue of contact angle. In the majority of literature, Mersmann's analogy[120] of successive hole occupation in sieve trays is followed to derive a theoretical model and in most of the efforts, the results obtained from single hole orifice can be extended towards sieve plates. According to this analogy, gas first passes through a single hole and then it goes to the next until the first hole attains jet regime. In the bubbling regime, bubbles are of a constant size. Before studying the various available mechanisms, it is essential to note that in a bubble column, four different regimes viz. bubbling, froth, cellular foam, and jetting are observed as a result of bubble generation at submerged sieve and perforated plates at various gas flow rates.

Similar to that of the single submerged orifice, the mechanism here can also be understood through the force balance, which includes surface tension force, pressure force, viscous force, drag force, gravity and two more features in the column i.e., liquid circulation and liquid turbulence influence the bubble formation. On porous plates with small holes, small bubbles are formed and gas momentum is too small to cause any gas density influence on the bubble formation size. Average bubble size depends on the bubble size at the sparger hole. The mechanism of bubble formation is considered to take place in two or more stages. Neck formation at the tray hole takes place in very small span and especially in this case, due to high gas velocity, the momentum is imparted by primary bubbles onto secondary and the surrounding liquid motion is high. This momentum is not only because of the effect of earlier bubble but also because of liquid motion due to bubbles generating from surrounding holes. As a result of these forces, shape of bubble under formation no longer remains spherical and changes to ellipsoidal and then to spherical cap (depending on the liquid properties) as it goes away from sieve tray holes and experiences coalescence/dispersion. In the process of bubble formation by jet breaking,[36] the level at which bubbles are formed is given by average jet penetration depth. For a bubble generating from an upward facing orifice, its center of gravity rises and results in reduction in the pressure on the downstream side of the orifice. Since the pressure drops across the orifice, it further causes pressure variation inside forming bubbles and thus a decrease in the surface tension pressure can be seen.

The observations by Klug and Vogelpohl[126,127] support the Mersmann criteria for generation of bubbles in jet regime while the mechanism of bubble formation on sieve trays is found similar to that at single submerged orifice. At high Weber numbers, secondary bubbles are smaller than those generated at the single hole plate and bubbles are generated through all the holes, though they do not approach the jet regime. In the case of sieve plates having the closest distance between holes, no individual bubbles are formed. Even before primary bubbles form, they coalesce to larger agglomerates which detach from the plate and again disintegrate due to shear stress of the surrounding liquid. This motion of liquid above the sieve plate is a considerable resistance in forming primary bubbles, which also follows Mersmann's criteria.

Miyahara and Tanaka[114] observed that all the bubbles ascend individually without coalescence and all that get dispersed have uniform size from a sintered mesh plate. Miyahara and Hayashino's[115] observation for perforated plates shows that bubble coalescence takes place after certain time immediately after formation yielding a log-normal probability distribution of the bubble sizes. In another extensive study on bubble formation on perforated plates Bowonder and Kumar[128] suggested the mechanism based on an assumption that the number of effective sites (active holes at any instant) such that the bubbles formed cover the whole area as if from single nozzles when arranged in close packing. Thus, their analysis accepts the same mechanism as for single orifice. Wraith[53] has considered it as a two-stage phenomenon considering the line of contact between bubble and the edge of slot.

2.9.3. Models of Bubble Formation in Multi-Orifice Configuration. Under the crowded source conditions that are likely to apply at high flow rates, lateral interaction between growing bubbles will impede formation and a model based upon spherical growth may not be adequate. Effectively, all of the models are the same as for single orifice except some times it is represented in terms of size distribution.

2.9.3.1. Li et al. Model[121]. According to Rayleigh-Taylor instability criteria,[129] horizontal interface between two stratified fluid layers at rest is generally observed to be unstable in a gravity or acceleration field if the density of the upper fluid is larger than that of the lower fluid. When gas flows vertically through a narrow, slot-shaped nozzle submerged in liquid, the gas liquid interface within the slot can be considered cylindrical. The meniscus is unstable because gas underlies liquid, and its radius of curvature is likely to vary with gas pressure. On this basis, the interface is assumed to get disturbed by the presence of peaks or nodes distributed along the slot at the most dangerous wavelength (λ_d) based on acceleration field developed in the vicinity of nozzle mouth which results in the generation of bubble. This dangerous wavelength can be given by

$$\lambda_d = 2\pi\sqrt{\frac{3\sigma}{g(\rho_1 - \rho_2)}} \tag{61}$$

For the present case, the analogous dimensionless form can be given as follows

$$\lambda_d^* = \frac{2.067 + 0.3108\sqrt{3}R^{*1.434}}{1 + 0.3108R^{*1.434}} \frac{2\pi}{\sqrt{1 + (1/R^{*2})}} \tag{62}$$

where λ_d^* is the dimensionless dangerous wavelength and $R^* = R_o\sqrt{\rho_L Q/\sigma}$ is the dimensionless radius of curvature. Model of bubble formation considering each hole as independent source on the same slot is proposed and at low gas flow rates, the bubbles generated by

capillary action are represented by force balance as

$$V_B = F_S/(\rho_L - \rho_G)g \tag{63}$$

where F_S effective surface tension force at the nozzle defined in terms of the total length (L) of contact at the orifice mouth. At large gas flow rates force balance yields

$$V_B = K_B Q^{6/5}/g^{3/5} \tag{64}$$

where K_B is the constant that depends on the bubble detachment condition. From the independent analysis, they have estimated the values of λ for different slot spacings ($w = L/N$) with N sources and correlated it with the system We as

$$\frac{\lambda}{w} = 17.6(\rho_L/\rho_G)^{0.16} We^{-0.25} \tag{65}$$

And further, these values are used for the calculation of bubble volume using the superficial gas velocity (V_G) as

$$V_B = 0.01(V_G w\lambda)^{1.37} \tag{66}$$

This formulation is later modified[130] to achieve the bubble sizes directly from the superficial gas velocity and the properties of the gas−liquid system and given as

$$V_B = 26.2\left(\frac{(V_G w)^2}{g}\right)\left(\frac{\rho_L}{\rho_G}\right)^{0.192}(Fr^{4/3}We)^{-3/10} \tag{67}$$

2.9.3.2. Miyahara and Takahashi (1986)[113] Approach. According to this model, bubble volume at the end of detachment remains the same for all the bubbles generated from all holes on a porous plate. Referring to this assumption, these investigators calculated the volume of individual bubble based on experimentally observed number of bubbles that are generated due to supply of certain volume of gas and then by force balance on a single bubble, diameter of individual bubble (d_B) was given as

$$d_B = \left(\sum 6V_B/\pi n\right)^{1/3} \tag{68}$$

For plate geometries, equation for d_B changes owing to change in shape of bubble. Similarly, for the case of sieve trays, Biddulph and Thomas[131] have used just the buoyancy and surface tension forces and employed the detachment point condition to predict the bubble sizes as

$$d_{B,Max} = (6\sin\theta)^{1/3}\left[\frac{d_h\sigma}{(\rho_L - \rho_G)g}\right]^{1/3} \tag{69}$$

To consider the actual size distribution, the diameter of generated bubble was considered to be Sauter mean diameter neglecting viscous drag force acting on bubble.[115,119]

$$d_{30} = 2.9[\rho g/\sigma d_h]^{-1/3} \tag{70}$$

which is reasonably close to Tate's law ($d_B = 1.8\sqrt[3]{d_h\sigma/\rho g}$).

2.9.3.3. Loimer et al. (2004) Single Bubble Approach.[132] In a recent work, Loimer et al.[132] have investigated the bubble formation over porous plates and sieve plates. Their theoretical analysis is based on the assumption that every bubble forms singularly without any hindrance due to surrounding bubbles and used Tate's law for the estimation of bubble size under quasi-steady regime as well as the dynamic regime. For single bubble formation in the dynamic regime, they have used the relative variation between the surface tension force and the pressure force to estimate the gas flow rate (Q_{SI}) for the transition from the quasi-steady to dynamic regime as $Q_{SI} = \pi(0.66/g^2k^3)^{0.17}(d_h\sigma/\rho)^{0.83}$, where k is the added mass force. For the case of wetted sieve plates, they estimated the minimum flow rate for the bubble formation at more than one orifice as $Q_{min} = 2\pi\sqrt{\sigma d_h^3/\rho_G}$ and the number of active orifices is estimated in terms of the ratio of total gas volume flux to the Q_{min}. For a densely packed sieve plate, their analysis yield the bubble sizes

$$R = 1.881V_G^2/g \tag{71}$$

where V_G is the superficial gas velocity. On the nonwetted sieve plates, the analysis also includes the dynamic regime. Their analysis assumes that below the sieve plate, no spatial pressure variations exist and hence the formation is a random process. However, this assumption is contradictory to the visual observations,[133] with Mersmann's criteria and also the CFD results by Dhotre et al.[134] The approach can be considered valid for porous plates which offer very high pressure drop across them yielding practically negligible pressure gradient below the plate. However, the pressure variation below a sieve plate is not only spatial but also has temporal dynamics associated with it, which makes the process complicated. Moreover, the visual observations indicate that the dynamics are well organized and follow systematic patterns, which can make the mathematical analysis simpler.

For the wetted porous plates, the analysis assumes a pressure field variation below the plate and a characteristic radius (R_C) is identified for the simultaneous bubble formation at two locations separated by a locus of circle of R_C. Since the formulation for Q_{min} is based on Darcy's law, it is independent of pore size and the bubble size is given as

$$R = \sqrt{(8\pi\sigma k/3\sqrt{3}V_G\mu_G)} \tag{72}$$

Similar analysis is also done for a nonwetted porous plate. The analysis has shown a reasonably good match between the experimental and predicted results. However, the random distribution of the bubbling positions mainly depends on the pore/hole size and their distribution and the observations need not be valid for large systems, due to the dynamics of bubble formation at large holes and the associated liquid flow in its vicinity. Nevertheless, the approach is simple and may be tested for large systems as well.

2.9.4. Factors Affecting Bubble Formation at Sieve Plates. 2.9.4.1 Gas Flow Rate. Similar to the single submerged orifice, for sieve trays bubble size increases with increase in gas velocity,[114] and they ascend individually without coalescence and get dispersed with uniform sizes. According to Miyahara and Haga,[135] at low gas flow rates, bubbles ascend individually, whereas at some higher flow rate formation of the secondary bubble is affected by the primary one because

bubbles from two holes ascend in close proximity with each other. At low pitch to hole-diameter ratio, gas velocity has no effect on bubble formation. Kumar and Kuloor[17] have reported above observations for sieve trays. At small flow rates, bubble size increases with hole-diameter and bubbles are formed at certain frequency and this has a unimodal distribution in size. With an increase in flow rates, relative influence of surface tension goes down resulting in diminishing of difference between bubble volumes obtained from different pore diameters and bubbles of nonuniform sizes are formed (bimodal distribution). At medium flow rates, single bubble formation takes place due to coalescence before detachment (multimodal distribution). At very high rates, the effect of surface tension is totally eliminated and a continuous linear blanket of gas forms at surface along the slot mouth and local getting and subsequent break-up takes place; also, bubbles ascend in groups and thus formation of the new bubble has to face the resistance due to turbulence by liquid in its vicinity. When spacing between sources is larger than the free bubble diameter the sources are discrete and independent and the performance is least affected at the orifice mouth. Li et al.[121] have also shown that even for a system having several bubbling sources, the bubble size increased with the gas flow rate; however, the nature of variation differed with the orifice configuration.

2.9.4.2. Pitch of Holes on Sieve Trays. For small pitch on the sieve trays, bubbles get coalesced to larger ones before it detaches. Smallest bubbles are formed at sieve plates with the closest hole-spacing of 6 mm as the momentum transfer becomes intensified with increasing proximity of bubbles in swarm. At high viscosities, smallest bubbles are formed at sieve plates with the largest spacing. Generally, large hole-spacing is required in order to suppress the increased coalescence in the sparger region. In dispersion zone, arrangement of bubbles is not affected by hole-spacing. Varying hole-spacing leads to different bubble sizes, and it affects the ascending velocity of bubbles. Decrease in pitch below less than bubble diameter stretches a bubble in vertical direction,[100] and consequently shape changes to an oblate shape, the pressure inside the bubble keeps reducing and finally produce a larger gas flow rate through the orifice and thus a larger detachment bubble volume. In a systematic analysis, Li et al.[121] have shown that with increase in the distance between two holes, larger bubble size is achieved even at smaller gas flow rates, while at high gas flow rates (gas flow rate per bubble source > 0.7 mL/s), the bubble sizes are not significantly affected by the pitch. When estimated for the various slot sizes they have used, the nozzle velocities were seen to be closer to the transition region between the steady jet and pulsating jet depending on the depth of orifices. Since very little has been studied and known about the bubble formation in sieve plats and porous plates, it is required to understand the bubble formation process to have a control on the process by creating only required interfacial area and by reducing back mixing.

In a bubble column reactor, the regime of operation i.e., homogeneous, heterogeneous and transition are basically governed by the bubble sizes and their slip velocities. In many of the cases, the homogeneous regime prevails at low gas velocities, whereas at higher V_G heterogeneous regime is attained. It is possible that, at low V_G, transition or heterogeneous regime can be attained by using a sieve plate having either large hole diameter[124,125] or very small pitch. This way, it is possible to control the regime of operation to some extent by making proper choice of the sparger design.

2.10. Experimental Techniques. Motion of bubbles in liquids can be observed experimentally either by visualization or by taking photographs at high speed. This is possible only in the case of transparent or semitransparent liquids. Here, we discuss the above two methods in brief followed by their pros and cons. Further, we also discuss the possible experimental methods of visualization, which would be possible using advanced flow visualization techniques. We have also tabulated the methods used by various investigators for this analysis in Table 1.

2.10.1. Image Visualization/Analysis. Most commonly used methods for the experimental observation of bubble formation and its rise is image visualization through stroboscopy or high-speed photography and X-ray.[136] The Stroboscopic method and high-speed photography is reliable even for jetting regime as the number of bubbles formed and their sizes can be measured from the photographs. However, this method is limited by its applicability in transparent and semitransparent liquids in near wall region. This limitation can be overcome by the use of X-ray as it can even be used in opaque systems but at higher cost of measurement and includes the danger of exposure to hazardous rays. The details of these techniques are explained in the third section of this Review.

2.10.2. Volume of Displaced Liquid. In this method, bubbles are continuously generated in a pool of liquid at certain known frequency (usually measured through visual observation) and the increase in liquid volume is measured. From the knowledge of the frequency of bubbling (under the assumption of constancy in size) bubble size is estimated. This method is suitable even for the opaque medium, provided the frequency of bubbling should be measured using some invasive/noninvasive methods for the recording of event on an oscilloscope. This method is limited for the generation of single bubbles and cannot be used for the cases, where primary and secondary bubbling or even bubbling through jet break-up occurs. Further, for very small sized bubbles, it is required to measure the exact change in liquid volume, which can make significantly large errors in results.

2.11. Conclusion and Recommendations. Bubble formation at a single orifice has been given sufficient attention and various research groups have developed this concept very well. Published literature shows that approaches for studying the bubble formation can be classified mainly as, (i) the experimental analysis by stroboscopic method, (ii) modeling the process through simple force balance/dimensional analysis, and finally, (iii) solving the equations of motion and continuity by potential flow approach for various conditions. A few of the recent studies illustrate that a combination of any of the above two is very useful.

Single stage bubble formation model holds well only for a few cases, viz. in the case of liquid flow where the bubble detachment is very fast and the volume occupied by bubble neck is negligible. The results from the single-stage bubble formation model do not compare very well with the experiments at high gas velocity and in non-Newtonian liquids since the contribution of bubble neck

to the overall bubble volume is not taken into account. Since the stroboscopic pictures have shown that the process is not a single stage process, it is needed to divide it in various stages and model it subsequently. The predicted results can be matched with the experimental ones only when the process of formation, growth and detachment are studied separately by applying the equations of motion to the system in consideration. Further, for a multi-stage consideration, it can be clearly seen that the predictions are improved over a wide range of operating and system parameters. This is because, the process of bubble growth is being taken into account very carefully and even the elongation of neck at low gas flow rates is also considered. The results of models based on the potential flow theory[18,102] look promising since the bubble growth at the orifice can be observed very neatly in time domain. Still, the force balance approach is simple, reliable and not computationally intensive as for the potential flow approach.

In most of the proposed models, bubbles are assumed to be spherical, which is not true always. For high gas flow rates in a pool of viscous liquid with large orifice diameters, the bubbles generated are either ellipsoids or hemispheres and pressure inside the bubble will be different at all the surface elements. Also, for nonspherical bubbles formed in the case of continuous phase flows, the detachment condition and the nonidealities in the shape also need to be considered. Similarly, to understand the phenomenon at high temperatures, where the gas does not remain ideal and becomes compressible, further modifications need to be made. With increased computational power, it seems possible to release such assumptions from the existing models and formulate a generalized approach. The approach of dividing the interface in various small parts and then applying the force balance on each surface can be combined with the potential flow method to meet the above requirement with appropriate inclusion of the thermodynamic laws.

As mentioned earlier, when the liquid is in motion, the bubble detachment occurs at an early stage and hence an additional term of the virtual mass force is taken into account. The results obtained even by the potential flow approach show little deviation from the experiments, which focuses on the empirical nature of the virtual mass coefficient and brings out the requirement of modifying it.

Various investigators have shown that the chamber volume and the orifice shape are important design parameters affecting the bubble sizes. The first parameter needs to be studied more methodically since the effect of back pressure has rarely been taken into account while modeling the process. This is mainly because, at higher flow rates, the primary bubble has noticeable effect on the secondary bubble volume and also in multipoint sparger, the hole-to-hole interaction and variation in the pressure drop across neighboring holes is mainly governed by the pressure fluctuations in the chamber. Also, in the case of column type of reactors, the near sparger region shows a complex flow pattern, which is greatly affected by the chamber dynamics and can be discerned by characterizing the bubble formation using advanced measurement techniques[137] and by using fast cameras to capture required features.

In practice, the single point spargers have limited applications and multipoint spargers are used commonly. The process of bubble formation at the multipoint spargers has not been studied thoroughly and needs to be understood by applying the first principals. The bubbling at the multipoint sparger is accompanied with weeping. Since the type of liquid and orifice material decide the wettability, conditions and hence the possibility of weeping and bubble formation in the presence of weeping[24,109−111] from multipoint spargers needs to be studied. Also, the bubble formation at different temperature−pressure conditions and for liquids of various types needs to be studied since many of the industrial operations run at nonambient conditions with different liquids with various properties. Most of the industrial columns are operated in jetting regime, where the effect of chamber volume is negligible it is required to improve upon the design of trays to minimize weeping.

In the published literature, the focus is on the effects of various experimental conditions on the bubble sizes generated from the orifice, which shows discrepancies in the observations. It is a requirement to compare them on a common basis and suggest the scope for further work to reach to a conclusion or a generalized approach to study this phenomenon.

New approach of employing neural network-parameter estimation technique toward this problem by Jamialahmadi et al.[60] looks very interesting. However, efforts in reducing the deviation from the experimental data need to be made and more attempts toward increasingly complex systems (liquid flow, bubble swarm, extreme operating conditions, etc.) are required.

Approaching the complex problem of formation of bubbles in the presence of hindrance seems difficult at this stage. An attempt can be made by formulating a model, which takes into account the effect of presence of surrounding bubbles, associated liquid motion and the various additional forces acting on it. The local bubble number density, bubble size distribution, the variations in the local liquid velocity in the vicinity of each hole, the dynamics of formation process, unequal pressure distribution over the orifice can be used to formulate a population balance based model along with Navier−Stokes equations for both the phases may be the next step in solving this problem.

Since the discrepancy in the various experimental observations is critical in some cases, it would be now more realistic to develop the further understanding of this phenomenon through rigorous CFD, which will help in visualizing the contribution of individual forces and parameters over a wide range of systems to a better extent.

3. Bubble Rise Velocity in Liquid

After the detachment of a bubble from the orifice, the buoyant forces cause its rise in the liquid. The dynamics associated with rise are mainly due to temporal variation in bubble characteristics or even the variation in the system properties. The phenomenon is very simple and observed very commonly in many industrial gas−liquid contactors viz. absorbers, flotation tanks, bubble columns, stirred gas−liquid hydrogenation reactors, viscbreaking, etc. Bubble rise in liquid is a classical example of flow past immersed bodies and shows different behavior under the conditions of with and without slip at the boundary. Rise velocity (generally termed as the terminal rise velocity in stagnant liquids and slip velocity in the case of moving liquids) of gas

bubbles in liquid dispersions is one of the parameters, which decide the gas phase residence time and hence the contact time for the interfacial transport and subsequently contributes to the performance of the equipment. In the applications of flotation, bubble rise velocity decides the operation time[138] and for enhancing the performance of the equipment, bubble size and rise velocity are important controlling parameters. The phenomenon of bubble rise in liquid in different conditions, i.e., quiescent and bubble swarm is under investigation over many decades. In the early years of attempting this problem,[139] it was assumed that the fluid surrounding the bubble has zero viscosity, and there is no slip at the boundary which simplifies the case to a greater extent when compared with the case of real fluids, where the complexity is higher. In the case of a system where fluid is real, gas bubbles experience a slip and the presence of viscous and inertial forces makes the analysis complicated and understanding meager.

The regimes of bubble motion in liquid are grossly classified as Stokes regime, Hadamard regime, Levich regime, and Taylor regime.[140] All of these regimes have specific conditions for a bubble motion conditional to their size, shape and nature of interface, i.e., free or rigid. The phenomenon is very interesting as the characteristics of a rising bubble (i.e., its size, rise velocity, trajectory, etc.) show dynamic behavior from system to system, making it very tedious to develop a general understanding for all the cases and also to develop a generalized correlation for rise velocity in all above regimes for different gas−liquid systems. The subject of bubble motion in liquid has been very interesting for the physicists (Auton,[141] Eames & Hunt,[142] Magnaudet & Eames,[143] Mei & Klausner[144]) and this problem is generally attempted through the force balance. The main forces, which act on a bubble during its motion in liquid are gravity, buoyancy, drag, surface tension, viscous forces, added mass force, history force (arising out of the unequal distribution of vorticity), and finally lift force (either due to baroclinically developed pressure gradients or unsteadiness of the flow). The contribution of individual forces varies from the case to case and most of the earlier work involves the development of suitable formulation for the same. However, in this section of the review, we have focused our attention mainly on the rise of bubbles in liquids and the effect of various physicochemical parameters on the rise velocity. Many investigators (Astarita,[145] Davis and Acrivos,[146] Haque et al.,[147] Clift et al.,[148] Abou-el-Hassan,[149,150] Chhabra,[151,152] Rodrigue[153,154]) have worked extensively in various gas−liquid systems and developed several correlation for a specific range of conditions. Since the chronological development in this area is not very important (pertaining to the development of generalized correlation) the attempts in this direction can be grossly classified on the basis of the nature of liquid phase (Newtonian, non-Newtonian, aqueous, organic etc.). Only the recent attempts by Nguyen[155] and Rodrigue[153,154,156,157] on developing generalized correlation for various liquid systems can be considered to be applicable over a wide range; however, still many important deviations from the regularity need to be incorporated. In view of this, here we have made an attempt to review the published literature on bubble rise velocity and have compared the existing correlation for the experimental data by various investigators for recommending the most suitable correlation applicable over a wide range of parameters. In addition to this, we have also compared all these observations and identified the possible reason behind every result and the physical significance of the particular experimental observation is also discussed in detail. This part of the review is arranged as follows: In the next subsection, we discuss the various parameters governing the phenomenon of bubble rise and effect of them on bubble rise velocity. Further, a qualitative description of bubble trajectories and different modes of oscillation is given. In the fourth subsection, we have reviewed the observations by various investigators on bubble rise velocity, and their analogy for development of correlation for the same is discussed and finally recommendations are given for the use of the same.

3.1. Factors Affecting the Rise Velocity. The rise of a bubble in liquid is a function of several parameters viz. bubble characteristics (size and shape), properties of gas−liquid systems (density, viscosity, surface tension, concentration of solute, density difference between gas and liquid), liquid motion (direction), and operating conditions (temperature, pressure, gravity). Here, we have discussed a few of these in regard to the importance given to them in many studies.

3.1.1. Effect of Purity of Liquid (Surface Tension) on Bubble Rise Velocity. As mentioned earlier, the regime of bubble motion in liquid shows the effect of various parameters on rise velocity and thus varying the physicochemical properties of liquid the regime of operation can be manipulated. In the case of Newtonian inviscid liquids, the rise velocity depends on bubble size, temperature, extent of contamination, and pressure in the system. The viscous forces have no noticeable influence on the rise velocity and only the gravity, buoyancy, and drag matter. Typical observations in such systems are shown in Figure 11A. It can be clearly seen that at ambient conditions the plot of rise velocity versus size in clean (pure) liquid, the velocity increases with size and attains a peak followed by a decrease in velocity over a very small range of bubble size after which it attains a weakly positive dependence on bubble size. Depending upon the type of contamination, i.e., surfactant, electrolyte and their concentration, the rise velocity characteristics of a bubble change significantly. In the case of the electrolyte solution, the effect is similar to that of surfactants; however, the additional electrokinetic forces repel them further causing existence of smaller bubbles rising with still lower velocity.

The mechanism by which surfactants modify the velocity field in the vicinity of a fluid−fluid interface was first described by Frumkin & Levich[158] and Levich,[159] who proposed that surfactants tend to be advected along the bubble surface and accumulate in the rear region. Since the surface tension gradient produced by any gradient of the surface concentration of surfactant must be balanced by a jump of the shear stress across the interface (Marangoni effect), this mechanism implies that a shear-free boundary condition is no longer imposed in the liquid at the gas−liquid interface, and this leads to an increase in the drag force. This is known as stagnant cap hypothesis and has been used successfully for the estimation of bubble rise velocity and also used for the prediction of drag coefficient with respect to extent of surface contamination.

Although the effect of surfactants/contaminants (may be even polymers) on bubble rise velocity is known for

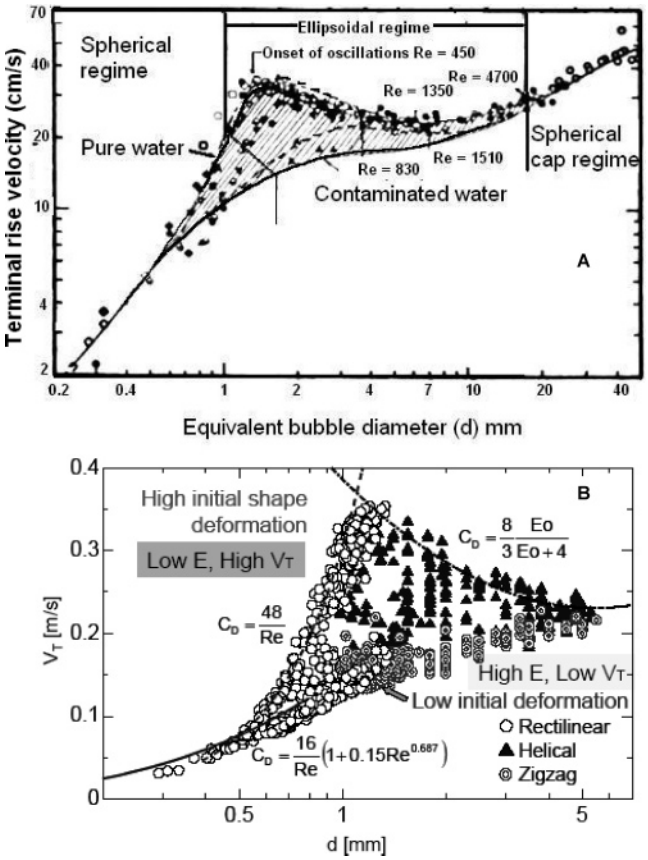

Figure 11. (A) Typical trends in rise velocity with bubble size for pure and contaminated liquids (reproduced with permission from Clift et al.[148]). (B) Effect of initial bubble deformation on terminal rise velocity in Distilled water. (reproduced with permission from Tomiyama[185]).

a while, very few detailed investigations exist where the effects of surfactants are studied. Since bubble size and its characteristics form an important component of design of a multiphase system operated in industries and in reality the industrial liquids are not always pure/clean, the laboratory studies with such liquids are important. Surfactants mainly modify the surface of a bubble resulting in change in its characteristics in both Newtonian and non-Newtonian liquids in a different manner. In the case of Newtonian contaminated liquids, if the contamination is due to surface active agents, as bubble rises, the bubble surface is dragged backward along with the liquid. The surfactants, specifically, are known to bridge the gap between solid rigid bodies and clean bubbles by immobilizing the bubble surface thus modifying the velocity field. In the front portion of the bubble, the surface is stretched and the new surface is constantly generated. As a result, surface tension gradients are generated resulting in increase in drag and reduction in the mobility of the gas−liquid interface. Thus, the internal circulation is reduced and also the tendency to coalesce with other bubbles. As a result of formation of rigid interface and enhancement in drag, the rise velocity is lesser than the clean bubble of the same size. For the case of liquid drops, the critical diameter increases with increasing surfactant concentration.[160] However, the effect is significant depending upon the solubility of the surfactant. Kopf-Sill and Homsey[161] have used Hele-Shaw cell for analyzing the effect of surfactants and have used the capillary number and Bond number for identifying six different shapes.

Studies by De Kee et al.[162] have shown that the reduction in surface tension (by addition of 0.042 mass% of sorbitan monolaurate) in the solution of 1 mass% polyacrylamide (AP-30) in 50/50 water/glycerine mixture results in the decrease of bubble rise velocity of small bubbles without any discontinuity. In another attempt, Rodrigue et al.[156] have studied the velocity of single bubble in Newtonian (three different concentrations of glycerine in distilled water) and non-Newtonian (solutions of CMC, gellan gum, poly(ethylene oxide) and PAA) fluids containing impurities (by adding several concentrations of SDS). They have reported that with increase in surfactant concentration the bubble rise velocity decreases till certain critical bubble volume, after which the bubble velocities are not affected by the surfactant concentration. The critical volume is a function of the solvent composition for their system. Radius of bubble at the critical volume can be estimated as $r_C = \sqrt{\sigma/g\Delta\rho}$ (Bond and Newton[163]). Thus, the observed reduction in the rise velocity is a function of the reduction in surface tension as well as higher liquid viscosity, which cumulatively lead to lowering of interfacial motion and hence the rise velocity. According to their observation, the effect of surfactants is noticeable only at relatively larger bubble volumes (beyond Stokes regime). For larger bubbles, which move at higher velocity, although more area is exposed to the fluid, diffusion rates of the surfactant do not allow for a significant immobilization and hence the effect of surfactants is negligible.

For the case of non-Newtonian liquids, the effect of surface tension on bubble rise velocity is similar to the earlier case, however, the observations for viscoelastic liquids are significantly different. In viscoelastic liquids such as solutions of PAA, bubble experiences a jump in the liquid velocity. The role of surface tension in this phenomenon is important as the jump is a result of the transformation of the rigid interface to a flexible one, and the extent of rigidity of the interface is decided by the surface tension to some extent. Several investigators have studied this phenomenon and proposed various possible explanations based on their observations. One of the possible explanations comes from the surface tension model by Zana and Leal,[164] where the existence of a bubble is proposed only under its surface being either totally covered or totally free of surfactants and also the elasticity plays an important role. However, the liquid viscosity is equally important and needs careful analysis. The remaining analysis of this phenomenon is explained in detail later at appropriate position in this Review.

For the case of power-law non-Newtonian liquids (CMC), Tzounakos et al.[165] have studied the effect of surfactants (SDS) in detail through the analysis of the drag curve. According to their investigation, the motion of bubble in a shear thinning liquid can be explained on the basis of two equations. For rigid bubbles having immobile surface

$$C_D = \frac{24}{Re}(1 + 0.173\,Re^{0.657}) \text{ where } Re = \rho_L d_b^{\,n} V_T^{2-n}/m \quad \text{for } Re < 135 \quad (73a)$$

and

$$C_D = 24/Re \text{ for } Re > 135 \quad (73b)$$

while for the bubbles having mobile surface, since the

shape deviations are possible at larger bubble volume, the correlation comes out to be

$$C_D = \frac{16}{Re}(1 + 0.173\, Re^{0.657}) \text{ where } Re = \frac{\rho_L d_b{}^n V_T^{2-n}}{mE^n} \quad \text{for } Re < 60 \quad (74a)$$

and

$$C_D = 16/\text{Re for } Re > 60 \quad (74b)$$

where m is the consistency index. Thus, there exists a difference in the respective drag curves and the addition of surfactant to the solution. Thus, for a given solution of fixed concentration, with increase in the bubble volume, the drag curve experiences a smooth transition from the curve explained by eq 74a to the curve explained by eq 74b. Details of this effect are quantified later.

Recently quantitative experiments performed with carefully controlled contamination have allowed the time evolution of the rise velocity of the bubble to be correlated to the physicochemical properties and the concentration of surfactant in the surrounding liquid.[166,167] On carrying out the experiments with bubbles rising in water contaminated with several surfactants, it was observed that below a critical bulk concentration, the final rise velocity is insensitive to the presence of the surfactant, whereas the rise velocity decreases abruptly to the value corresponding to a solid sphere above the critical bulk concentration. The critical concentration is reported to depend on the nature of the surfactant and also the bubble diameter. This also showed that a higher concentration is required to cover larger bubbles. Very recently, in a systematic experimental investigation by Ybert and Di Meglio,[168] bubbles were released preloaded with the surfactant, the measured rise velocity as a function of distance traveled indicated that after the initial stage of acceleration from rest, the instantaneous rise velocity of a given bubble depends only on the total amount of surfactant adsorbed on the bubble surface. It was also shown that the surfactants are not only absorbed onto the bubble surface, but may also be desorbed, which result in rise in the bubble velocity owing to remobilization of the interface finally reaching a constant equilibrium value of the surfactant concentration. This observation rules out the proposition by Zana and Leal[164] that no intermediate stages of surfactant presence on bubble surface can exist.

In an elegant approach, Alves et al.[169] have shown that with increase in the extent of contamination over a bubble surface, the drag coefficient of a 1.5 mm diameter bubble increases gradually and reaches a plateau after an exposure for about 960 s, which is even seen to be consistent for other bubble sizes. The experimental analysis by these authors in terms of the rise velocity of bubbles for a range of contamination level is consistent when compared with the classical bubble rise velocity plot (Figure 11A).

3.1.2. Effect of Liquid Viscosity on Bubble Rise Velocity. In Newtonian viscous liquids[160] (viz. aqueous solutions of glycerol) modes of bubble rise show different behavior than the inviscid liquids as well as some of the non-Newtonian liquids. Rodrigue et al.[156] have reported an almost linear relationship between rise velocity and the bubble volume dependent on the liquid viscosity of the aqueous solutions of glycerine at different concentrations. Further, the bubble rise velocity is also reported to decrease with viscosity with the possibility of reduction of the interfacial motion due to viscous forces.

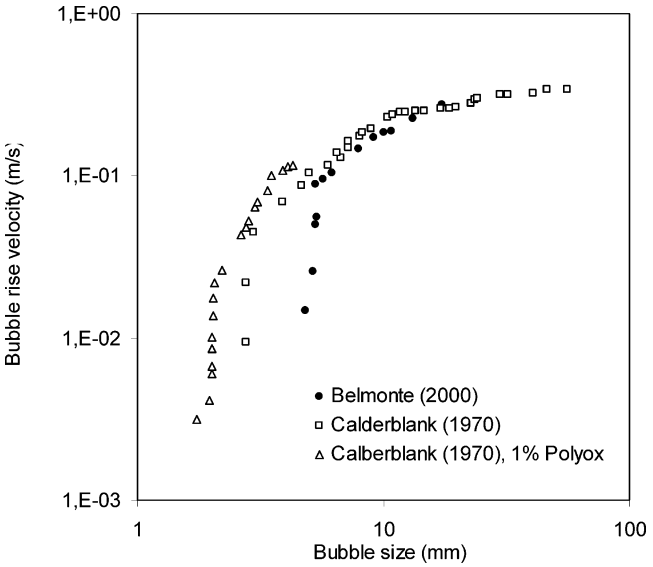

Figure 12. Typical experimental data showing the regime transition during the motion of a bubble in non-Newtonian liquids. Several such transition plots for various liquids may be seen in Tzounakos et al.,[165] Rodrigue et al.[157,173]

For the case of different non-Newtonian liquids, the relationship between the bubble size and rise velocity shows different nature depending upon the nature of viscosity. In certain viscoelastic liquids (viz. aqueous solutions of PAA), terminal rise velocity (V_T) exhibits a discontinuity at certain critical value of bubble size while in other shear thinning liquids (viz. solutions of different polysaccharide, CMC)[167] such an observation is never reported. Leal et al.,[173] Astarita and Apuzzo,[140] Acharya et al.,[55] and Rodrigue[173] have investigated this phenomenon in detail. It has been proposed that the jump in the velocity is an effect of the transition from the Stokes regime to the Hadamard regime where the viscoelasticity shows its dominance. These authors have carried out their analysis for various viscoelastic liquids of different concentrations and found that the transition size is a function of the concentration of the solute. Further, their analysis has shown that the effect of elastic forces prohibits any regime transition and also the contribution of elastic forces is independent of the presence or absence of no slip condition. However, the observations of Acharya et al.[174] have shown that in the creeping flow regime (i.e. the size below the transition size) elasticity has no effect on the rise velocity, which they have shown through C_D–Re relationship. These observations are concordant with the earlier inference and clearly indicate that the transition in rise velocity follows from a deviation in shape from sphere. Also, the transition from Stokes to Hadamard regime is gradual in the case of Newtonian purely viscous shear thinning liquids, and not sudden as in the case of viscoelastic liquids. Figure 12 shows the regime transition in the case of various viscoelastic liquids. In contrast to the above observation, Carreau et al.,[175] Margaritis et al.,[167] Dekee et al.[176] have observed no discontinuity in the respective solutions and their observations are supported even in the case of dissolution of a bubble in liquid. To verify the existence of this transition even in

liquids with very low surface tension Belmonte,[177] has studied the effect of micellar concentration on the modified viscosity of a cetltrimethylammonium bromide solution, and the overall effect of modification of the properties on bubble rise velocity. This attempt is different from the earlier as the surface tension was reduced to form micelles, which reduces the surface mobility. They have observed change in bubble shape at the transitional bubble size that results in discontinuity in the velocity. The details of this phenomenon and the possible reasons behind it are discussed separately.

3.1.3. Effect of Temperature on Bubble Rise Velocity. It is well-known that for ideal gases, at constant pressure, with increase in temperature, the volume of gas increases and the average density goes down. But, generally, to maintain the liquid state of the liquid phase reactant the condition of high temperature is accompanied with high pressure. There are very few studies made on the effect of temperature on the rise velocity of bubble. At ambient conditions, the rise velocity follows certain trend with bubble size. Two different cases may be considered: rise of a gas bubble in insoluble liquid and rise of vapor bubble in liquid at relatively low temperature. Both the cases are common, while only the second case is studied very systematically and the complexity of accompanied condensation makes it more complicated. In the first case of rise of a bubble of ambient condition in heated liquid, the heat transfer across the interface causes increase in the bubble volume. Also, at higher temperature the density difference between two fluids goes down, the buoyancy experienced by the bubble decreases causing the subsequent reduction in the rise velocity. Thus, the counteracting effects are dominant in different ranges of temperature and in certain temperature range rise velocity is a strong function of size. This particular case is important but still remains unattended in many respects and very meager information is available. Leifer et al.[178] have studied the effect on small bubbles of 0.1 to 3.5 mm diameter. Under the assumption of the no slip at the surface and no internal circulation, the kinematic viscosity, and the densities are expressed as a function of temperature in clean water as

$$\nu = \frac{0.01}{\rho_w} e^{[-24.71 + 4209/T + 0.04527T - 3.37 \times 10^{-5}T^2]} \quad (75)$$

where $\rho_w = 1 + 8.124 \times 10^{-5}T - 1.018 \times 10^{-5}T^2 + 1.146 \times 10^{-7}T^3 - 9.246 \times 10^{-10}T^4 + 2.986 \times 10^{-12}T^5$ which can be substituted in Stokes equation $V_T = (2gr_B^2)/9\nu$ to estimate the bubble rise velocity. Few of the most important observations by these authors include: (i) The oscillatory nature of bubble for varying temperature ranges (0−40 °C). (ii) For the bubble sizes below 0.3 mm, the rise velocity increased with temperature, (iii) For bubble sizes greater than 0.3 mm (~0.67 mm), at lower temperatures, the observations followed the above trend, (iv) above 25 °C, the rise velocity decreased with temperature (Figure 13). For larger sizes, the rise velocity is shown to have a weak negative dependence on temperature, whereas on the other hand, the oscillation amplitude was found to increase positively. In reality, the situation is quite different in terms of contamination of liquid, nonisothermal operations, wide bubble size distribution, coalescence-break-up phenomenon, and so forth, and hence, it is required to quantitatively understand the dynamics of bubble motion in such systems.

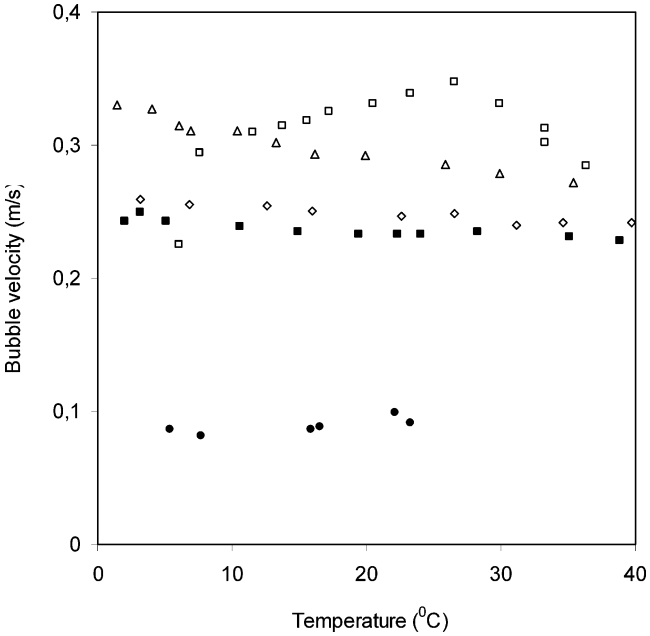

Figure 13. Experimental data on the effect of temperature variation on bubble rise velocity. ◆ d_h = 0.375 mm, □ d_h = 0.677 mm, Δ d_h = 1.003 mm, ◇ d_h = 2.0 mm, ■ d_h = 3.462 mm.

Since liquid density (ρ_L) is inversely proportional to the temperature, the possible effect of liquid density on bubble rise velocity can be realized from the above explanation. Higher liquid density results in increased buoyant forces which lead to faster bubble rise. However, this effect is not significant when compared to other physical properties of the liquid that that affect the bubble rise velocity.

3.1.4. Effect of External Pressure on Rise Velocity. Although most of the laboratory scale investigations on bubble dynamics are carried out at ambient conditions, the operating conditions in industrial systems are significantly different from the ambient ones. For example, at elevated pressure, the hydrodynamic conditions in the column type of reactors are very much different as the increased outside pressure affects the bubble dynamics, the mode of bubble formation and hence the overall flow pattern. To be specific, as a result of rise in the outside pressure, bubbles are formed only after a sufficient minimum gas velocity is reached (which is higher than at ambient conditions), while their sizes are relatively smaller. This is mainly because, to withstand the outside pressure, the bubbles prefer to have as smaller size as possible and hence their rise velocities are lesser than that at the ambient condition. Due to the elevated external pressure, pressure head on bubble is very high resulting in a slow rise. Another reason behind the existence of smaller bubbles is the increased bubble break-up frequency with increase in size. Letzel[179] has systematically analyzed the effect of gas density on the rise velocity of large bubbles. In a similar attempt, under the assumption of homogeneous nature of the suspension, Luo et al.[180] have studied the effect of external pressure on bubble rise velocity in a gas−liquid-solid fluidized bed (Newtonian viscous system). It can be clearly seen from Figure 14 that, with increase in pressure, for the same solid loading, the rise velocity had a manifold decrease at two temperature conditions. Further, the increased pressure was found

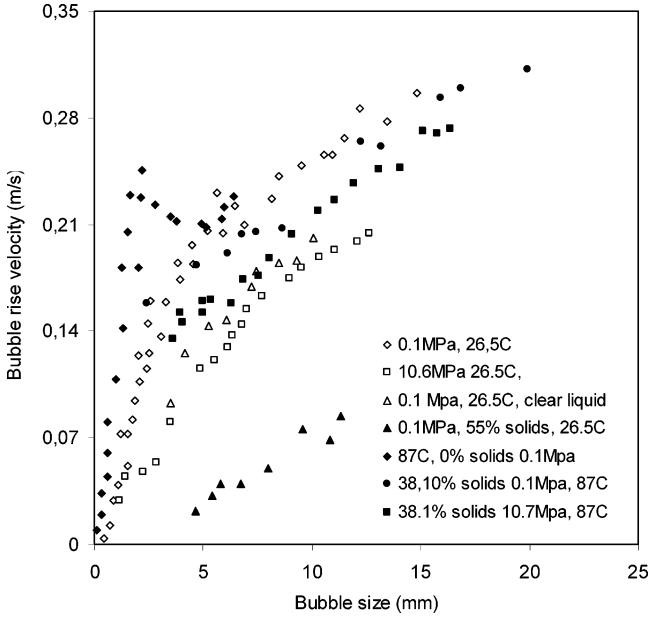

Figure 14. Experimental data on the effect of external pressure on bubble rise velocity (Luo et al.[180]) for different liquid viscosities.

to have low effect for higher temperatures, mainly because, the difference between the vapor pressure of liquid and external pressure goes down.

3.1.5. Effect of Initial Bubble Detachment Condition. In Figure 11A, the plot of bubble terminal rise velocity vs size is shown for an inviscid liquid. As mentioned in published literature (Clift et al.,[148] Fan and Tsuchiya[181]), the upper bound of the V_T data is considered to correspond to the bubbles in pure liquids while in the presence of trace amount of surfactants, drastic increase in the drag, causes the reduction in velocity leading to a scatter in the data below the curve for pure liquid. In a recent analysis, Tomiyama et al.[182,183] and Wu and Gharib[184] have reported that the main reason behind this scatter is not the extent of contamination but the difference in the way of bubble release from the orifice i.e., the initial condition before detachment. According to their analysis, for low initial shape deformation, bubble rise occurs at lower velocity with its trajectory being either a rectilinear or zigzag path. For large initial shape deformation terminal velocity is high and produces wide scatter depending on the different possible release conditions and deformations. This observation is depicted in Figure 11B, which is obtained from the measurements at 170 mm above the nozzle tip. Recently Tomiyama[185] has shown that the Figure 11B is comprised of data points that can be bounded with three different drag curves. Basically, for bubble having constant equivalent diameter increase in the aspect ratio is shown to reduce V_T. Also, for constant aspect ratio, V_T was found to decrease with increasing equivalent bubble diameter. It is however required to check the validity of such observation with the bubble shape map (Figure 15) proposed by Grace[186] on the basis of dimensionless numbers.

3.2. Formulations for Rise Velocity Correlations. In view of the important contribution of rise velocity in deciding the overall hydrodynamics of the system, it is required to know the bubble rise velocity in a system of known physicochemical properties and also possibly the bubble size. Since the rise velocity shows varying nature with the system properties, many investigators have developed empirical, semiempirical and theoretical formulation for the rise velocity, which many times remain subjective to a narrow range of governing parameters. We begin with the fundamental approach based on simple force balance and then move to empirical and semiempirical ones.

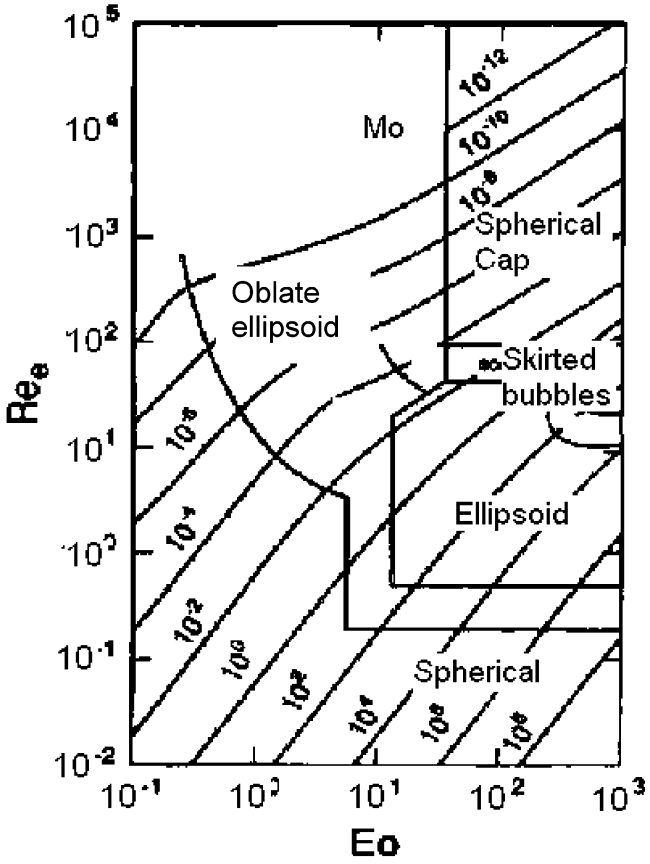

Figure 15. Bubble shape map. (reproduced with permission from Fan and Tsuchiya[181]).

3.2.1. Force Balance Approach. One of the earliest investigations in the bubble rise have shown that for small spherical bubbles, the drag force can be calculated and combined with the buoyancy force to yield Stokes' law as

$$V_{St} = \frac{2g(\rho_L - \rho_G)R_b^2}{9\mu} \tag{76}$$

under the assumption that the bubbles do not have any internal circulation and no slip exists at the boundary. Peebles and Garber[187] have done extensive experimental measurements of the drag coefficient analysis of bubbles in liquids with wide range of physical properties. Their correlation is given in Table 4 and the comparison of the predictions with experiments is shown in Figure 16.

The authors have obtained different correlations for different size regions, which bring out the need for developing a generalized correlation, which would work independent of the region. Davies and Taylor[198] have correlated the bubble rise velocity and the radius of curvature in an innovative way for the case of spherical cap bubbles (6.9 mm $< R_b <$ 36 mm). They assumed that the pressure over the front of the cap shaped bubble is the same as on a completely spherical bubble and the rise velocity was independent of the liquid properties. They proved that the rise velocity $V_T \approx (R_C)^{0.5}$.

3.2.2. Approach based on Dimensional Analysis. The main forces, which govern the phenomenon of

Table 4. Correlations for Bubble Rise Velocity in Newtonian and Non-Newtonian Liquids

investigator	system	physicochemical properties	correlation	remarks
Stokes[188]	Pure gases- clean liquids		$V_T = \frac{2g\rho r_B^2}{9\mu}$	Simple in formulation, however applicable only for the cases, where slip at interface as well as internal circulation in bubble is negligible.
Haberman & Morton[189]	Air-cold, hot water, mineral oil, varsol, turpentine, methanol, corn syrup-in water, glycerin-water, ethanol−water, olive oil	$782 < \rho < 1480$ kg/m^3 $0.02 < \sigma < 0.72$ N/m $0.52 < \mu < 18000$ cP	$V_T = 1.02\sqrt{gr_B}$	Although simple in formulation, not applicable to most of the systems, except where effect of physical properties is negligible.
Mandelson[190]	Published data of Habberman and Morton (1953)	$782 < \rho < 1480$ kg/m^3 $0.02 < \sigma < 0.72$ N/m $0.52 < \mu < 18000$ cP	$V_T = \sqrt{\frac{\sigma}{r_B\rho_L} + gr_B}$	Suits well for medium sized bubbles (>2 mm) in most of the pure liquids. Modification is required for including very small bubbles and contaminated liquids.
Peebles and Garber[187]	Measured data for: Air−water, acetic acid, ethyl ether, oil, ethyl acetate-oil, aniline, acetone, methanol, butanol, benzene, toluene, nitro benzene, pyridine, 2-propanol	$626 < \rho < 1071$ kg/m^3 $0.016 < \sigma < 0.72$ N/m $0.22 < \mu < 31$ cP	$V_{T1} = 2g\rho_L r_B^2/9\mu$, $Re < 2$ $V_{T2} = \frac{0.33g^{0.76}\rho_L^{0.52}r_B^{1.28}}{10\mu^{0.52}}$, $2 < Re < 4.02Mo^{-0.214}$ $V_{T3} = 1.35\sqrt{\frac{\sigma g}{r_B\rho_L}}$, $4.02Mo^{-0.214} < Re < 3.10Mo^{-0.25}$ $V_{T4} = 1.18\left(\frac{\sigma g^2}{\rho_L}\right)$, $3.10Mo^{-0.25} < Re$	Applicable for certain ranges of Re and Mo.
Harmathy[191]			$V_\infty = 1.53\left[\frac{g\Delta\rho\sigma}{\rho_L^2}\right]^{1/4}$, moderately distorted ellipsoids $V_\infty = \lambda\sqrt{\frac{g\Delta\rho D}{\rho_L}}$ for cylindrical slugs	Applicable for bubbles with $Re > 500$.
Astarita and Apuzzo[140]	Air-viscous liquids (Separan AP30, J100 in water)		Hadamard region $V_T = \frac{126V_B^{0.66}}{\nu}$ Levich region $V_T = \frac{42V_B^{0.66}}{\nu}$ Taylor region $V_T = \frac{2}{3}(gR')^{0.5}$ R' − Radius of curvature	Known correlations are categorized for different regions in terms of shapes and bubble sizes. Since it is similar to Stoke's formulation, applicability is limited.
Angelino[192]	Air-Viscous liquids		$V_T = K(4r_B^3)^m/3$ where $K = 25/(1 + 0.33\text{Mo}^{0.29})$; and $m = 0.167(1+0.34\text{Mo}^{0.24})$	Equation suits well for spherical cap shaped bubbles in various liquids[204]. Needs modification in terms of verification against complete force balance.
Dumitrescu[193]	Air-PVA		$V_\infty = 0.35\sqrt{2gr_b}$	Applicable for slugs with clean interface and potential flow of liquid in its vicinity.
Lehrer[194]	Published data of Habberman and Morton (1953)	$782 < \rho < 1480$ kg/m^3 $0.02< \sigma < 0.72$ N/m $0.52 < \mu < 18000$ cP	$V_T = \sqrt{\frac{3\sigma}{\rho d_B} + \frac{d_B g\Delta\rho}{2\rho}}$	Modification of waveanalogy. Fits well for experimental in a better way than wave theory.
Clift et al.[148]	Published data Air-Newtonian liquids over wide range of properties	$782 < \rho < 1410$ kg/m^3 $0.015 < \sigma < 0.72$ N/m $0.72 < \mu < 29000$ cP	$VT = \left(\frac{\mu}{\rho_L G}\right)Mo^{-0.149}(J - 0.857)$ $J = 0.94\,H^{0.747}$ for $2 < H < 59.3$ $J = 3.42\,H^{0.441}$ for $H > 59.3$ $H = -\frac{4}{3}EoMo^{-0.149}\left(\frac{\mu}{\mu_w}\right)^{-0.14}$	Equation is suitable for pureliquids over wide range of properties. Deviation is visible for spherical cap shaped bubbles.
Abou-el Hassan[150]	Published data Air-Newtonian liquids over wide range of properties	$835 < \rho < 1039$ kg/m^3 $0.015 < \sigma < 0.072$ N/m $0.233 < \mu < 59$ cP	$V = 0.75(\log F)^2$ V − Velocity number F − Flow number	Excellent match with experimental data in terms of Velocity and Flow number.

Nickens et al.[195]	Published data Air-Newtonian liquids over wide range of properties by White and Beardmore (1962)	$803 < \rho < 1420$ kg/m^3 $0.022 < \sigma < 0.77$ N/m $0.8 < \mu < 20900$ cP	$V_T = 0.361(1 + 4.89/Eo)^{0.25}$	Correlation is valid for contaminated low-density liquids as well as pure viscous liquids.
Jamialahmadi et al.[196]	Data by Peebles and Garber (1959)	$626 < \rho < 1071$ kg/m^3 $0.016 < \sigma < 0.72$ N/m $0.22 < \mu < 31$ cP	$V_{sp} = \dfrac{4(\rho_G - \rho_L)gr_B^2(3\mu + 3\mu_G)}{18\mu\left(2\mu + 3\mu_G\right)}$ $V_w = \sqrt{\dfrac{2\sigma}{2r_B(\rho_L + \rho_G)} + gr_B}$ $V_T = \left(\dfrac{-V_{sp}V_w}{\sqrt{V_{sp}^2 + V_w^2}}\right)$	Since the derivation is modification of a fundamental approach, it has excellent fit for the predictions for pure liquids over a wide range of gas–liquid properties.
Karamanev[197]	Published data Air-Newtonian liquids over wide range of properties	$790 < \rho < 1350$ kg/m^3 $0.02 < \sigma < 0.487$ N/m $0.8 < \mu < 120$ cP	$V_T = 1.16\left[\dfrac{d_{BG}^{0.5}\rho^{b'}Mo^{0.23b'}}{\mu^{b'}C_D^{0.5}}\right]^{1/1-b'}$ where, $C_D = 24(1 + 0.173Re^{0.65})Re + 0.143/(1 + 16300Re^{-1.09})\}$	Suitable for various Newtonian liquids, provided, the values of 'a' and 'b' needs verification over a range of Ta.
Nguyen[155]	Air–water (contaminated)	$Mo < 10^{-6}$ $Eo < 40$	$V_T = d_B\left[\dfrac{g\mu_L}{\rho_L}\right]^{0.33}\left(\dfrac{4aMo^{0.46b'}}{2.85^{1/2-2b'}}\right)\left(\dfrac{\rho_L^2 g}{\mu^2}\right)^{2-2b'/6-6b'}{}^{2-2b'/2b'+1}$	Applicable for contaminated Newtonian liquids only. Needs further validation over a wide range of physical properties of liquids
Rodrigue[154]	Published data Air–liquids over wide range of properties	$722 < \rho < 1380$ kg/m^3 $0.015 < \sigma < 0.091$ N/m $0.0022 < \mu < 18$ Pa s	$V_T = \dfrac{V_T\mu^{0.33}\sigma^{0.33}}{(2r_B)^{2/3}\rho^{2/3}}$	Fits well for available experimental data for few Newtonian pure liquids, however, for low-density liquids, the predictions are underestimated.

bubble motion in a pool of liquid, are buoyancy, gravity, viscosity, drag, interfacial tension, and the memory force (arising through the gradient of vorticity on the surface of a bubble). Since few of the forces are formulated using the simple physicochemical parameters, the simplest approach for correlating the bubble size and rise velocity is through the use of density of gas, density of liquid, viscosity of liquid, surface tension, gravity, equivalent bubble diameter, and obtain a relation between drag coefficient and Reynolds number. Several authors have used this approach of using the above parameters for dimensional analysis of the phenomenon and express the dependence of bubble rise on various other parameters. Among one of the initial attempts, Abou-elhassan[149] has used the force ratios of buoyancy to inertial, viscosity and interfacial tension respectively and expressed as

$$[g(\Delta\rho)d^{5/3}/(u(\rho\mu\sigma)^{1/3})] \tag{77}$$

He obtained two dimensionless numbers, flow number (F) and velocity number (V)

$$F = [gd^{8/3}(\Delta\rho)\rho^{2/3}/\mu^{4/3}\sigma^{1/3}] \tag{78}$$

$$V = [V_T d^{2/3}\rho^{2/3}/\mu^{1/3}\sigma^{1/3}] \tag{79}$$

The range of physicochemical parameters considered by him is given in Table 4. The correlation proposed by him, which fits very well for the data in the range of studies is

$$V = 0.75(\log F)^2 \tag{80}$$

Further, he has considered various flow regimes by varying the index of flow regime and modified the earlier correlation as

$$V_T \propto (g\Delta\rho)^{n'}\mu^{(1-4n')/3}\sigma^{(1-n')/3}\rho^{(2n'-2)/3}d^{(8n'-2)/3} \tag{81}$$

where n' is the index of flow regime. Further, for non-Newtonian fluids, he replaced the viscosity by a correction term based on the consistency (k) and pseudoplasticity index (n) as

$$\mu = kF(n)(u/d)^{n-1} \tag{82}$$

which results into

$$V_T \propto (g\Delta\rho)^{1/n}[kF(n)]^{1/n}d^{(n+1)/n} \tag{83}$$

These correlations are found to be independent of flow regimes and the bubble shapes and are applicable for the range of Reynolds numbers from Stokes region to Newton's law region. Recently, this methodology was adapted by Rodrigue[157] to develop a general correlation for the rise velocity of single gas bubbles in Newtonian liquids.

Recently, Tomiyama[185] and Rodrigue[157] have proposed excellent correlations based on the dimensional analysis. For the first, the approach is mainly oriented to capture the bubble shape variation in the Newtonian liquids and it gives excellent way of understanding the trends in rise velocity for different liquid properties and for different bubble shapes over a wide range of possible distortions. The correlation by Rodrigue[157] extends the approach of Abou-El-Hassan[150] and derives the bubble rise velocity in terms of velocity number and flow

AP

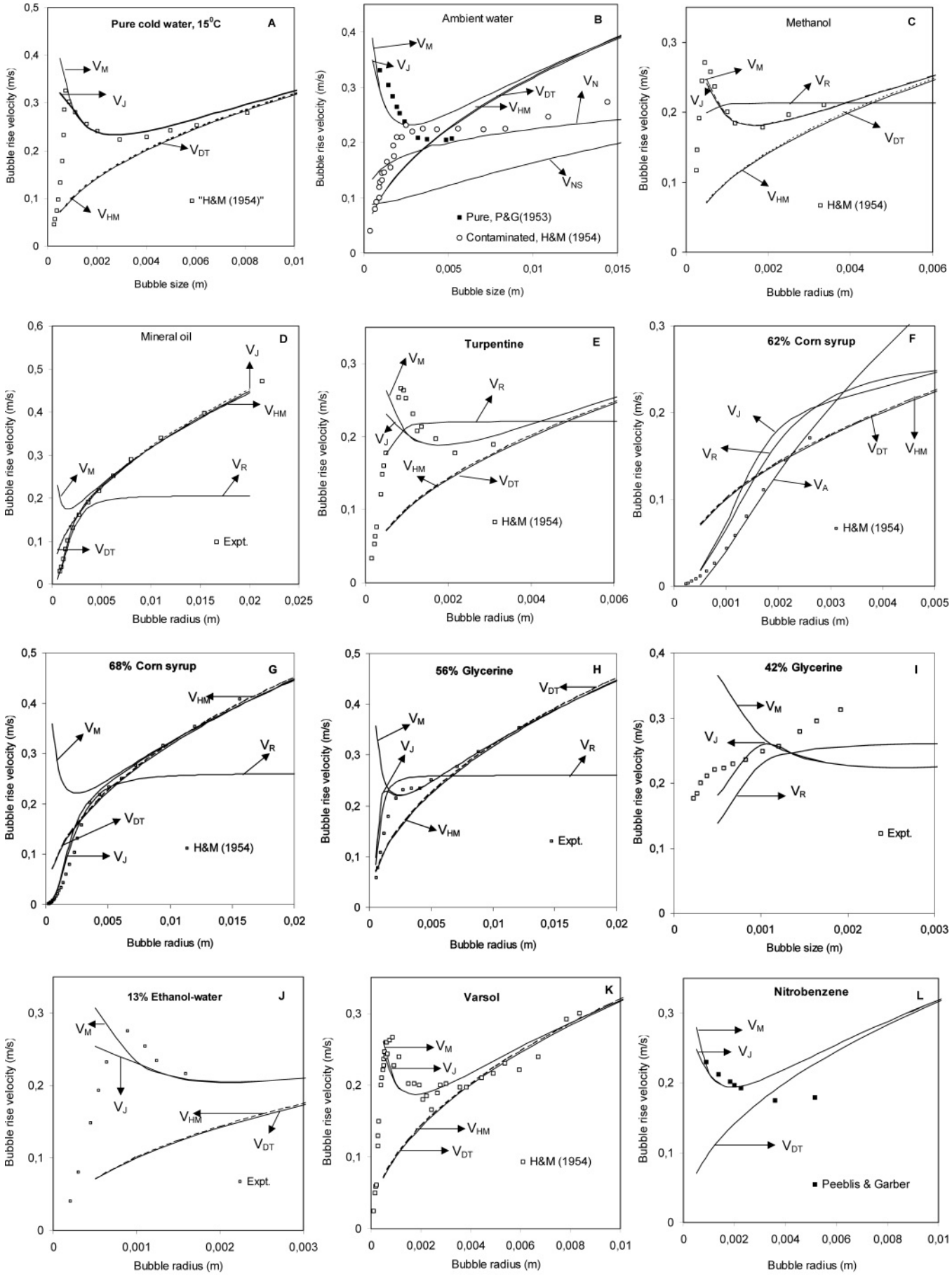
Pure cold water, 15°C
A
Bubble rise velocity (m/s)
Bubble size (m)
"H&M (1954)"
Ambient water
B
Pure, P&G(1953)
Contaminated, H&M (1954)
Methanol
C
H&M (1954)
Bubble radius (m)
Mineral oil
D
Expt.
Turpentine
E
62% Corn syrup
F
68% Corn syrup
G
56% Glycerine
H
42% Glycerine
I
Bubble size (m)
13% Ethanol-water
J
Varsol
K
Nitrobenzene
L
Peeblis & Garber

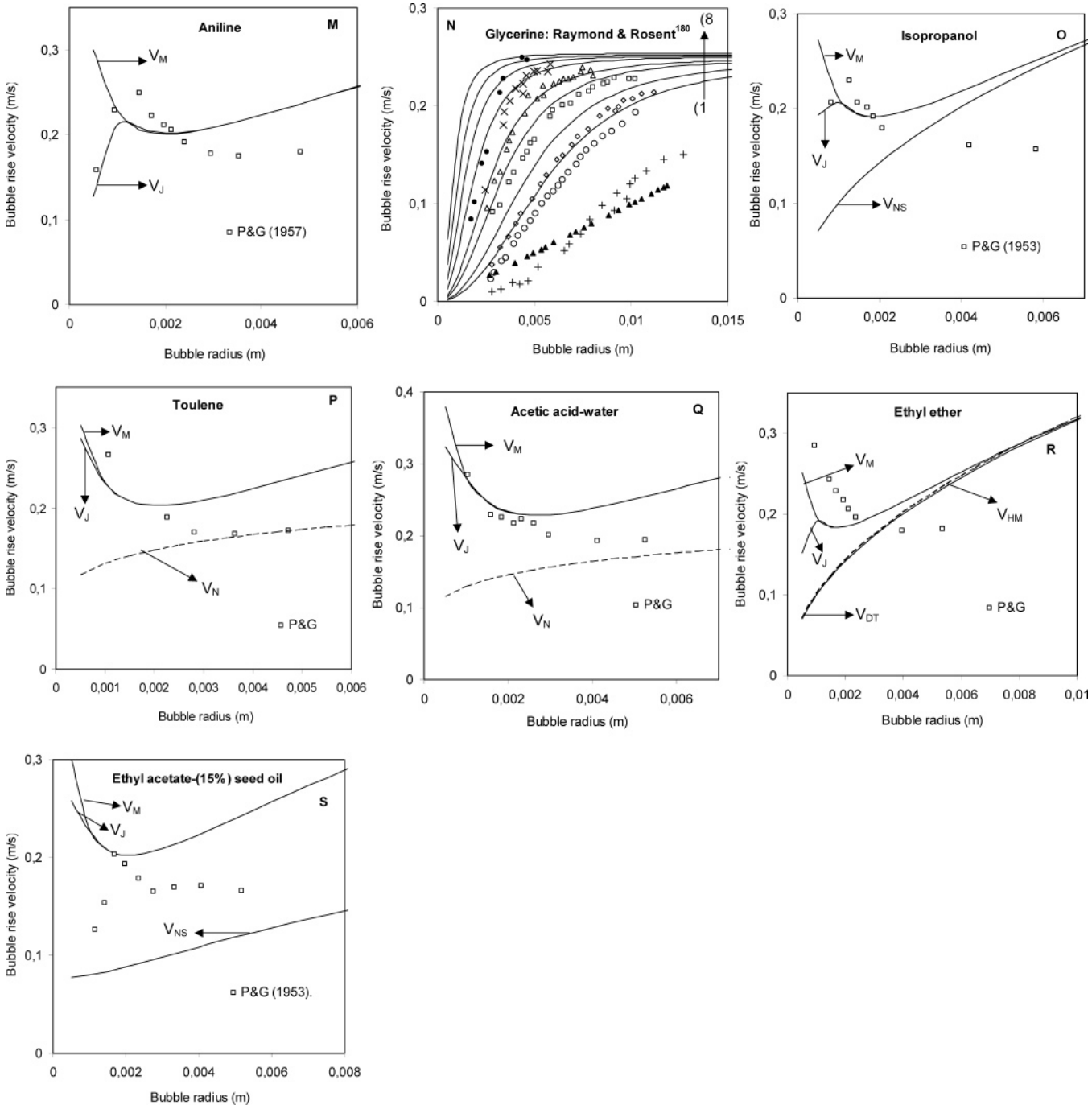

Figure 16. Comparison of predictions by various correlations with published experimental data. (Abbreviations for the different authors: Abou-el-Hassan[149] [V_A], Davies and Taylor[198] [V_{DT}], Haberman & Morton[207] [V_{HM}], Mandelson[190] [V_M], Nickens and Yannitell[195] [V_{NS}], Nguyen[155] [V_N], Rodrigue[153] [V_R], Jamialahmadi et al.[196] [V_J]). Experimental data is shown in symbols and lines indicate the predictions. For the data by Raymonds & Rosent[209] (N) for Glycerine solution of different viscosities (cP), the numbers in the bracket ( ) indicate the predictions while symbols indicate the experimentally measured rise velocities in the respective viscous solutions. (1) + 1250, (2) ▲ 1245, (3) ○ 1230, (4) ◇ 1222, (5) □ 1205, (6) Δ 1190, (7) × 1172, (8) ● 1150.

number. According to his correlation

$$V = \frac{F}{12}\left[\frac{(1 + 1.31 \times 10^{-5}\mathrm{Mo}^{11/20}\mathrm{F}^{73/33})^{21/176}}{(1 + 0.02F^{10/11})^{10/11}}\right]$$

where

$$V = V_T\left(\frac{\rho^2 d_b^{\ 2}}{\sigma\mu}\right)^{1/3} \text{ and } F = g\left[\frac{\rho^5 d_b^{\ 8}}{\sigma\mu^4}\right]^{1/3} \qquad (84)$$

3.2.3. Approach through Wave Analogy. In an innovative attempt, Mendelson[190] proposed wave theory for prediction of bubble rise velocity. In his analogy, he assumed bubbles interfacial disturbances for which their dynamics are similar to those of waves on an ideal fluid and can be correlated in terms of the fluid properties and bubble size (r) for the terminal rise velocity of a bubble as

$$V_T = \sqrt{\frac{\sigma}{r\rho} + gr} \qquad (85)$$

The results have shown very good agreement with the experiments except for very small bubbles (<0.5 mm),

where the surfaces are rigid and as no interfacial disturbances are present no waves are formed. Figure 16 shows the comparison of the predictions from wave analogy for different experimental data. The theory was modified by Lahrer[194] who argued that during rise, potential energy associated with bubble is converted into kinetic energy, followed by its dissipation in the wake, which on incorporation in the wave analogy resulted in

$$V_T = \left(\frac{3\sigma}{2\rho r} + \frac{rg\Delta\rho}{\rho}\right)^{0.5} \quad (86)$$

Mendelson's wave theory was extended by Maneri[199] for two special cases of rise of a planar bubble and the rise in a rectangular duct. The final equations for the bubble rise velocity follow the wave analogy but their applicability is restricted toward the limited cases, which are not common in practice. The comparison of the various experimental data sets over a wide range of liquid properties is shown in Figure 16.

Jamialahmadi et al.[196] has used the wave analogy and modified the correlation by Hadamard,[144] i.e., no slip at the boundary for the rise velocity of bubbles for a wide size and shape range. The correlation is given in Table 4 and it is worth mentioning that for the case of pure liquids, correlation by Jamialahmadi et al.[196] yields excellent results when compared with the experimental data for various pure liquids (Figure 16).

In addition to the few known approaches of understanding the variation in terminal rise velocity with bubble size in various liquid that are discussed earlier, one of the ways is through the variation in the drag coefficient (C_D) with Re. This particular approach and the corresponding developments are discussed separately.

3.3. Bubble Rise Velocity in Non-Newtonian Liquids. Rheological behavior of non-Newtonian liquids is complex and the motion of bubbles in these liquids has different characteristics than observed in Newtonian liquids. As mentioned earlier, the jump in rise velocity and early transition in the shapes are few of the peculiar characteristics of bubbles in a special class of non-Newtonian liquids. Depending upon the type of liquid, the rheological properties change and hence the critical bubble size. Chhabra[200] has reviewed the published literature in detail, whereas Dekee et al.[176] has listed the transition bubble volumes for various viscous Newtonian and non-Newtonian liquids. However, it is required to compare the different methods of investigation and results from different theoretical studies. Most of these studies are carried out to develop a correlation between the C_D and Re. The complexity in the estimation of C_D as well as Re is due to the time dependent viscosity as well as its effect on the bubble shape. Non-Newtonian liquids mainly considered in most of the studies can be categorized in two classes, shear thinning liquids and structural viscous liquids. In shear thinning liquids, the apparent viscosity (i.e., ratio of shear stress by strain rate) decreases with increasing shear rate. Prediction of the thinning characteristics is solely a function of the time dependent shear rate variation and can be written as a power-law model in terms of the consistency index (m) and flow index (n), where for these kind of liquids, $n < 1$. Typically, the shear stress (τ) can be given a function of shear rate (γ) as $\tau = m\gamma^n$. Depending upon the nature of flow and the operating conditions, the formulation for viscosity takes different forms. Before starting with various models, for the case of viscous Newtonian and power-law non-Newtonian liquids it is important to note that, in these cases, the modified viscosity i.e., $\mu = m(U/D)^{n-1}$ is used instead of molecular viscosity. With the earlier explained reasons behind the jump in rise velocity in Section 3.2, here we have given stress on the attempts that are made to possibly explain this phenomenon theoretically and some of the experimental observations by various investigators.

Recently, Rodrigue et al.[173] has developed criteria for jump conditions based on the drag analysis. According to their analysis, the drag coefficient in an incompressible fluid can be given as

$$C_D = \frac{16}{Re}\left[2^{n-1}3^{(n-1)/2}\frac{1 + 7n - 5n^2}{n(n+2)}\right] \quad (87)$$

where Re is for the non-Newtonian fluids. According to their analysis, for meeting the jump condition, a bubble has to follow a condition, $\alpha = CaDe/Ma \sim 1$, where $Ca = \eta_0 V_T/\sigma$ is the capillary number, $De = N(\gamma)/2\tau$ is the Deborah number (with $N = a\gamma^b$ represents the power law relation for primary normal stresses) and $Ma = \Delta\sigma/(\tau R)$ is the Marangoni number with $\Delta\sigma$ being the difference in the surface tension of the pure solvent, and the solution and R is the equivalent bubble radius. Here, α represents the balance between different forces acting on bubble and it clearly indicates that it is required to reach a particular condition where all the parameters lead to $\alpha = 1$ causes a jump in the bubble velocity. Thus, at the rear stagnation point, the local stresses are large and cause high curvature and local deformation. Generation of high normal stresses in this region cause the contaminant molecules to get stretched and induce a change in the fluid properties. Thus, the action of the normal forces in the vicinity of the bubble result in removing the contaminant molecules from the bubble surface causing a sudden change in the interfacial conditions, which finally may lead to the jump in rise velocity. Further, since on the rear stagnation point the unidirectional flow is continuous it may lead to removal of contaminant molecules thus helping the jump condition. However, this process need not be restricted for certain bubble size but needs to be verified for smaller bubbles for longer time, which may show similar features depending upon the extent of surface contamination.[200]

We begin with an industrial process where the nature of liquid has utmost importance in controlling the flow regime. In fermentation processes, the rheological behavior of the liquid changes from Newtonian in the beginning to non-Newtonian at the end of the reactions. Although very less attention has been paid in this interesting phenomenon, recent studies by Margaritis et al.[171] on the effect of such a transition on the rise velocity of single bubble are encouraging in terms of experimental observations. The important feature being the dynamics associated with the rise velocity, it is indeed required to follow the dynamics of viscosity, which would decide the nature of C_D vs Re curve. Since the flow index of the liquids used here is in the range of 0.63 and 0.68, these authors have followed the suggestion of estimating the drag coefficient using Hadamard−Rybczynsky[202] correlation by Miyahara and Yamanaka.[203] Their observations in CMC, xanthan gum, Na-alginate, dextran and pullulan showed that for constant shear rate, the shear stress decreases with

concentration and can be correlated by power law. Further, they have also reported that for same concentration of the above six liquids, the mean rise velocity was a strong function of the K and n, and for the same fluid, the drag coefficient plot did not show much variation for different concentration values. For the solutions of pullulan they observed different nature of the drag curve for bubbles of different shapes. Unlike other investigators, these studies did not show any jump in the velocity with change in the regime of bubble motion. The generalized correlation proposed by these authors clearly shows deviation from the experimental data where the drag coefficient is proposed to remain constant after $Re > 135$. Further, the conclusion based on the experimental drag curve that most of the bubbles would be in Stokes region in Newtonian liquids is not acceptable as the spread in the data clearly shows the discrepancy and demands modification in the correlation in terms of the dynamic nature of viscosity. Rodrigue[154] has followed the similar approach for the prediction of drag coefficient in various power law non-Newtonian liquids as in Newtonian liquids. Since the approach adopted here is the same as discussed earlier, the dimensional analysis has suppressed the actual information to a great extent and error in the predictions makes the model unacceptable. However, the modification in the formulation based on the variable Morton number has shown that the following correlation for velocity and bubble diameter at the minimum in the C_D-Re curve hold very well.

$$V_{Tm} = 1.37\left(\frac{g\sigma}{\rho}\right)^{1/4} \text{ and } C_{Dm} = \left(39.9\frac{m}{\rho g}\right)^{1/(n+1)}(V_{Tm})^{n/(n+1)} \quad (88)$$

The above discussion evidently shows a requirement for the development of correlation based on the dynamics of bubble shapes and their rise velocity.

Few other attempts include Barnett et al.,[204] Haque et al.,[205] Margaritis et al.,[171] Miyahara and Yamanaka[203] who studied the rise velocity in highly viscous Newtonian and non-Newtonian liquids. Their analysis mainly focuses on the shape variation in bubble at various ranges of physicochemical properties and it indicates that irrespective of type of liquid, the rise velocity increases with bubble size, however, it brings out the need to incorporate the extent of deformation and associated oscillation frequency in the model. Dekee et al.[176] have shown that for the viscous Newtonian liquids, the rise velocity is a weak function of the bubble volume, while for non-Newtonian liquids, it has a linear dependence but the velocities in the earlier case are much higher than the later. Their observations are correlated and given in Table 4. Their experimental observations clearly show that with addition of a shear thinning liquid (1% PAA) in a viscous Newtonian solution (glycerol−water), the rise velocity decreases drastically. Figure 17A shows the comparison of predictions from the correlations by Miyahara and Takahashi[206] for pure liquids, where different correlation are used for different ranges of Re.

3.4. Comparison of Correlation for Bubble Rise Velocity in Pure and Contaminated Liquids. Stokes[188] derived the simplest and the earliest known correlation resulting from force balance on very small bubbles in a quiescent liquid (eq 76), however, the applicability of this equation is indeed limited for the very small sized bubbles mainly in contaminated liquid,

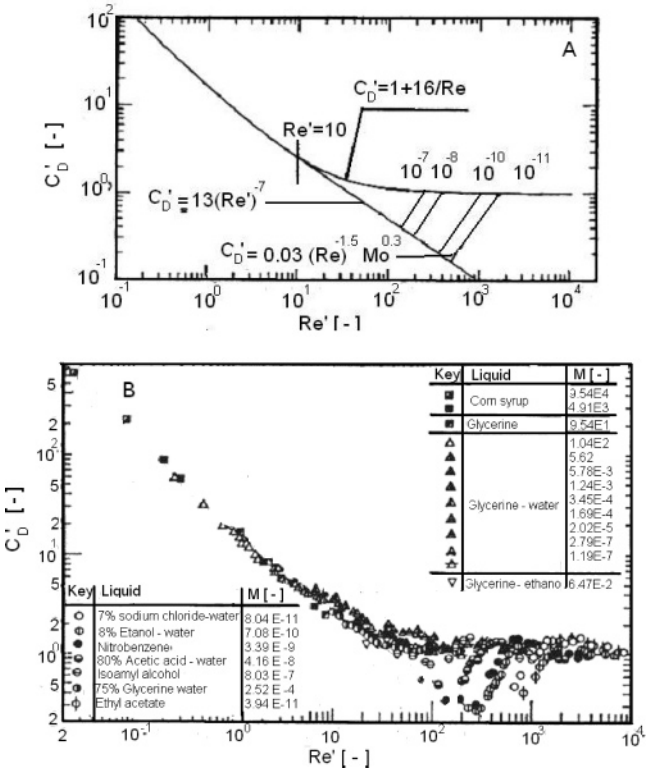

Figure 17. Typical drag curves for bubble motion in liquid. (C_D vs. Re for different liquids) (reproduced with permission from Peelis and Garber[187]).

where the internal circulation is almost minimal. The above statement is found true for the polymeric liquids (Newtonian) where for very small sized bubbles the viscous forces are strong enough to resist any surface motion as well as internal circulation and result in a rigid surface. The comparison of the experimental data for very small bubbles in a pure liquid system is found never to match with the predictions by the Stokes formulation as the rise velocities are always higher, while for the contaminated liquids with low viscosity, the deviation between predictions and experimental data is noticeable which diminishes with increase in the liquid viscosity. It shows an inherent inability to show a good match with most of the experimental data, except for the viscous non-Newtonian liquids below critical bubble size. In the next attempt in this direction Habberman and Morton,[207] (will be referred hereonward as HM) proposed rise velocity only as a function of bubble size under the assumption that the velocity is independent of the physical properties of liquid. Although the resulting correlation is simple, its limited applicability may be only for the data by few investigators[17,51,52,58] who have observed negligible effect of viscosity on size and Davidson and Schuler[4] who propose no effect of surface tension specifically for the case of constant gas flow rate system. A poor agreement was observed on comparison of the predictions from the correlation by HM with the experimental data for several pure liquids (Figure 16). Density difference between the two phases being the most important parameter for rise of a bubble (which is not taken into account), the validity of this correlation is suspicious. Its applicability is restricted for very small bubbles in contaminated liquid, where (i) irrespective of viscosity bubble surface is rigid, (ii) Eo is also very small, and (iii) it does not depend on viscosity. As a result, although Mo varies over a wide range bubble rise velocity is

simply a function of its size. However, a large number of other studies have shown a noticeable effect of viscosity and surface forces on size. We prefer to mention that, the discussion in this subsection is based on the results available in the literature and comparison we have shown in Figure 16.

For pure Newtonian liquids, the correlation by Davis and Taylor[198] is applicable only for large size spherical cap bubbles which for the available experimental data of Devenport et al.,[208] shows a very good match in low-density liquids. Correlation by Clift et al.[148] gives good predictions for the pure liquids as it even takes into account the shape variation in a bubble through the use of dimensionless numbers (viz. Ta), however, the method of estimation includes numerous iterations to reach the final value of velocity for each size. It is generally preferred to follow simpler formulation for design purpose. Formulation by Karamanev[197] is an extension to that by Clift et al.[148] which is generally applicable under the assumption of rigid surface irrespective of its shape and this procedure also requires tedious iterative calculations. The interesting part is that this formulation is bubble shape dependent and hence can be used for the correct estimation of the drag coefficient over a wide range of *Re*, however, it is required to quantify the difference in the drag coefficient arising out of a rigid and a free surface. In a recent attempt Rodrigue[153] has correlated most of the published data on pure Newtonian liquids. It is to be noted from the method of analysis that the dimensional analysis loses the sensitivity for few of the parameters whereby the effect of physical properties cannot be understood from the variation in velocity with size. The comparison of the predictions by Rodrigue's[153] formulation with the experimental data of Reymonds et al.[209] for bubble rise in aqueous glycerol solutions shows excellent match for liquids with relatively low viscosity, while for higher viscosities, predictions deviate by about 15%.

Correlation by Nguyen[155] for contaminated liquids stands well for the Newtonian liquids. The correlation suits very well for a range of bubble sizes and follows the curve for contaminated liquids given in Clift et al.[148] The available data for such studies is from the flotation of minerals and the correlation is found to give excellent match for such data. However, the lack of data in contaminated liquids of different properties is the bottleneck for the thorough validation of this correlation over a range of parameters.

Wave analogy based correlation by Mendelson[190] is found to be suitable for various pure liquids only after the region of very small bubbles where the rise velocity increases with size and reaches maximum followed by a decrease in the velocity. The correlation is not suitable for the bubbles in viscous systems viz. glycerol solution, corn syrups, except for the glycerin solutions of various concentrations and few of the oils. However, in low viscosity oils and other organic liquids the comparison is reasonable but not completely acceptable. Indeed, the experimental data would also get corrupted to some extent due to the possible small trace of impurity/contamination present in the liquid or even in the gas phase. But the other modified forms of the wave analogy by various investigators have shown some success for pure liquids. The predictions from correlation by Jamailamhadi[196] show an excellent agreement with the experimental data for liquids over a wide range of physical properties (i) low viscosity organic liquids (i.e. Aniline, nitrobenzene, etc.), (ii) low-density viscous oils (olive oil, caster oil, mineral oil, hydrocarbon oil, cotton seed oil, turpentine, etc.), (iii) viscous Newtonian liquids (aqueous solutions of glycerin and glycerol, varsol, etc.). For the case of viscous solutions of Glycerol in water, the correlation is found to agree with the experimental data discretely indicating that, the correlation should follow a smooth variation in bubble shape provided the surface tension should also vary with viscosity. In most of the cases, the surface of bubbles is rigid approaching the state of contaminated Newtonian liquids with higher viscosity either due to dominant surface forces or viscous forces. The correlation also gives excellent match with the data for pure water in cold as well as ambient conditions.

Trends obtained from the geometry based correlation by Davis and Taylor[198] are restricted for spherical caps in various systems, but the deviation of the predictions shows that even for spherical cap shapes, since the shape depends on the physical properties of liquid, it would be unsafe to use a geometry based correlation. Similar analysis also applies for Habberman and Morton's correlation.[210] Correlation by Abou-al-hassan[149] successfully correlates the flow number (F) and velocity number (V) estimated for a range of experimental data, however, in the form of dimensionless numbers, the denominator of the dimensionless numbers is very high as compared to the numerator and thus sensitivity to the variation with respect to various parameters is lost. This correlation may be used to check the validity of the experimental data by checking the nature of variation in terms of V and F for Newtonian liquids. Here, we can conclude that correlation by Jamialahmadi et al.[196] can be used for various pure liquids however the correlation needs to be modified for its applicability even for contaminated liquids, for which one by Nguyen[155] can be used.

The results from the correlation, when compared with the experiments, clearly show that the region of rise velocity being independent of the size does not show any match and hence it is required to improve-upon the correlation for that particular region.

3.5. Drag Coefficient for Bubbles in Liquids. Since it is not always possible to obtain the rise velocity directly, its variants viz. drag coefficient (C_D), *Re* are estimated and a correlation is developed for understanding the relationship between size and velocity. Most commonly, the relation between bubble rise velocity and the size is seen through the variation in C_D with *Re*, provided, for nonspherical bubbles the effect of physicochemical properties of gas−liquid system is incorporated into the correlation. The most important effect of viscosity on the displacement of a flow past body is to produce a drag force which slows down its relative motion in the surrounding fluid. Conceptually, drag coefficient is analogous to Fanning friction factor[211] but the formulation is complex as it is a result of both, the form drag and skin drag. In the past decade, Karamanev and Nikolov[212] experimentally showed that the trajectory of free rising solid particles in Newtonian fluids is different from the free falling particles, until then it was assumed that the free rise of buoyant particles should obey the laws of free settling of heavy particles. They also reported that the terminal rise velocity of free rising particles is much lesser than the falling ones. For the detailed analysis of this phenomenon, reader may refer to Karamanev,[213] where it is shown that the free rise

characteristics of light rigid particles are similar to those of bubbles. Before discussing more onto the drag coefficient of bubbles, here we briefly discuss the subject of the drag force.

Production of drag force that tends to slow the relative motion of a body is one of the most important effects of viscosity on the displacement of a body in a fluid. Although the theory is well characterized for the low *Re* regime, a complete understanding of bluffed bodies moving at high *Re* needs more careful analysis. For the contaminated bubble surfaces, the low *Re* theory is well applicable. This is mainly because of the zero shear stress for the tangential component of the liquid velocity which allows the liquid to slip along the surface of the bubble leading to unseparated flow in its wake and changes the mechanism of the vorticity production on the surface of the bubble.[214] The drag force (F_D) determined from a balance between the rate of work done by the drag force and the viscous dissipation within the fluid interior, which leads to its formulation as

$$F_D = \frac{C_D \rho V_T^{\,2} A}{2g} \tag{89}$$

where C_D is the proportionality constant and for low *Re*, it can be given as

$$C_D = 48/\mathrm{Re} \tag{90}$$

In reality, this correlation[215,159] changes depending on the range of *Re* and also the physicochemical properties of the liquid. Importantly, Kang and Leal[216] have shown that the pressure variation over a bubble surface accounts for one-third of the total drag in eq 90, while the rest of it is provided by the normal viscous stress. The formulation in eq 90 is further corrected by Moore[217] by taking into account the boundary layer thickness at different surface regions of a bubble. Several numerical attempts in this direction can be seen in the literature.[218−226] It is known that C_D decreases linearly with increase in Re. The most general formulation for C_D can be given as

$$C_D = \frac{24}{Re}\frac{2 + 3(\mu_D/\mu_C)}{3 + 3(\mu_D/\mu_C)} \tag{91}$$

i.e., for the case of passage of gas bubble into liquid, value of the term in bracket is negligible and correlation tends to $C_D = 16/Re$, whereas for the case of solid−liquid system, $C_D \approx 24/Re$. thus the value of C_D at a particular *Re* are bounded in this range. However, the experimentally obtained C_D values have shown different trends in variation with *Re*, which has encouraged many investigators to propose various formulation for C_D. Here, we have reviewed many such attempts and have compared their results to recommend the most suitable formulation applicable over a wide range of parameters. For the detailed discussion of the drag force in a bubbly flow, reader may refer to Magnaudet and Eams[143] and Miyahara and Takahashi.[206]

The values of C_D depend on the system's physicochemical properties and the bubble dimensions. Before discussing the dependence of the drag coefficient on different parameters, here we summarize three distinct regions that show a different dependence on the bubble rise velocity. (1) A first region (viscosity-dominated), for very low Reynolds number, in which bubbles are spherical, viscosity forces dominate the terminal motion and terminal velocity increases with diameter. (2) An intermediate region (surface-tension-dominated), in which surface tension and inertia forces determine the terminal velocity. Bubbles are no more spherical in this region and terminal velocity may increase or remain constant or decrease with equivalent diameter. According to Clift et al.,[148] at least for air−water systems this regime holds for about $0.25 < Eo < 40$, however the boundaries (especially the lower one) are somewhat arbitrary. (3) A last region (inertia-dominated), for high *Eo*, in which the bubbles are spherical-cap or bullet-shaped and the motion is dominated by the inertia forces. Velocity increases with equivalent diameter in this regime.

In continuation to the above explanation, for very small sized bubbles, ($Re < 2$) Stokes law is obeyed, whereas for $Re > 2$, departure from Stokes law is significant and correlation for the drag coefficient shows relatively weak dependence on *Re*. However, with departure from Stoke's regime bubble shape also changes and also with transition from the clean to contaminated liquids, the extent of internal circulation also changes which requires the surface properties also to be incorporated into the correlation.[227] The nature of bubble rising in pure liquids and the contaminated liquids are completely different and the same is with its rise velocity. For example, air bubble behaves like solid spheres only until a certain critical *Re*, beyond which, it changes its shape and a slip will be associated with its motion. Rosenberg[227] has made an attempt to identify critical *Re* (Re_{crit}) and found that Re_{crit} for the distilled and contaminated water are 40 and 130, respectively. In the case of the rigid spherical bubbles, internal circulation is absent and this condition can even be achieved if the liquid is contaminated with surfactants resulting into constant drag coefficient. Many investigators have formulated several correlation for the prediction of drag coefficient in Newtonian[148,187,206,223] and non-Newtonian[151,153,173,228] liquids which are summarized in Table 5 and few are discussed here.

For the case of contaminated Newtonian liquids, Karamanev[213] has formulated the drag coefficient as

$$C_D = \frac{24}{Re_t}(1 + 0.173 Re_t^{\,0.657}) + \frac{0.413}{1 + 16300 Re_t^{\,-1.09}} \quad \text{for } Re < 135 \tag{92}$$

and $C_D = 0.95$ for $Re > 135$, where the value of Re_t for a spherical particle in power-law fluid can be given as $Re_t = d_p^{\,n} V_t^{\,2-n}\rho/K$, which for nonspherical axisymmetric particles becomes $Re_t = d_h^{\,n} V_t^{\,2-n}\rho/K$, where d_h is the diameter of the horizontal projection of bubble.

Kamaranev[197] has given the rise velocity of single bubble in quiescent liquids in terms of the drag curve under the assumption that the difference between the drag coefficients given in the literature and that of the solid particles is only due to the use of equivalent diameters as measure of the bubble size. Further, for taking into account the departure from spherical shapes, the surface area was determined using the projected diameter of the horizontal plane and the modified equation for drag coefficient appears as

$$C_D = \frac{4g\Delta\rho d_B^3}{3\rho d_h^2 V_T^2} \tag{93}$$

The range of parameters used for checking the validity

Table 5. Correlations for Drag Coefficient (C_D)

investigator	systems under consideration/ bubble shapes	correlation	applicability
Levich[215]	Single clean bubble in water	$C_D = 48/Re$	Applicable for the systems, with free surface and energy transferred to liquid is directly dissipated into internal energy.
Peebles & Garber[187]	Single bubble rise in water, 2-propanol, ethyl ether, pyridine, nitrobenzene, aniline, acetone, *n*-butanol, methanol, benzene, toluene, ethyl acetate, cotton seed oil, glacial acetic acid	$C_D = 24Re^{-1}$	Bubbles with $Re < 2$ rise rectilinearly. Applicable for the region where C_D decreases with Re.
		$C_D = 18.7\ Re^{-0.68} = \frac{8rg}{3V_\infty^2}$	$Re > 2$, till the range where CD abruptly starts increasing with Re.
		$C_D = 0.0275\left(\frac{g\mu^4}{\rho\sigma^3 g^3}\right)Re^4,\ Re > 4.02Mo^{-0.21}$	Region, where C_D increases with Re and depends on the Mo to a noticeable extent.
		$C_D = 0.82\left(\frac{g\mu^4}{\rho\sigma^3 g^3}\right)Re$	C_D is independent of Re, dominance of physicochemical properties of liquid is more than Re.
Moore[217]	Clean spherical bubbles	$C_D = \frac{48}{Re}\left(1 - \frac{2.21}{Re^{0.5}}\right) + O(Re^{-11/6})$ and $C_D = 5.66Mo^{0.2}We^{-3/5}f^{4/5}$	Bubble is associated with a thin boundary layer and wake. The formulation takes into account the dissipation occurring in the above two regions.
		$We = 4x^{-4/3}(x^3 + x - 2)\left[\begin{matrix}x^2\sec^{-1}x \\ -(x^2-1)^{1/2}\end{matrix}\right]^2(x^2-1)^3$	x is the deformation factor or the aspect ratio in the case of ellipsoidal bubbles.
		$f = 0.4x^{4/3}\left[\frac{(x^2-1)^{0.5} - (2-x^2)\sec^{-1}x}{x^2\sec^{-1}x - (x^2-1)^{0.5}}\right]$	
Taylor and Acrivos[223]	Clean spherical bubbles	$C_D = \frac{16}{Re} + 2$	Limited applicability mainly in contaminated liquids with negligible internal circulation.
Takahashi et al.[228]	1.19e-7 < Mo < 1.04e2	$C_D' = 1 + \frac{16}{Re'}$	Applicable for $Mo > 10^{-7}$, where C_D decreases with Re.
		$C_D' = 13Re'^{-0.7}$	$Mo < 10^{-7}$, $Re > 10$, where C_D increases with Re.
Bhaga and Weber[229]	Bubbles in viscous fluids	$C_D = [2.42 + (16/R)^{0.9}]^{1/0.9}$	Excellent match for various viscous liquids for Mo > 0.004.
Miyahara & Takahashi [206]	$Mo > 10^{-7}$	$C_D' = 0.03(Re')^{1.5}Mo^{0.3}$	Applicable also for nonspherical bubbles in the range, where Takahashi's correlation cannot be applied. Prior knowledge of the shape factor is required.
Turton and Levenspiel[230]	Spherical bubbles in contaminated liquids.	$C_D = \frac{24}{Re}(1 + 0.173Re^{0.657}) + \frac{0.413}{1 + 16300Re^{-1.09}}$	Applicable for rigid bubbles with Re < 130.
Delnoij et al.[231]	Spherical bubbles in water.	$C_D = \frac{24}{Re}(1 + 0.15Re^{0.687})$ for $Re < 1000$	Applicable for a bubble swarm with
		$C_D = 0.44$ for $Re > 1000$	
Ford & Loth[232]	Ellipsoidal clean bubble	$C_D = e^{[2.1785\ln(\mathrm{Re}) - 15.054]}$	Formulation is yielded from the measured terminal velocity for successively increasing bubble diameters. Applicability is limited for the case where C_D increases with Re.
Kendoush[233]	Bubble swarm in Newtonian liquid	$C_D = 48/Re(1-\alpha)^2$, α: void fraction	For known bubble size, its velocity can be predicted at various gas void fractions in bubble swarm.
Rodrigue[153]	Viscous fluids	$C_D = \frac{16}{Re}\left[\left(\frac{1}{2} + 32\Theta + \frac{1}{2}\sqrt{1 + 128\Theta}\right)^{1/3} + \left(\frac{1}{2} + 32\Theta - \frac{1}{2}\sqrt{1 + 128\Theta}\right)^{1/3} + 0.036\left(\frac{128}{3}\right)^{1/9} Re^{8/9}\, Mo^{1/9}\right]^{4/9}$ where $\Theta = (0.018)^3\left(\frac{2}{3}\right)^{1/3} Re^{8/3}Mo^{1/3}$	Applicable for a wide range of bubble sizes rising through various viscous liquids.
Margaritis et al. [171]	Applicable for deformed bubbles	$C_D = \frac{16}{Re}(1 + 0.173Re^{0.657}) + \frac{0.413}{1 + 16300Re^{-1.09}}$	Suitable for bubbles in viscous non-Newtonian liquids. Modification is necessary to incorporate the region, specific to correlation by Miyahara and Takahashi[81]

Mei & Klausner[144]	Clean spherical bubbles	$C_D = \frac{16}{Re}\left\{1 + \left[\frac{8}{Re} + \frac{1}{2}(1 + 3.315Re^{-0.5})\right]^{-1}\right\}$	Valid for all Re.
Sadhal and Johnson[234] (1983)	Clean bubble rising in contaminated liquid	$C_D = \frac{C_{D,rigid} - C_{D,mobile}}{2\pi}(2\phi + \sin\phi - 2\sin(2\phi) - 0.33\sin(3\phi)) + C_{D,mobile}$ where ϕ is cap angle dependent on the truncation point.	Useful for analyzing the effect of contamination on the rise velocity of spherical cap shaped bubbles.
Tomiyama[185]	Newtonian liquids	$C_D = \begin{cases} \frac{8}{3}\frac{Eo}{(\gamma E)^{2/3}(1-E^2)^{-1}\,Eo + 16E^{4/3}}F^{-2} & \text{for } E < 1 \\ 6\gamma^{-1/3} & \text{for } E = 1 \\ \frac{8}{3}\frac{\gamma^{1/3}Eo}{(\gamma E)^{2/3}(E^2-1)^{-1}\,Eo - 16E^{4/3}}G^{-2} & \text{for } E > 1 \end{cases}$ where $E = b/a$, γ is the distortion factor $F = \frac{\cos^{-1}E - E\sqrt{1-E^2}}{1-E^2}$ and $G = \frac{E\sqrt{E^2-1} - \tanh^{-1}(E^{-1}\sqrt{E^2-1})}{E^2-1}$	Applicable for pure and contaminated bubbles of all possible shapes in Newtonian liquids.
Rodrigue[157]	Newtonian liquids	$C_D = \frac{16}{Re}\frac{(1 + 0.02Y^{10/11})^{10/11}}{X^{21/176}}$ where $X = (1 + 1.31 \times 10^{-5}Mo^{11/20}Y^{10/11})$ $Y = \left[\frac{3}{4}C_D\,Re^2\,Mo\right]^{8/9}$	Suitable for all Newtonian inviscid and viscous liquids. It gives an excellent fit even for the region, where the effect of surface tension is taken over by the viscous forces that mobilize the bubble surface. Shows excellent comparison for the data for water, different concentrations of glycerin in water, ethanol, mercury, and molten silver.

of this equation is given in Table 5. From his experimental studies and the observations based on the solid bubbles' motion, it has been concluded that the internal recirculation has no detectable effect of the dynamics of the bubble rise in contaminated liquids. The semi-analytical correlation for the rise velocity from above observations is given as

$$V_T = 40.3V^{1/6}\frac{d_e}{d_h} = 40.3V^{1/6}aTa^b \tag{94}$$

where 'a' and 'b' are empirical constants. Further, since the correlation takes into account the variation in aspect ratios, it can be transformed into various other correlations specific to particular bubble shape. Tadaki number (Ta) can have various ranges pertaining to different bubble shapes and hence the coefficients 'a' and 'b' change accordingly. Since the Ta and C_D both depend on the bubble rise velocity, the equation becomes complex and solution procedure to converge at a particular value is tedious.

Since in the above correlation, the rise velocity is dependent on the bubble drag coefficient and the procedure for the estimation of drag coefficient is numerically tedious. In view of this, Nguyen[155] has developed simplified approach for the prediction of terminal rise velocities in contaminated liquids through the use of Archimedes number ($Ar = D^3\delta^2 g/\mu^2$) and Lyashchenko number ($Ly = V_\infty^3\delta/g/\mu$). The correlation for C_D follows the improvement by expressing it in terms of Mo and Re as

$$C_D = \frac{8a^2Dg}{3V_T^2}Mo^{0.46b}Re^{2b} \tag{95}$$

and used the same for expressing modified Ar and Ly. Since the bubble shape also reflects into the values of Re, different correlations were developed for various ranges of Re, i.e., different shapes (Figure 15). For the range below $Re < 130$, the correlation is a modified version of Stokes' equation.

$$V_T = V_{St}\left\{1 + \frac{Ar/96}{(1 + 0.079Ar^{0.749})^{0.755}}\right\}^{-1} \tag{96}$$

It even takes into account the deviation in terminal rise velocity with rigidity of bubble. For higher Re, it was assumed that terminal rise velocity is independent of Re and the correlation was modified in terms of only Ar and Mo as

$$V_T = \sqrt[3]{\frac{g\mu}{\delta}}\left\{\frac{4a^2Mo^{0.46b}}{3C_D}\right\}^{1/(2-2b)}Ar^{(2b+1)/(2-2b)} \tag{97}$$

where the drag coefficient was considered to be constant in that range as taken by Karamanev[197] for rising solid spheres. Since the formulation is specific for the contaminated liquids, the assumption of a rigid interface supports the formulation. However, for the liquids contaminated with electrolytes or polymeric dilute solutions, the nature of the drag curve is different, since the bubble shapes deviate from the spherical ones, and hence, checking the validity of this equation against such experimental data is required. The distinct feature of this correlation is its ability to predict the transition point in the Re (~130), where the shape deviates from spherical and also the equation can be reduced to

specific expressions suitable for specific conditions, viz. for very small bubbles, rise velocity can be expressed as a simple function of bubble size and gravity. For a very critical analysis of the drag coefficient based on the comparison of the predictions from various proposed correlation and the experimental values, we recommend the reader to refer to Marco et al.[235] Typical drag curves from the literature are shown in Figure 17. The different correlations for drag coefficient by several investigators (discussed here and also given in Table 5) when put together on the same plot could not clearly bring out their distinct features (due to several overlaps) and hence here we prefer to discuss the nature of different drag curves from the various correlations and their rage of validity.

An empirical drag law (given in Table 5) was proposed by Mei and Klausner[225] is considered to yield accurate drag coefficient at almost all *Re*. In a recent attempt, Tomiyama et al.,[236] have developed a generalized correlation with four coefficients

$$C_D = \max\left\{\min\left[\frac{C_1}{Re}(1 + 0.15Re^{0.687}), \frac{C_2}{Re}(1 - C_3Re^{-0.5})\right], \frac{8}{3}\frac{Eo}{Eo + 2C_4}\right\} \quad (98)$$

and it gives an excellent match with the whole drag curve. The range of the coefficients $C_1 \approx 16-24$, $C_2 \approx 48 - \infty$, $C_3 = 0$, $C_4 = 2$ were found suitable to cover the whole range of Re for different gas−liquid systems. We have discussed the comparison of the predictions from this formulation for different cases in subsection 3.6.

On the basis of the approach by Abou-al-hasan,[149] where *V* and *F* are used for characterizing the rise velocity, recently Rodrigue[153,156] has developed excellent method in correlating bubble rise velocity with governing parameters for various liquids. He has used dimensional analysis to modify the flow number and velocity number and proposed generalized correlation for bubble rise velocity in pure liquids. The results from the model have shown that it gives a very good match with the experimental values for a wide range of data. The rise velocity is shown to follow three different relationships $V_T \propto \mu^{-1}d^2$, $V_T \propto \mu^0 d^0$, $V_T \propto g^{7/16}d^{1/2}$ in laminar, turbulent and intermediate regimes, respectively, which clearly shows its applicability for pure and clean liquids only. For the case of inviscid and viscous Newtonian liquids, the correlation by Rodrigue[157] gives excellent comparison the data experimental for water, different concentrations of glycerin in water, ethanol, mercury and molten silver. The single correlation is capable of even following the trends of the *Re*, where the drag coefficient goes through a minimum and then increases to attain a plateau. However, in this particular region, the correlation seems to under predict the drag coefficient with decreasing *Mo*, and the error is seen to increase with lowering *Mo* value.

Non-Newtonian Liquids. In general, for the non-Newtonian liquids, the drag coefficient is given as

$$C_D = \frac{24}{Re}\frac{2 + 3X_E}{3 + 3X_E}X \quad (99)$$

where $Re = \rho V_T^{2-n}d^n/m$, $X_E = \mu_d/m(V_\infty/d)^{n-1}\}$, and *X* is the drag correction factor. Although the values of '*m*' and '*n*' are the properties of liquid and *X* for various fluids can be expressed in different forms. Chhabra[200] has listed known formulations for *X*. The value of *X* is unity for Newtonian liquids and increases for shear thinning liquids.

Since eq 92 over predicts the drag coefficient for non-Newtonian shear thinning liquids, in an extensive experimental analysis, Margaritis et al.[171] have studied the drag coefficient variation for bubbles over a wide range of *Re* in different non-Newtonian polysaccharide solutions and proposed the following correlation

$$C_D = \frac{24}{Re}(1 + 0.173Re^{0.657}) + \frac{0.413}{1 + 16300Re^{-1.09}} \quad \text{for } Re < 60 \quad (100)$$

and $C_D = 0.95$ for $Re > 60$, where *Re* is estimated using the equivalent bubble diameter. This correlation is shown to give very good match with the experimental data, except in the region of transition and the reason is attributed to the shape changes. However, it is important to notice that the region where the drag curve changes its direction, it goes though a minimum and it mainly depends on the local fluid phase physical properties and hence the local turbulence. Thus, change in shape needs to be taken into account correctly to yield a good understanding of this region, which demands substantial modification of above correlation. This requirement is noticeable from Figure 12 of Margaritis et al.[171]

Recently, Rodrigue et al.[173] has developed a correlation for the bubbles in non-Newtonian viscoelastic liquids. According to their analysis, the drag coefficient in an incompressible fluid can be given as and

$$C_D = \frac{16}{Re}X_{(n)} \quad (101)$$

$$C_D = \frac{16}{Re}Y_{(n)}, \text{ where } Y_{(n)} = [2^{n-1}3^{(n-1)/2}(1 + 7n - 5n^2)/n(n + 2)] \quad (102)$$

depending upon the bubble surface characteristics. $X_{(n)}$ is a correction function dependent on the power-law index *n*. Thus, when the surface is rigid, $X_{(n)}$ can be used, which represents a correlation dependent on the power law index (*n*), while for the case of mobile bubble surface, $Y_{(n)}$ can be used, which characterizes the viscoelastic nature of the fluid. They have shown that in a typical plot of C_D vs *Re*, for viscoelastic liquids, at low *Re*, the variation of C_D follows eq 101 while, on the jump of velocity, the nature of surface changes and it follows the properties of viscoelastic liquid. Thus, before the jump, the drag coefficient can be given using eq 101, while after the jump, it can be correctly given through eq 102. For the case of viscous liquids Rodrigue[154] has made an attempt to take into account the bubble shapes by expressing C_D in terms of *Re* and *Mo*. The correlation is given in Table 5. The predictions from it show excellent comparison for the experimental data by Peebles and Garber[187] and Moore[237] over a wide range of *Mo* ($1.93 \times 10^{-1} < Mo < 7.71 \times 10^{-12}$) for various viscous fluids.

3.5.1. Comparison of the Correlation for Drag Coefficient for Newtonian Liquids. From the various data and comparison available in the literature, we have made the following observations. The selection of the correlation should be made on two bases: applicability for a certain range of *Re* and variation in the shape which reflect upon the nature of drag curve. Correlations given by Miyahara and Takahashi[206] are

sufficiently good to track the experimental drag curve in different ranges however the change in shape (which should be known a priory) is incorporated by modifying the values on abscissa and ordinate through the ratio of equivalent diameter to major axis. The results of the various gas−liquid systems have shown that data matches very well for the modified C_D and *Re*. For the case, where *Mo* is sufficiently high (high viscosity and low surface tension), drag curve follows curve close to that of a rigid bubble. Correlation by Turton and Levelspiel[230] can be used with some modifications toward changing viscosity (for the case of shear thinning liquids). These set of correlation are even found to give excellent match for the experimental data (Figure 17B) by Margaritis et al.,[171] except for the region, where drag coefficient increases with *Re*, where correlation by Miyahara and Takahashi[206] shows excellent agreement. Correlation by Mei and Kalusner[144] suits well for very small bubbles. The plots of comparison of the predictions with the experimental ones show that the drag coefficient cannot be predicted simply from a single correlation and various correlations are applicable for different shape regimes. Among all, the recent correlation by Rodrigue[157] seems to be excellent for the Newtonian liquids (the extent of variation in the C_D in the region, where the shape changes show an effect should be verified with the correlation by Miyahara and Takahashi[206]) properties change, while for the non-Newtonian liquids, (i) correlation by Margaritis et al.[171] is suitable for shear thinning power law fluids, and (ii) for the viscoelastic liquids, the correlation by Rodrigue et al.[173] can be used provided, the correction function should be changed appropriately to account for the variation in the surface properties of bubble.

3.6. Bubble Trajectories. As mentioned in the introductory part, the rise velocity is associated with certain dynamics. So far, we have discussed only the magnitude part of it, while directional component is equally important to understand this vectorial quantity. General aspects of the rise of single medium-sized bubbles (between 1 and 10 mm diameter) produced from an underwater nozzle have been well documented.[148] A detailed observation is discussed in de Vries et al.,[239] where they have experimentally investigated the motion of gas bubbles in highly purified water. In the beginning of bubble size range (<2 mm), smaller bubbles undergo axisymmetric shape oscillations. At a certain height, depending on the conditions and hence the size (>2 mm), bubbles establish an approximately ellipsoidal shape. Feng and Leal[240] have discussed the various possible bubble trajectories in different shape regimes. A single bubble can follow a zigzag path ($Re \approx 600$), coordinated with vortex shedding behind the bubble. However, under the same experimental conditions, the bubble might also follow a spiral trajectory without vortex shedding.[241] The sideways motion of bubbles may contribute significantly to the turbulence generated by bubbles in mixing situations. Furthermore, the overall length of the trajectory influences the residence time of the bubble in the liquid. This is very important for gas absorption. Generally, the dynamics of bubble rise are nonlinear and the extent of nonlinearity increases with bubble size. In a bubble swarm, the trajectories are strongly dominated by the surrounding liquid flow and associated dynamics is more complex. The observations have shown that bubble trajectories have a primary and secondary structure. The primary structure probably represents the greatest kinetic energy, i.e., the sideways oscillation within the spiral part of the trajectory.[242] The secondary structure is the large-scale shape of the trajectory. This is a single path up to a critical height, where it bifurcates into a pair of (or several) intertwined spirals. For smaller bubbles (2.10 ± 0.05 mm) in stagnant liquid, a stable, curved trajectory is reported up to a critical height, which here is about 17 bubble diameters, after which several spiral trajectories may begin. They are also reported to oscillate within the trajectories, but this is less noticeable than similar oscillations made by the larger bubbles. The cross-flow causes the bubbles to spiral immediately and spread of trajectories is proportional to the cross-flow velocity. For bubbles of sizes 4.3 ± 0.2 mm in diameter, without any liquid cross-flow, Yoshida and Manasseh[241] have found that bubbles follow a perfectly repeatable trajectory with slight curvature (mainly due to lift forces and vorticity gradients developed on the surface of a bubble) up to a critical height about 45 mm (10 bubble diameters) above the orifice. At the critical height, axisymmetric oscillations are found to become complex associated with nonaxisymmetric surface distortion, followed by a spiral path. In fact, their observation has shown that the trajectory bifurcates into two spirals at the critical height, beyond which their amplitude increases with height with sideways oscillations to certain extent. In the cross-flow situation, the critical height is lowered and multiple trajectories (spirals) can be seen. The shape of the bubble at the critical height may be what determines the trajectory it will follow. For the case of viscous Newtonian and non-Newtonian liquids, irrespective of the size of the bubble, the trajectories are rectilinear,[242] mainly because of the large viscous drag. In the simulations of bubble dynamics, Blanko[243] and Takagi and Matsumoto[244] have performed detailed axisymmetric computations of transient evolution of a deforming bubble rising in a stagnant liquid. Blanko[243] has reported that these oscillations occur when the capillary time $\sqrt{8\rho r^3\sigma}$ is larger than the gravitational time $\sqrt{2r/g}$, which supports the experimental observations related to the path instability of a rising bubble. The relationship between the wake structure and trajectory of clean bubbles (helical or zigzag) has been clarified by the flow visualizations of Lunde & Perkins.[245] They have showed that the helical path is associated with a steady wake made of two vortex threads, whereas the zigzag path is observed when hairpin vortices are shed in the wake. Thus, there should possibly exist a close correspondence between the wake structure and the bubble trajectory. Similar experiments with expanded-polystyrene spheroids also showed zigzag motion with relatively larger angular displacements from the vertical, which shows that path instability does not require shape variations or for liquid to slip along the interface. These experiments appear to indicate that the path instability is controlled by the mode by which the bubble sheds its vorticity, and this mode itself depends on the amount of vorticity produced on the bubble surface. Thus, bubble deformability in an inviscid flow is not able to produce path instability, although wake dynamics seem sufficient to qualitatively explain most of the observations. However, the contribution of the bubble deformation on the trajectory or the mode is not negligible as the wake dynamics are inherently governed by bubble shape. However, details of the bubble trajectories are not well understood;

moreover, the nature of the trajectories when a stream of bubbles is produced deserves further investigation. For further reading on this subject, readers are recommended to refer to Fan and Tsuchiya[181] (specifically on the effect of wake structure and dynamics on the bubble motion), Wu and Gharib[184] and Feng and Leal.[240]

3.7. Experimental Methods for Measurement of Rise Velocity. The most commonly used methods for the measurement of rise velocity include high-speed photography and use of intrusive and nonintrusive methods. For detailed information about these different techniques the readers may refer to the review by Adrian.[246] Here, we give a brief account of the various experimental techniques that are employed for the measurement of bubble rise velocity and associated parameters.

3.7.1. Nonintrusive Methods of Bubble Rise Analysis. 3.7.1.1. Photographic Methods. This method is one of the most commonly used experimental technique for the measurement of bubble size and rise velocity in transparent systems. Most often, high-speed photography (500−2000 fps) is used for the rise velocity measurements and for tracking the rise trajectories (Willert and Gharib,[247] Lunde and Perkins,[245] Hsieh et al.,[248] Lu and Zang,[249] Wu and Gharib,[184] Tomiyama et al.,[183] Takemura and Magnaudet[250]). The optimum choice is made based on the possible coalescing tendency of bubble and speed of photography. This methodology suits very well for the case of two-dimensional transparent systems, and even for 3-D systems (only when single or very few bubbles are rising in stagnant/flowing liquid). Further, for opaque systems and turbid liquids, this method is not suitable. Although the spatial resolution achieved by these techniques is excellent, its reliability goes down with increase in number of moving particles, nature of curvature of the system and also with the extent of turbulence. Trajectory analysis using combination of mirrors is possible with a single camera. Such a procedure and details are given by de Vries et al.[239] In many cases, to analyze the oscillations of a gas bubble, bubble motion is recorded using a rotating mirror camera and acoustic waves radiated by the bubble are monitored using a needle hydrophone.[251] It is also possible to carry out the analysis using laser induced fluorescence that helps in tracking the bubble trajectory based on the wake movement as well as the movement of bubble interface from the fluorescence emitted by the photosensitive dye.

With the existing techniques, it is difficult to analyze the effect of gradual contamination on bubble characteristics. To be able to follow bubble dissolution for much longer periods of time, Vasconcelos et al.[252] and Alves et al.[169] have adapted a technique where individual bubbles are kept stationary in a downward liquid flow. The liquid flow is in a closed circuit, allowing continuous cleaning of the liquid. By keeping the individual bubbles stationary in a downward liquid flow, it is possible to simultaneously (i) follow mass transfer to/from a single bubble as it inevitably gets contaminated; (ii) follow its shape as it increases its sphericity; and (iii) periodically measure its terminal velocity along the process of contamination. The experimental setup allows a bubble to be visually followed for an indefinite period time as it gathers contaminant. Periodic measurement of terminal velocity as a function of bubble age can be easily achieved just by stopping the pump and allowing the bubble to ascend along the tube. This technique can even be used for analyzing the gradual changes in the wake dynamics.

3.7.1.2. PIV Measurements. Many studies of the bubble motion in liquid shows that the size, shape, and position of the moving bubbles are unsteady and these changes are aperiodic. Such an unsteady-state analysis of the bubble motion is possible through the use of digital image processing techniques (image filtering, edge detection, thresholding and binary images, etc.). One such method is the use of particle image velocimeter (PIV) for the measurement of time varying bubble characteristics.[253,254] This technique has the capability to track detailed characteristics of individual bubbles moving through a turbulent flow field, e.g., size, shape, velocity, and acceleration, and simultaneously to measure the instantaneous fluid velocity field on a two-dimensional plane. Typical system configurations and method of data analysis can be seen in Raffel et al.[255] Important features of this technique are the ability to capture bubble trajectories for long periods of time and the use of bubble images which appear as two fine point images for each instant, from which centroid and diameter can be deduced. For the details of using PIV or particle tracking velocimetry (PTV), readers may refer to the extensive work by Murai[256] and Yamamoto.[257]

3.7.1.3. LDA Measurements. The method of employing photographic technique to quantify the rise velocity and departure frequency of bubbles requires a significant time investment to provide accurate time-averaged results. It is possible to use LDA to quantify these parameters. On the passage of air bubbles through the measurement volume the data acquisition unit receives a time gap, frequencies of which can be estimated directly from the signal. Recent attempts by Kulkarni et al.[258] have shown that LDA can be successfully used in forward scatter mode for the exact measurement of bubble rise/slip velocity even in a bubble swarm without any hindrance to the flow. The advantage of a system with a facility to measure three velocity components simultaneously can be used to get the magnitude as well as the direction of bubble motion. The fiber optic based LDA makes the system simple but the applicability is limited due to the measurements in backscatter mode. Recently, Terasaka et al.[259] have developed a novel sensing system using three coupled laser sensors, which is capable of yielding measurement of 3-dimensional shape and behavior of single bubble in liquid in real time.

3.7.2. Intrusive Measurements. 3.7.2.1. Optical Probes. For intrusive techniques, the performance must be rated based on the quality of data and hindrance caused to the local flow in their presence. The probes based on the principal of utilizing the difference in optical reflectivity of the liquid and gas phases are known as optical probes and are known for their excellent de-wetting property. In the presence of bubbles, they produce a pulse of voltage which due to nonwettability gives accurate time for the presence of bubbles. Most commonly, a pair of probes is used under the assumption that the rise is rectilinear. The method of estimation of velocity is simple and just requires input in terms of time required for bubble for interception between two probe tips with known separation distance. However, for the systems where bubble passage is not rectilinear but moves in different directions, more than two probe tips with known distance of separation are required. Saberi et al.[260] have given a detailed account

of the previous attempts in this direction and have made systematic analysis of the experimental data using this method for a bubble column. Similar analysis is also carried out by Chabot et al.,[261] where the spherical bulb fiber optic probes are applied for bubble characterization. The principle of operation of these optical fiber probes is based on the difference in refractive indices between the gas and the liquid phases. The investigators have verified the method through simultaneous photographic measurements.

3.7.2.2. Conductive/Capacitance Probes. The probes based on the principal of utilizing the difference in electrical conductivity between the liquid and gas phases are widely used for the measurement of bubble velocities and sizes to some extent.[262,180] Conductive probes have wetting characteristic and hence their applicability is restricted for the bubbling systems with higher gas fraction. The discussion for optical probes regarding the direction of bubble motion and number of probe tips required also applies for the capacitance probes. Kuramoto et al.[263] have used high-speed photography accompanied with hot-wire probe for the measurement of detailed flow structure and properties of dispersed as well as continuous phase transport phenomena in a 2D column.

3.7.3. Imaging in Opaque Systems. 3.7.3.1. Dynamic Imaging by Neutron Radiography for Opaque Systems. For opaque test systems, it is possible to characterize bubble motion using neutron flux method (Mishima et al.,[264] Hibiki et al.,[265] Saito et al.[266]). The penetrated neutron flux conveys the information of two-phase flow in the test section, since the incident neutron flux is attenuated when the neutron beam passes through the test section. Generally, a neutron source is followed by a converter having high sensitivity and quick light decay characteristics, and for the imaging system, silicon intensifier target (SIT) tube camera for dynamic imaging or a high-speed video camera for high frame-rate imaging is used. The bubble images are other parameters are analyzed on the basis of different image brightness with gas single-phase, liquid single-phase, and two-phase flow based on the scaling method.

3.7.3.2. X-ray Imaging. X-rays have the advantage that they are not affected by the various refraction indices of the multiphase system and penetrate the multiphase flow in undistorted straight lines. The technique falls within a broad array, including gamma, beta, and neutron radiations, but as a general rule, quantitative measurements have remained local (i.e., narrow beams), and mostly steady state. Hence, in contrast to optical methods, both of these X-ray-based methods are independent of the void fraction and are applicable to opaque liquids. Recently, Seeger et al.[267] have developed a methodology that extracts the information concerning continuous or discreet phase is extracted using X-ray-based flow visualization and X-ray-based particle tracking velocimetry (PTV). Heindel[268] has used flash X-ray radiography (FXR) to visualize rising air bubbles in fiber suspension. The FXR technique allows for bubble visualization in the bulk suspension and the images of bubbles reveal that the bubble rise characteristics and patterns are highly dependent on suspension properties. Theofanous et al.[269] have given detailed information about the techniques based on X-ray radiography.

Controlled Experiments. In most of the experiments where the terminal bubble rise velocities are measured, the observation is made based on the equivalent bubble diameter, its possible deformation (through some a priory known rules or photographic images) and the rise velocity. However, the important factor of detachment condition or bubble release condition is rarely observed. In the available literature that accounts for this kind of an analysis, the generation of bubble is made in different manners. Typically, orifices of different diameter are used for analyzing the release condition or using an orifice of fixed dimensions the bubble is generated either by direct injection or by injection assisted with transportation of bubble using the same fluid as in the tank. Using the former method the deformation can be enhanced by using larger orifice diameters. The later method is considered to reduce the extent of deformation. Details of this method can be seen in Wu and Gharib[184] and Tomiyama.[185]

3.8. Conclusions. Experimental methods for the measurement of bubble rise velocity include photography, which is useful for the analysis in stagnant liquids or even for the dispersed two-phase flows, the reliability of the results in the second case is limited by bubble frequency. Recent attempts to measure the rise velocity based on the use of intrusive or nonintrusive anemometers are encouraging and can be used over a wide range of operating conditions provided the noise part of the data should be carefully eliminated. Further, extensive data should be collected for the rise of bubbles in stagnant and flowing liquids of various properties to understand the sensitivity of rise velocity to different physical properties and their combined effects.

Formulation for bubble rise velocity should be based on the complete force balance on a rising bubble. In many cases, the forces, which are taken into account are always taken either for convenience in simplification of the formula or based on the understanding and compared with the experiments. However, the minute details viz. vorticity on the surface of a bubble (which varies over the surface itself) has an important contribution in deciding the shape and hence the rise velocity of a bubble, are bypassed. The approach based on the potential flow or the solution of equation of motion and continuity would give better predictions than the empirical correlation. Results from the approach based on the dimensionless numbers are acceptable to certain range of system parameters however the attempts to make it generalized or robust result in the loss of sensitivity toward few parameters.

Wave-based analogy of bubble rise and its anomalies show a good comparison with the experimental conditions for a wide range of parameters. However, they show poor agreement for the contaminated liquids in the range of bubbles of $d_B < 5$ mm. For the operations, where, deformed, large size bubbles exist the correlation based on wave analogy[190] may even be used for the prediction of rise velocity. Nevertheless, the correlation needs modification in terms of the effect of external pressure and temperature on the rise of a bubble.

Acknowledgment

Authors acknowledge the permission from (i) Elsevier for the reproduction of Figures 1, 2 7, 9, and 10, (ii) Professor R. Clift and Elsevier for Figure 11A, (iii) Professor Tomiyama for Figure 11B, (iv) Professor L. S. Fan for Figure 15, and (v) AIChE for Figure 17. (Sources of the individual Figures are mentioned in the Figure caption) Amol Kulkarni gratefully acknowledges

(i) the financial support from Professor M. M. Sharma Endowment (University of Mumbai) during this work and also (ii) the Alexander von Humboldt Foundation (Bonn) and the Max-Planck-Institute for Dynamics of Complex Technical Systems, Magdeburg for the financial support and facilities, respectively during the revision of this paper.

Nomenclature

a = radius of bubble (eq 25−27), bubble acceleration at the end of bubble detachment (eq 17), constant in Eq. (95, 97), maximum bubble diameter (Table 3, Sada[74])
a_o = cross-sectional area of the orifice eq 55 (m^2)
Ar = Archimedes number (−)
b = constant in Eq. (95, 97) (−), minimum bubble diameter (Table 3, Sada[74])
Ca = Capillary number (−)
C_D = drag coefficient (−)
C_{Dm} = minimum drag coefficient in C_D-Re plot (−)
d = bubble diameter (m)
d_{30} = sauter mean diameter
d_B, = bubble diameter
d_e = equivalent diameter of bubble (m)
d_h = hole diameter on sieve plates, horizontal projection of a bubble (eq 92) (m)
d_m = maximum horizontal bubble diameter
De = Deborah number (−)
D_i = orifice inner diameter
E= distortion factor (Table 5, Tomiyama[185])
F = Flow number (−)
F_b, f_b = buoyancy force, bubble frequency
F_d = drag force
F_i = inertial force
F_m = gas momentum force
F_p = pressure force
F_R = Froude number
F_s = surface tension force (Nm/s)
g = acceleration due to gravity (m/s^2)
H = orifice coefficient (−)
Q_G, G = gas flow rate (m^3/s)
k = added mass force (N)
K = pulsation parameter
L = parameter in eq 20, length of contact/perimeter of orifice (m)
La = Laplace number (−)
Ly = Lyashchenko number (−)
$\bar{m}$, M = virtual mass of the bubble
m = flow index
Ma = Marangoni number (−)
Mo = Morton number (−)
n = number of holes on sieve plate, consistency index
n' = the index of flow regime (eq 81)
N = number of sources (−)
N_C = capacitance number (−)
P, P_b = Pressure in the bubble (N/m^2)
P_B, P_h = pressure with in the bubble and the static head (N/m^2)
P_C, P_B = pressures in the gas chamber and in the bubble (N/m^2)
P_G = gas pressure (N/m^2)
P_O = hydrostatic pressure at the orifice plate (N/m^2)
Q = gas flow rate at any one of sources on a slot (m^3/s)
Q_t = volumetric flow rate at any instant 't' (m^3/s)
Q_{min} = minimum gas flow rate required for bubbling (m^3/s)
Q_{SI} = gas flow rate for transition from quasi-steady state to dynamic regime (m^3/s)
r,R = radius (m)
r_C = radius of bubble at critical bubble volume (m)
r_O = orifice radius (m)
R' = radius of elemental circle (eq 40)
R_C = radius of curvature, characteristic radius (m)
R_E = equivalent radii (eq 40)
Re = Reynolds number (−),
r_e, r_E = radius of bubble reaching to the end of first stage/ expansion stage (m)
Re_{crit} = critical Reynolds number (−)
R_o = orifice radius (m)
s = distance of center of bubble from point of gas supply (m)
S = bubble surface
S_D = perpendicular distance between bubble center and orifice
Ta = Tadaki number (−)
T, T_c, T_i = temperature (°C)
t_e = bubble expansion time (s)
U_b = bubble rise velocity for spherical cap shaped bubbles (m/s)
U_i = velocity of the surface element (m/s) (eq 51)
V = velocity number (−), bubble volume (eq 1), bubble rise velocity (m/s)
V_B = bubble volume at any instant (m^3)
V_C = chamber volume (m^3)
V_e = velocity relating to first stage (m/s)
V_E = volume of the force balance bubble (m^3)
V_F = final volume of a bubble (m^3)
V_L = mean velocity of liquid (m/s)
Vs = slip velocity (m/s)
V_T = terminal rise velocity (m/s)
V_{Tm} = terminal rise velocity at minimum in C_D-Re plot (m/s)
w = slot spacing (eq 65, 66)
We = Weber number (−)
X = drag correction factor (−)
$X_{(n)}$ = correction function dependent on the power-law index n (eq 101)
z = Eulerian axial coordinate

Greek Letters

α = orifice coefficient (−), void fraction (−)
β = bubble growth angle (eq 52)
$\Delta\rho$ = density difference between gas and liquid
ϕ = cap angle dependent on the truncation point (degrees)
ϕ = velocity potential
γ = shear rate (1/s)
λ = wavelength (m)
μ = viscosity (Pas)
θ = contact angle (degrees)
ρ = density (kg/m^3)
σ = surface tension (Nm/s)
τ = shear stress (m^2/s^2)
υ =kinematic viscosity of the liquid
χ = virtual mass coefficient (−)
ζ = pulsation function

Subscript

0 = initial stage
b, B = bubble
e = indicates the first stage of formation
G = gas
h = hemispherical geometry, orifice/hole
i = time unit
L = liquid
O = orifice
q = angular coordinate on the hemispherical surface (eq 26, 29)
w = water

Superscript

* = dimensionless quantities

Literature Cited

(1) Tate, T. On the magnitude of a drop of liquid formed under different circumstances. *Philosophical Magazine* **1864**, *27*, 176.

(2) Bashforth, F.; Adams, J. C. An attempt to test the theories of capillary action, Cambrige University Press: Cambrige, 1883.

(3) Davidson J. F.; Schuler B. O. G. Bubble formation at an orifice in a viscous liquid. *Trans. Inst. Chem. Eng.* **1960**, *38*, 144.

(4) Davidson J. F.; Schuler B. O. G. Bubble formation at an orifice in an inviscid fluid. *Trans. Inst. Chem. Eng.* **1960**, *38*, 335.

(5) Tsuge, H.; Hibino, S. I. Bubble formation from an orifice submerged in liquids. *Chem. Eng. Commun.* **1983**, *22*, 63.

(6) Tsuge, H. Hydrodynamics of bubble formation from submerged orifices. In. *Encyclopaedia of Fluid Mechanics*; Gulf Publishing Company: New York, 1986, Vol. 3, 191.

(7) Tsuge, H.; Rudin, P.; Kammel, R. Bubble formation from a vertically downward facing nozzle in liquids and molten metals. *J. Chem. Eng. Jpn.* **1986**, *19*, 326.

(8) Tsuge, H.; Nakajima Y.; Terasaka K. Behaviour of bubbles formed from a submerged orifice under high system pressure. *Chem. Eng. Sci.* **1992**, *47* (13/14), 3273.

(9) Tsuge, H.; Treasaka, K.; Koshida, W.; Matsue H. Bubble formation at submerged nozzles for small gas flow rate under low gravity. *Chem. Eng. Sci.* **1997**, *52* (20), 3415.

(10) Tsuge, H.; Treasaka, K.; Koshida, W.; Matsue H. Bubble formation in flowing liquid under reduced gravity. *Chem. Eng. Sci.* **1997**, 52 (20), 3671.

(11) Terasaka, K.; Tsuge, H. Bubble formation under constant flow conditions. *Chem. Eng. Sci.* **1993**, *48* (19), 3417.

(12) Terasaka, K.; Tsuge, H. Bubble formation at orifice in viscoelastic liquids. *A. I. Ch. E. J.* **1997**, *43* (11), 2903.

(13) Terasaka, K.; Tsuge H.; Matsue, H. Bubble formation in co-currently upward flowing liquid. *Can. J. Chem. Eng.* **1999**, *77*, 458.

(14) Ramkrishnan, S.; Kumar, R.; Kuloor, N. R. Studies in bubble formation − I, Bubble formation under constant flow conditions. *Chem. Eng. Sci.* **1969**, *24*, 731.

(15) Satyanarayana, A.; Kumar, R.; Kuloor N. R. Studies in bubble formation − II, Bubble formation under constant pressure conditions. *Chem. Eng. Sci.* **1969**, *24*, 731.

(16) Khurana A. K.; Kumar R. Studies in bubble formation-III. *Chem. Eng. Sci.* **1969**, *24*, 1711.

(17) Kumar, R.; Kuloor, N. R. The formation of bubbles and drops. *Adv. Chem. Eng*.; Academic Press: New York, 1970, Vol. 8.

(18) Marmur, A.; Rubin, E. Equilibrium shapes and quasi-static formation of bubbles at submerged orifice. *Chem. Eng. Sci.* **1973**, *28*, 1455.

(19) Marmur A.; Rubin E. A theoretical model for bubble formation at an orifice submerged in an inviscid liquid. *Chem. Eng. Sci.* **1976**, *31*, 453.

(20) Rabiger, N.; Vogelpohl, A. Bubble formation and its movement in Newtonian and Non-Newtonian liquids. *Encyclopaedia of Fluid Mechanics*: Gulf Publishing: Houston, 1986, 59.

(21) Rabiger, N.; Vogelpohl, A. Calculation of Bubble-Size in the Regime of Bubble and Jet Gassing in Stationary and Moving Newtonian Liquids. *Chem. Ing. Technik*. **1982**, *54*(11), 1082.

(22) Gaddis E.; Vogelpohl A. Bubble formation in quiescent liquids under constant flow conditions. *Chem. Eng. Sci.* **1986**, *41*(1), 97.

(23) Tan, R. B. H.; Chen, W. B.; Tan, K. H. A nonspherical model for bubble formation with liquid cross-flow. *Chem. Eng. Sci.* **2000**, *55*, 6259.

(24) Zhang, W.; Tan, R. B. H A model for bubble formation and weeping at a submerged orifice. *Chem. Eng. Sci.* **2000**, *55*(24), 6243.

(25) Xie, S.; Tan, R. B. H. Bubble formation at multiple orifices—bubbling synchronicity and frequency. *Chem. Eng. Sci.* **2003**, *58*(20), 4639.

(26) Chen, W. B.; Tan, R. B. H. Theoretical analysis of two-phase bubble formation in an immiscible liquid. *A. I. Ch. E. J.* **2003**, *49*(8), 1964.

(27) Zhang, W.; Tan, R. B. H. A model for bubble formation and weeping at a submerged orifice with liquid cross-flow. *Chem. Eng. Sci.* **2003**, *58*(2), 287.

(28) Xiao, Z.; Tan R. B. H. An improved model for bubble formation using the boundary-integral method. *Chem. Eng. Sci*. **2005**, *60*(1), 179−186.

(29) Loimer, T.; Machu, G.; Schaflinger, U. Inviscid bubble formation on porous plates and sieve plates. *Chem. Eng. Sci.* **2004**, *59*(4), 809−818.

(30) Gerlach, D.; Biswas, G.; Durst, F.; Kolobaric, V. Quasi-static bubble formation on submerged orifices. *Int. J. Heat Mass Transfer* **2005**, *48*(2), 425−438.

(31) Loubière, K.; Hébrard, G. Influence of liquid surface tension (surfactants) on bubble formation at rigid and flexible orifices. *Chem. Eng. Proc.* **2004**, *43*(11), 1361−1369.

(32) Loubière, K.; Castaignède, V.; Hébrard, G.; Roustan, M. Bubble formation at a flexible orifice with liquid cross-flow. *Chem. Eng. Proc*. **2004**, *43*(6), 717−725.

(33) Byakova, A. V.; Gnyloskurenko, S. V.; Nakamura, T.; Raychenko, O. I. Influence of wetting conditions on bubble formation at orifice in an inviscid liquid: Mechanism of bubble evolution. *Colloids and Surfaces A: Physicochem. Eng. Aspects* **2003**, *229*(1−3), 19−32.

(34) Gnyloskurenko, S. V.; Byakova, A. V.; Raychenko, O. I.; Nakamura, T. Influence of wetting conditions on bubble formation at orifice in an inviscid liquid. Transformation of bubble shape and size. *Colloids and Surfaces A: Physicochem. Eng. Aspects* **2003**, *229*(1−3), 73−87.

(35) Loubière K.; Hébrard, G. Bubble formation from a flexible hole submerged in an inviscid liquid. *Chem. Eng. Sci.* **2003**, *58*(1), 135−148.

(36) Tse, K. L.; Martin, T.; McFarlane, C. M.; Nienow, A. W. Small bubble formation via a coalescence dependent break-up mechanism. *Chem. Eng. Sci*. **2003**, *58*(2), 275−286.

(37) Valencia, A.; Cordova, M.; Ortega, J. Numerical simulation of gas bubbles formation at a submerged orifice in a liquid. *Int. Commun. Heat Mass Trans.* **2002**, *29*(6), 821−830.

(38) Li, H. Z.; Mouline, Y.; Midoux, N. Modelling the bubble formation dynamics in non-Newtonian fluids. *Chem. Eng. Sci.* **2002**, *57*(3), 339−346.

(39) Chen, W. B.; Tan, R. B. H. A model for steam bubble formation at a submerged nozzle in flowing subcooled water. *Int. J. Heat Fluid Flow* **2001**, *22*(5), 552−560.

(40) Zhang, L.; Shoji, M. Aperiodic bubble formation from a submerged orifice. *Chem. Eng. Sci.* **2001**, *56*(18), 5371.

(41) Terasaka, K.; Tsuge, H. Bubble formation at a nozzle submerged in viscous liquids having yield stress. *Chem. Eng. Sci.* **2001**, *56*(10), 3237−3245.

(42) Tritton, D. J.; Egdell, C. Chaotic bubbling. *Phys. Fluids* **1993**, *5*, 503−505.

(43) Femat, R.; Alvarez-Ramírez, J.; Soria, A. Chaotic flow structure in a vertical bubble column. *Phys. Lett. A* **1998**, *248*(1), 1−91, (2) 67−79.

(44) Tufaile, A.; Sartorelli, J. C. Chaotic behavior in bubble formation dynamics. *Physica A: Stat. Mech. Appl.* **2000**, *275*(3−4), 336−346.

(45) Kulkarni, A. A. Effect of sparger design on the local flow field in a bubble column: Analysis using LDA. *Chem. Eng. Res. Des*. **2005**, *83*(A1), 1.

(46) Muller, R. L.; Prince R. G. H. Regimes of bubbling and jetting from submerged orifices. *Chem. Eng. Sci.* **1972**, *27*(8), 1583.

(47) Schnurrmann, R. *Z. Physic. Chem*. **1929**, *143*A, 456.

(48) Eversole, W. G.; Wagner, G. H.; Stachhouse, E. Rapid formation of gas bubbles in liquids. *Ind. Eng. Chem.* **1941**, *33*, 1459.

(49) Krevelen, D. W.; Hoftijzer, P. J. Studies of gas bubble formation. *Chem Eng. Prog*. **1950**, *46*(1), 1950.

(50) Benzing, R. A.; Mayers, J. E. Low-frequency bubble formation at horizontal circular orifices. *Ind. Eng. Chem.* **1955**, *47*, 2087.

(51) Hughes, R. R.; Handlos, A. E.; Evans, H. D.; Maycock, R. L. The formation of bubbles at simple orifices. *Chem. Eng. Prog.* **1955**, *51* (12), 557.

(52) Leibson, I.; Holcomb, E. G.; Cacoso, A. G.; Jacmic J. J. Rate of flow and mechanics of bubble formation from single submerged orifices. *A. I. Ch. E. J.* **1956**, *2*, 296.

(53) Wraith, A. E. Two-stage bubble growth at a submerged plate orifice. *Chem. Eng. Sci.* **1971**, *26*, 1659.

(54) Acharya, A.; Ulbrecht, J. J. Note on Influence of Viscoelasticity on Coalescence Rate of Bubbles and Drops. *AIChE J.* **1978**, *24*(2), 348.

(55) Nahra, H. K.; Kamotani, Y. Prediction of bubble diameter at detachment from a wall orifice in liquid cross-flow under reduced and normal gravity conditions. *Chem. Eng. Sci.* **2003**, *58*(1), 55−69.

(56) Quingley, C. J.; Johnson, A. I.; Harris, B. L. *Chem. Eng. Prog. Symp. Ser.* **1955**, *16*, 31.

(57) Datta, R. L.; Napier, D. H.; Newitt, D. M. The properties and behaviour of gas bubbles formed at a circular orifice. *Trans. Inst. Chem. Eng.* **1950**, *28*, 14.

(58) Vasilev, A. S. Laws governing the outflow of a jet of gas into a liquid. *Theor. Found. Chem. Eng.* **1970**, *4*(5), 727.

(59) Siemes, W.; Kaufmann, J. F. Die periodische entstechung von gas blasen an dusen. *Chem. Eng. Sci.* **1956**, *5*, 127.

(60) Jamialahmadi, M.; Zehtaban, M. R.; Muller-Steinhagen, H. et al., Study of bubble formation under constant flow conditions. *Chem. Eng. Res. Des.* **2001**, *79* (A5), 523.

(61) Liow, J. L. Quasi-equilibrium bubble formation during top-submerged gas injection. *Chem. Eng. Sci.* **2000**, *55*, 4515.

(62) Hsu, S. H.; Lee, W. H.; Yang, Y. M.; Chang, C. H.; Maa, J. R. Bubble formation at an orifice in surfactant solutions under constant flow conditions. *Ind. Eng. Chem. Res.* **2000**, *39*, 1473.

(63) Idogawa, K.; Ikeda, K.; Fukuda, T.; Morooka, S. Formation and flow of gas bubbles in a pressurized bubble column with a single orifice or nozzle gas distributor. *Chem. Eng. Comm.* **1987**, *59*, 201.

(64) Wilkinson, P. M. *Physical aspects and scale-up of high-pressure bubble columns*. Ph.D. Thesis, University of Groningen. **1991**.

(65) Kupferberge, A.; Jameson, G. J. Bubble formation at a submerged orifice above a gas chamber of finite volume. *Trans. Inst. Chem. Engrs*. **1969**, *47*, 241.

(66) Antoniadis, D.; Mantzavinos, D. Effect of chamber volume & diameter on bubble formation at plate orifices. *Trans. Inst. Chem. Eng.* **1992** *70A*, 161.

(67) Mccann, D. J.; Prince R. G. H. Regimes of bubbling at a submerged orifice. *Chem. Eng. Sci.* **1971**, *26* (10), 1505.

(68) Park, Y.; Tyler, A. L.; Nevers, N. de, The chamber orifice interaction in the formation of bubbles. *Chem. Eng. Sci.* **1977**, *32*, 907.

(69) Davidson, L.; Amick, E. H. Formation of gas bubbles at horizontal orifice. *A. I. Ch. E. J.* **1956**, *2*, 337−342.

(70) Berdnikov, V. I.; Levin, A. M.; Shakirov, K. M. Size of bubbles during injection of metal. *Steel USSR* **1974**, *4*(10), 804−807.

(71) Szekely, J.; Fang, S. D. On bubble formation at the tip of a capillary with downward gas flow. *Chem. Eng. Sci*. **1971**, *26*, 1123.

(72) Iliadis, P.; Douptsoglou, V.; Stamatoudis, M. Effect of orifice submergence on bubble formation. *Chem. Eng. Technol*. **2000***, 23*(4), 341.

(73) Ponter, A. B.; Surati, A. I. Bubble emissions from submerged orifice-a critical review. *Chem. Eng. Technol.* **1997**, *20*, 85.

(74) Sada, E. Bubble formation in molten $NaNO_3$. *Ind. Eng. Chem. Process Des. Dev.* **1986**, *25*, 838.

(75) Rice, R. G.; Lakhani, N. B. Bubble formation at a puncture in a submerged rubber membrane. *Chem. Eng. Commun*. **1983**, *24*, 215.

(76) Marshall, S. H.; Chudacek, M. W.; Bagster, D. F. A model for bubble formation from an orifice with liquid cross-flow. *Chem. Eng. Sci*. **1993**, *48*(11), 2049.

(77) Wilkinson, P. M.; van Dierendonck, L. L. A theoretical-model for the influence of gas properties and pressure on single-bubble formation at an orifice. *Chem. Eng. Sci.* **1994**, *49*(9), 1429.

(78) Pamperin, O.; Rath, H. J. Influence of Buoyancy on Bubble Formation at Submerged Orifices. *Chem. Eng. Sci.* **1995**, *50*(19), 3009.

(79) Buyevich, Yu. A.; Webbon, B. W. Bubble formation at a submerged orifice in reduced gravity. *Chem. Eng. Sci.* **1996**, *51*(21), 4843.

(80) Rielly, et al. 1998, personal collection.

(81) Forrester, S. E.; Rielly, C. D. Bubble formation from cylindrical flat and concave sections exposed to a strong liquid cross-flow. *Chem. Eng. Sci.* **1998**, *53*(8), 1517.

(82) Hooper, A. P. A study of bubble formation at a submerged orifice using the boundary element method. *Chem. Eng. Sci.* **1986**, *41*(7), 1879.

(83) Pinczewski, W. V. The formation and growth of bubbles at the submerged orifice. *Chem. Eng. Sci*. **1981**, *36,* 405.

(84) Tan, R. B. H.; Harris, I. J. A model for nonspherical bubble growth at a single orifice. *Chem. Eng. Sci.* **1986**, *41*(12), 3128−3175.

(85) Chuang, S. C.; Goldschmidt, V. W. Bubble formation due to a submerged capillary tube in quiescent and coflowing streams. *J. Basic. Eng*. **1970**, *92*, 705.

(86) Kumar, R. A unified approach to bubble and drop formation. *Chem. Eng. Sci.* **1971**, *26*(2), 177−184.

(87) Sada, E.; Yasunishi, A.; Katoh, S.; Nishioka, M. Bubble formation in flowing liquid. *Can. J. Chem. Eng.* **1978**, *56*, 669.

(88) Takahashi, T.; Miyahara, T.; Senzai, S.; Terakado, H. Bubble formation at submerged nozzles in co-current, counter current and cross-current flow. *Kagaku Kogaku Ronbunshu* **1980**, *6*, 563.

(89) Maier, C. G. Producing small bubbles of gas in liquids by submerged orifices. *US Bur. Mines Bull.* **1927**, *260*, 62−121.

(90) Stich, K.; Barr, A. Begasun Querstömenden Wassers durch einzelund mehrfachöffnungen sehr kleiner Durchmesser. *Vehrfahrenstechnik* **1979**, *9*, 671−681.

(91) Sullivan, S. L.; Hardy, B. W. Formation of air bubbles at orifices submerged below liquids. *AIChE J*. **1964**, *10*, 848.

(92) Kawase, Y.; Ulbrecht, J. J. Formation of drops and bubbles in flowing liquids. *Ind. Eng. Chem. Proc. Des. Dev*. **1981**, *20*(4), 636−640.

(93) Morgenstern, I. B.; Mersmann, A. Aeration of highly viscous liquids. *Ger. Chem. Eng.* **1982**, *5*, 374−379. Morgenstern, I. B.; Mersmann, A. *Chem. Ing. Technik.* **1983**, *55*, 580.

(94) Wace, P. F.; Morrell, M. S.; Woodrow, J. Bubble formation in a traverse horizontal liquid flow. *Chem. Eng. Commun*. **1987**, *62*, 93.

(95) Tsuge, H.; Nojima, Y.; Hibino, S. The volume of bubble formed from a submerged single orifice in flowing liquid. *Kagaku Kogaku Ronbunshu* **1980**, *6*(2), 136.

(96) Marshall, S. H., Thesis University Sydney, Australia 1990.

(97) Miyahara, T.; Takahashi, T. Bubble volume in single bubbling regime with weeping at a submerged orifice. *J. Chem. Eng. Jpn.* **1984**, *17*(6), 597.

(98) Tsuge, H.; Hibino, S.; Nojima, U. Volume of a bubble formed at a single submerged orifice in a flowing liquid. *Int. Chem. Eng.* **1981**, *21*(4), 630−636.

(99) Kim, I.; Kamotani, Y.; Ostrach, S. Modeling bubble and drop formation in flowing liquids in microgravity. *AIChE J.* **1994**, *40*(1), 19−28.

(100) Tsuge, H.; Terasaka, K.; Koshida W.; Matsue, H. Bubble formation under microgravity. *Proc. 5th World Congress of Chem. Eng.* **1996**, *1*, 420−425.

(101) Tsuge, H.; Treasaka, K.; Koshida, W.; Matsue H. Bubble formation in flowing liquid under reduced gravity. *Chem. Eng. Sci.* **1997**, *52*(20), 3671−3676.

(102) Bhunia, A.; Pais, S. C.; Kamotani, Y.; Kim, I. Bubble formation in a coflow configuration in normal and reduced gravity. *AIChE J.* **1998**, *44*(7), 1499−1509.

(103) Nahra, H. K.; Kamotani, Y. Bubble formation from wall orifice in liquid cross-flow under low gravity. *Chem. Eng. Sci.* **2000**, *55*, 4653−4665.

(104) Terasaka, K.; Tsuge, H. Bubble formation at a single orifice in highly viscous liquids. *J. Chem. Eng. Jpn*. **1990**, *23*, 160.

(105) Swope, R. D. Single bubble formation at orifices submerged in viscous liquids. *Can. J. Chem. Eng.* **1971**, *49*, 169.

(106) Ghosh, A. K.; Ulbrecht, J. J. Bubble formation from a sparger in polymer solutions in stagnant liquids. *Chem. Eng. Sci*. **1989,** *44*, 957.

(107) L'Ecuyer, R. D.; Murthy, S. N. B. Energy transfer from a liquid to gas bubbles forming at a submerged orifice. *NASA Tech. Note* **1965**, TN D-2547, Washington, DC.

(108) Favelukis, M.; Albalak, R. J. Bubble growth in viscous Newtonian and non-Newtonian liquids. *Chem. Eng. J. Biochem. Eng. J*. **1996**, *63*(3), 149−155.

(109) McCann, D. J.; Prince, R. G. H. Bubble formation and weeping at submerged orifice. *Chem. Eng. Sci*. **1969**, *24*, 801.

(110) Miyahara, T.; Iwata, M.; Takahashi, T. Bubble formation pattern with weeping at a submerged orifice. *J. Chem. Eng. Jpn.* **1984**, *17*(6), 592.

(111) Houghton, G.; McLean, A. M.; Ritchie, P. D. Mechanism of formation of gas bubble-beads. *Chem. Eng. Sci*. **1957**, *7*, 40.

(112) Mersmann 1962 A. VDI491 FORSCH.

(113) Miyahara, T.; Takahashi, T. Coalescence phenomena at the moment of bubble formation at adjacent holes. *Chem. Eng. Res. Des.* **1986**, *64*(4), 320.

(114) Miyahara, T.; Tanaka, A. Size of bubbles generated from porous plates. *J. Chem. Eng. Jpn.* **1997**, *30*(2), 353.

(115) Miyahara, T.; Hayashino, T. Size of bubbles generated from perforated plates in non-Newtonian liquids. *J. Chem. Eng. Jpn.* **1995**, *28* (5), 596.

(116) Koide, K.; Hirahara, T.; Kubota, H. Average bubble diameter, slip velocity and gas hold-up of bubble swarms. *Kagaku Kogaku* **1966**, *30*, 712.

(117) Koide, K. T.; Sato, S.; Tanaka, Y.; Kubota, H. Bubbles generated from porous plates. *J. Chem. Eng. Jpn.* **1968**, *1*, 51.

(118) Schwarzer, J.; Dewjanin, W.; Vogelpohl, A. Primary bubble formation on perforated plates. *Chem. Ing. Technol.* **1990**, *62*(2), 144.

(119) McCann, D. J.; Prince, R. G. H. Regimes of bubbling at a submerged orifice. *Chem. Eng. Sci*. **1971**, *26*, 505−1512.

(120) Mersmann, A. Bubble formation dynamics at sieve plates. *Chem. Ing. Technol.* **1980**, *52*(12), 933.

(121) Li, R. Q.; Wraith, A. E.; Harris, R. Gas dispersion phenomena at a narrow slot submerged in a liquid. *Chem. Eng. Sci.* **1994**, *49*(4), 531.

(122) Southern, S. M.; Wraith, A. E. Gas dispersion at diffuser sources for steel making, Proceedings of International Symposium on Developments in Ladle Steel making & Continuous Casting, 26−29 August, pp 1, C. I. M., Hamilton, Ontario. **1990**.

(123) Li, R.; Harris, R. Bubble formation from a very narrow slot. *Can. Met. Q.* **1993**, *32*(1), 31.

(124) Ruzicka, M. C.; Drahos, J.; Zahradník J.; Thomas, N. H. Intermittent transition from bubbling to jetting regime in gas−liquid two phase flows. *Int. J. Multiphase Flow* **1997**, *23*(4), 671−682.

(125) Ruzicka, M. C.; Drahos, J.; Zahradník J.; Thomas, N. H. Natural modes of multi-orifice bubbling from a common plenum. *Chem. Eng. Sci.* **1999**, *54*(21), 5223−5229.

(126) Klug, P.; Vogelpohl, A. Bubble formation with superimposed liquid motion at single-hole plates and sieve plates. *Ger. Chem. Eng.* **1983**, *6*, 311

(127) Klug, P.; Vogelpohl, A. Bubble formation at sieve plates—Effect on gas hold-up in bubble columns. *Ger. Chem. Eng*. **1986**, *9*, 93.

(128) Bowonder, B.; Kumar, R. Studies in bubble formation −IV, Bubble formation at porous discs. *Chem. Eng. Sci.* **1970**, *25*, 25.

(129) Taylor, G. I. The instability of liquid surfaces when accelerated in a direction perpendicular to their plane I. *Proc. Royal Soc. London A* **1950**, *201*, 192−196.

(130) Wraith, A E.; Li, R. Q.; Harris, R. Gas bubble volume at a narrow slot nozzle in a liquid. *Chem. Eng. Sci.* **1995**, *55*(6), 1057−1058.

(131) Biddulph, M. W.; Thomas, C. P. Effect of liquid surface-tension on small hole distillation sieve tray pressure-drop. *AIChE J.* **1995**, *41* (4), 819.

(132) Loimer, T.; Machu, G.; Schaflinger, U. Inviscid bubble formation on porous plates and sieve plates. *Chem. Eng. Sci*. **2004**, *59*, 809.

(133) Kulkarni, A. A.; Ramkrishna, D.; Joshi, J. B. Determination of bubble size distributions in bubble columns using LDA. *AIChE J.* **2004**, *50*(12), 3068.

(134) Dhotre, M. T.; Ekambara, K.; Joshi, J. B. CFD simulation of sparger design and height-to-diameter ratio on gas hold-up profiles in bubble column reactors. *Exp. Ther. Fluid Sci*. **2004**, *28*(5), 407.

(135) Miyahara, T.; Haga, N. Bubble formation at orifice at high gas flow rates. *Int. Chem. Eng.* **1983**, *23*, 524.

(136) Rowe, P. N.; Matsuno, R. Single bubbles injected into a gas-fluidized bed and observed by X-rays. *Chem. Eng. Sci*. **1971**, *26*, 923.

(137) Bisgaard, C. Velocity fields around spheres and bubbles investigated by laser Doppler anemometry. *J. Non-Newtonian Fluid Mech.* **1983**, *12*, 283−302.

(138) Jameson, G. J. Bubbles in motion, *Trans. Inst. Chem. Eng.* **1993**, *71*(A), 587.

(139) Lamb, H. *Hydrodynamics*, 6th ed.; Dover Publications. Co.: New York, 1945; p 600.

(140) Astarita, G.; Apuzzo, G. Motion of gas bubbles in non-Newtonian liquids. *AIChE J.* **1965**, *11*(5), 815.

(141) Auton, T. R. The lift force on a spherical body in a rotational flow. *J. Fluid Mech*. **1987**, *183*, 199.

(142) Eames, I.; Hunt, J. C. R. Inviscid flow around bodies moving in a weak density gradient in the absence if buoyancy effects. *J. Fluid Mech.* **1997**, 353.

(143) Magnaudet, J.; Eames, I. Motion of high Reynolds number bubbles in turbulent flows. *Annu. Rev. Fluid Mech*. **2000**, *32*, 659.

(144) Mei, R.; Klausner, J. F. Unsteady force on a spherical bubble at finite Re with small fucntions in the free stream velocity. *Phys. Fluids A* **1992**, *4*, 63.

(145) Astarita, G, Spherical gas bubble motion through Maxwell liquids. *Ind. Eng. Chem. Fund*. **1966**, *5*(4), 548.

(146) Davis, R. E.; Acrivos, A. The Influence of Surfactants on the Creeping Motion of Bubbles *Chem. Eng. Sci.* **1966**, *21*, 681.

(147) Haque, M. W.; Nigam, K. D. P.; Viswanathan, K.; Joshi, J. B. Studies on gas holdup and bubble parameters in bubble-columns with (carboxymethyl) cellulose solutions. *Ind. Eng. Chem. Res*. **1987**, *26* (1), 86.

(148) Clift, R.; Grace, J. R.; Weber, M. E. *Bubbles, Drops, and Particles*; Academic Press: London, 1978.

(149) Abou-el-hassan, M. E. A generalized bubble rise velocity correlation. *Chem. Eng. Commun.* **1983**, *2*, 243.

(150) Abou-el-hassan, M. E. Correlations for bubble rise in gas−liquid systems. *Encyclopaedia of Fluid Mechanics*; 1983; Vol. 3, 110.

(151) Chhabra, R. *Bubbles, Drops and Particles in Non-Newtonian Fluids*: CRC Press: Boca Raton. Fla., 1993.

(152) Gummalam, S.; Chhabra, R. P. Rising velocity of a swarm of spherical bubbles in a power law non-Newtonian liquid. *Can. J. Chem. Eng.* **1987**, *65*, 1004.

(153) Rodrigue, D. Generalized correlation for bubble motion. *AIChE J.* **2001**, *47*, 39.

(154) Rodrigue, D. A simple correlation for gas bubbles rising in power-law fluids. *Can. J. Chem. Eng.* **2002**, *80*(2), 289.

(155) Nguyen, A. V. Prediction of bubble terminal velocities in contaminated water. *AIChE J.* **1998**, *44*(1), 226.

(156) Rodrigue, D.; De Kee, D.; Chan Man Fong, C. F. An experimental study of the effect of surfactants on the free rise velocity of gas bubbles. *J. Non-Newt. Fluid Mech.* **1996**, *66*(2−3), 213.

(157) Rodrigue, D. A general correlation for the rise velocity of single gas bubbles. *Can. J. Chem. Eng.* **2004**, *82* (2), 382−386.

(158) Frumkin, A.; Levich, V. G. On the surfactants and interfacial motion. *Z. Fizicheskoi Khimii* **1947**, *21*, 1183−1204.

(159) Levich, V. G. *Physicochemical Hydrodynamics*; Prentice Hall: Englewood Cliffs, NJ, 1962.

(160) Gonzaleztello, P.; Camacho, F.; Jurado, E.; Bailon, R. Influence of surfactant concentration on the final rising rate of droplets. *Can. J. Chem. Eng.* **1992**, *70*(3), 426.

(161) Kopfsill, A. R.; Homsy, G. M. Bubble motion in a Hele-Shaw cell. *Phys. Fluids* **1988**, *31*(1), 18−26.

(162) Dekee, D.; Chhabra, R. P.; Dajan, A. Motion and coalescence of gas-bubbles in nonnewtonian polymer-solutions. *J. Non-Newtonian Fluid Mech.* **1990**, *37*(1), 1−18.

(163) Bond, W. N.; Newton, D. A. *Philos. Mag.* **1924**, *5*, 793.

(164) Zana, E.; Leal, L. G. Dynamics and dissolution of gas-bubbles in a viscoelastic fluid. *Int. J. Multiphase Flow* **1978**, *4*(3), 237−262.

(165) Tzounakos, A.; Karamanev, D. G.; Margaritis, A.; Bergougnou, M. A. Effect of the Surfactant Concentration on the Rise of Gas Bubbles in Power-Law Non-Newtonian Liquids. *Ind. Eng. Chem. Res.* **2004**, *43*(18), 5790−5795.

(166) Duineveld, P. C. The rise velocity and shape of bubbles in pure water at high Reynolds number. *J. Fluid Mech*. **1995**, *292*, 325−332.

(167) Fdhila, R. B.; Duineveld, P. C. The effect of surfactant on the rise of a spherical bubble at high Reynolds and Peclet numbers. *Phys. Fluids* **1996**, *8*(2), 310−321.

(168) Ybert, C.; Di Meglio, J. M. Ascending air bubbles in protein solutions. *Eur. Phys. J. B* **1998**, *4*, 313.

(169) Alves, S. S.; Orvalho, S. P.; Vasconcelos, J. M. T. Effect of bubble contamination on rise velocity and mass transfer. *Chem. Eng. Sci.* **2005**, *60*(1), 1−9.

(170) Calderblank, P. H.; Johnston, D. S. L.; Loudon, J. Mechanics and mass transfer of single bubble in free rise through some Newtonian and non-Newtonian liquids. *Chem. Eng. Sci*. **1970**, *25*, 235.

(171) Margaritis, A.; Te Bokkel, D. W.; Karamanev, D. Bubble rise velocities and drag coefficients in non-Newtonian polysaccharide solutions. *Biotech. Bioeng*. **1999**, *64*(3), 259.

(172) Leal, L. G.; Skoog, J.; Acrivos, A. On the motion of gas bubbles in a viscoelastic liquid. *Can. J. Chem. Eng*. **1971**, *49*, 569.

(173) Rodrigue, D.; De Kee, D.; Chan Man Fong, C. F. Bubble velocities: further developments on the jump discontinuity. *J. Non-Newt. Fluid Mech*. **1998**, *79*(1), 45.

(174) Acharya, A.; Mashelkar, R. A.; Ulbricht, J. Mechanics of bubble motion and deformation in non-Newtonian media. *Chem. Eng. Sci.* **1977**, *32*, 863.

(175) Carreau, P. J.; Devic, M.; Kapellas, M. Dynamique des bulles en milieu viscoélastique. *Rheol. Acta* **1974**, *13*, 477.

(176) De Kee, D.; Carreau, P. J.; Modarski, J. Bubble velocity and coalescence in viscoelastic liquids. *Chem. Eng. Sci.* **1986**, *41*, 2273.

(177) Belmonte, A. Self-oscillations of a cusped bubble rising through a micellar solution. *Rheol. Acta* **2000**, *39*, 554.

(178) Leifer, I.; Patro, R. K.; Bowyer, P. A study on the temperature variation of rise velocity for large clean bubbles. *J. Atm. Oceanic Tech*. **2000**, *17*(10), 1392.

(179) Letzel, M. Hydrodynamics and mass transfer in bubble columns at elevated pressures, Ph.D. Thesis, Delft University, 1998.

(180) Luo, X.; Zhang, J.; Tsuchiya, K.; Fan, L. S. On the rise velocity of bubbles in liquid−solid suspensions at elevated pressure and temperature. *Chem. Eng. Sci.* **1997**, *52*(21−22), 3693.

(181) Fan, L. S.; Tsuchiya, K., Bubble wake dynamics in liquids and liquid−solid suspensions, Butterworth and-Heinemann, 363. **1990**.

(182) Tomiyama, A.; Yoshida, S.; Hosokawa, S. Surface Tension Force Dominant Regime of Single Bubbles rising through Stagnant Liquids, on CD-ROM of 4th UK-Japan Seminar on Multiphase Flow, pp 1−6 2001.

(183) Tomiyama, A. Reconsideration of Three Fundamental Problems in Modeling Bubbly Flows, Proc. JSME- KSME Fluid Eng. Conf. Pre-Symp., pp 47−53 2002.

(184) Wu, M.; Gharib, M. Experimental studies on the shape and path of small air bubbles rising in clean water. *Phys. Fluids* **2002**, *14*, L49.

(185) Tomiyama, A. Drag, lift and virtual mass forces acting on a Single Bubble, 3rd International Symposium on Two-Phase Flow Modelling and Experimentation Pisa, 22−24 September 2004

(186) Grace, J. R. Shapes and velocities of bubbles rising in infinite liquids. *Trans. Inst. Chem. Eng.* **1973**, *51*, 116.

(187) Peeblis, F. N.; Garber, H. J. Studies on the motion of gas bubbles in liquids. *Chem. Eng. Prog.* **1953**, *49*, 88.

(188) Stokes, G. G. On the effect of the internal friction of fluid on the motion of pendulums. *Trans. Cambridge Phi. Soc.* **1851**, *9*, 8.

(189) Habberman, W. L.; Morton, R. K. *NAV. DEP. DW TAYL.* **1953**, *802*, 68.

(190) Mendelson, H. D. The prediction of bubble terminal velocities from wave theory. *AIChE J.* **1967**, *13*, 250.

(191) Harmathy, T. Z. Velocity of large drops and bubbles in media of infinite or restricted media. *AIChE J*. **1960**, *6*(2), 281.

(192) Anjelino, H. Hydrodynamique des grosses bulles dans les liquides visqueux. *Chem. Eng. Sci.* **1966**, *21*(6−7), 541

(193) Dumitrescu, D. T., Z. *Angew. Math. Mech*. **1943**, *23*, 139−49.

(194) Lehrer, H. G. A rational terminal velocity equation for bubbles and drops at intermediate and high Reynolds number. *J. Chem. Eng. Jpn.* **1976**, *9*, 237.

(195) Nickens, H. V.; Yannitell, D. W. The effects of surface tension and viscosity on the rise velocity of a large gas bubble in a closed, vertical liquid-filled tube. *Int. J. Multiphase Flow* **1987**, *13*(1), 57.

(196) Jamialahmadi, M.; Branch, C.; Steinhagen, H. M. Terminal bubble rise velocity in liquids. *Chem. Eng. Res. Des.* **1994**, *72*(A), 119.

(197) Karamanev, D. G. Rise of gas bubbles in quiescent liquids. *AIChE J.* **1994**, *40*, 1418.

(198) Davies, R. M.; Taylor, G. I. The mechanics of large bubbles rising through extended liquids and through liquids in tubes. *Proc. R. Soc. London* **1950**, *A200*, 375.

(199) Maneri, C. C. New look at wave analogy for prediction of bubble terminal velocities. *AIChE J.* **1995**, *41*(3), 481.

(200) Chhabra, R. Hydrodynamics of bubbles and drops in rheologically complex fluids. *Encyclopedia of Fluid Mechanics 7*; Gulf Publishing Co.: London, 1988; 253.

(201) De Kee, D.; Chhabra, R. P.; Rodrigue, D. Hydrodynamics of Free Rise of Bubbles in Non-Newtonian Polymer Solutions. In. *Handbook of Applied Polymer Processing Technology*; Cheremisinoff, N. P., Cheremisinoff, P. N., Eds.; Marcel Dekker: New York, 1996, 87−123.

(202) Hadamard, J. S. Mouvement permanent lent d'une sphere liquide et visqueuse dans un liquide viscquexe. *Comput. Rend. Acad. Sci. (Paris)* **1911**, *152*, 1735.

(203) Rybczynski, W. Uber die fortschreitende bewegung einer flussigen kugel in einem zaben medium. *Bull. Acad. Sci. Cracow* **1911**, *1A*, 40.

(204) Miyahara, T.; Yamanaka, S. Mechanics of motion and deformation of a single bubble rising through quiescent highly viscous Newtonian and non-Newtonian media. *J. Chem. Eng. Jpn*. **1993**, *26*, 297.

(205) Barnett, S. M.; Humphrey, A. E.; Litt, M. Bubble motion and mass transfer in non-Newtonian fluid. *AIChE J.* **1966**, *12*(2), 253.

(206) Haque, M. W.; Nigam, K. D. P.; Viswanathan, K.; Joshi, J. B. Studies on bubble rise velocity in bubble columns employing non-Newtonian solutions. *Chem. Eng. Commun*. **1988**, *73*, 31.

(207) Miyahara, T.; Takahashi, T. Drag coefficient of a single bubble rising through a quiescent liquid. *Int. Chem. Eng.* **1985**, *26*, 146.

(208) Habberman, W. L.; Morton, R. K. An experiment al study of bubbles moving in liquids. *Trans. ACSE* **1954**, *12*, 59.

(209) Davenport, W. G.; Richardson, F. D.; Bradshaw, A. V. Spherical cap bubbles in low-density liquids. *Chem. Eng. Sci.* **1967**, *22*, 1221.

(210) Raymond, F.; Rosant, J. M. A numerical and experimental study of the terminal velocity and shape of bubbles in viscous liquids. *Chem. Eng. Sci*. **2000**, *55*, 943.

(211) Haberman, W. L.; Morton, R. K. An experimental study of bubbles moving in liquids. *Trans. Am. Soc. Civil Eng.* **1956**, *121*, 227.

(212) Magnaudet, J.; Legendre, D. The viscous drag force on a bubble with a time-dependent radius. *Phys. Fluids* **1998**, *10*, 550.

(213) Karamanev, D. G.; Nikolov, L. N. Free rising bubbles do not obey Newton's law for free settling. *A. I. Ch. E. J.* **1992**, *38*, 1993−1997.

(214) Karamanev, D. G. Equations for calculation of the terminal velocity and drag coefficient of solid spheres and gas bubbles. *Chem. Eng. Commun.* **1996**, *147*, 75−84.

(215) Batchelor, G. K. *An Introduction to Fluid Dynamics*; Cambridge University Press: Cambridge, 1967.

(216) Levich, V. G. Bubble motion at high Reynolds numbers. *Zh. Eksp. Teoret. Fiz*. **1949**, *19*, 18−24.

(217) Kang, I. S.; Leal, L. G. The drag coefficient for a spherical bubble in a uniform streaming flow. *Phys. Fluids* **1988**, *31*, 233 37.

(218) Moore, D. W. Boundary layer on a spherical bubble. *J. Fluid Mech.* **1963**, *16*, 161.

(219) Brabston, D. C.; Keller, H. B. Viscous flows past spherical gas bubbles. *J. Fluid Mech.* **1975**, *69*, 179.

(220) Ryskin, G.; Leal, L. G. Numerical solution of free-boundary problems in fluid mechanics. Part 2. Buoyancy driven motion of a gas bubble through a quiescent liquid. *J. Fluid Mech.* **1984**, *148*, 19−35.

(221) Mei, R.; Klausner, J. F. Unsteady force on a spherical bubble at finite Reynolds number with small fluctuations in the free-stream velocity. *Phys. Fluids A* **1992**, *4*, 63−70.

(222) Magnaudet, J.; Rivero, M.; Fabre, J. Accelerated flows past a rigid sphere or a spherical bubble. Part I. Pure straining flow. *J. Fluid Mech*. **1995**, *284*, 97−135.

(223) Blanco, A.; Magnaudet, J. The structure of the high Reynolds number flow around an ellipsoidal bubble of fixed shape. *Phys. Fluids* **1995**, *7*, 1265−74.

(224) Taylor, T. D.; Acrivos, A. On the deformation and drag of a falling viscous drop at low Reynolds number. *J. Fluid Mech*. **1964**, *18*, 466−476.

(225) Golovin, A. M.; Ivanov, M. F. Motion of a bubble in a viscous liquid. *J. Appl. Mech. Technol. Phys. (USSR)* **1973**, *12*, 91−94.

(226) Mei, R.; Klausner, J. F. A note on history force on a spherical bubble with finite Reynolds number. *Phys. Fluids* **1994**, *6*, 418.

(227) Takagi, S.; Matsumoto, Y. Force acting on a rising bubble in a quiescent fluid. *Proc. ASME Summer Meeting Num. Methods Multiphase Flow,* San Diego, CA, 1996, pp 575−80.

(228) Rosenberg, B. The David W. Taylor model basin, Washington, DC, Rep. 727, **1950**.

(229) Takahashi, T.; Miyahara T.; Izawa, H. Drag coefficient and wake volume of single bubble rising through quiscent liquids. *Kagaku Kogaku Ronbunshu* **1976**, *2*, 480.

(230) Bhaga, D.; Weber, M. E. Bubbles in viscous-liquids—shapes, wakes and velocities. *J. Fluid Mech*. **1981**, *105*, 61.

(231) Turton, R.; Levenspiel, O. A short note on the drag correlation for spheres. *Powder Technol.* **1986**, *47*(1), 83.

(232) Delnoij, E.; Lammers, F. A.; Kuipers, J. A. M.; van Swaaij, W. P. M. Dynamic simulation of dispersed gas−liquid two-phase flow using a discrete bubble model. *Chem. Eng. Sci.* **1997**, *52*(9), 1429.

(233) Ford, B.; Loth, E. Forces on ellipsoidal bubbles in a turbulent shear layer. *Phys. Fluids* **1998**, *10*, 178.

(234) Kendoush, A. A. Hydrodynamic model for bubbles in a swarm. *Chem. Eng. Sci.* **2001**, *56* (1), 235.

(235) Sandhal, S. S.; Johnson, R. E. Stokes flow past bubbles and drops partially coated with thin films. Part I: Stagnant cap of surfactant film-exact solution. *J. Fluid. Mech.* **1983**, *126*, 237.

(236) Di Marco, P.; Grassi, W.; Memoli, G. Experimental study on rising velocity of nitrogen bubbles in FC-72. *Int. J. Thermal Sci*. **2003**, *42,* 435.

(237) Tomiyama, A.; Kataoka, I.; Zun, I.; Sakaguchi, T. Drag coefficients of single bubbles under normal and microgravity conditions. *JSME Int. J. Ser. D* **1998**, *41*(2), 472.

(238) Moore, D. W. The rise of a gas bubble in a viscous liquid. *J. Fluid Mech.* **1959**, *6*(1), 113.

(239) Mei, R.; Lawrence, C. J.; Adrian, R. J. Unsteady drag on a sphere at finite Reynolds number with small-amplitude fluctuations in the free stream velocity. *J. Fluid Mech.* **1991**, *233*, 613.

(240) de Vries, A. W. G.; Biesheuvel, A.; Wijngaarden, L. van, Notes on path and wake of a gas bubble rising in pure water. *Int. J. Multiphase Flow* **2002**, *28*, 1823.

(241) Feng, Z. C.; Leal, L. G. Feng Nonlinear bubble dynamics. *Annu. Rev. Fluid Mech*. **1997**, *29*, 201.

(242) Yoshida, S.; Manasseh, R. Trajectories of rising bubbles, The 16th Japanese Multiphase Flow Symposium, Touya, Hokkaido, July **1997**.

(243) De Kee, D.; Chhabra, R. P.; Dajan, A. Motion and coalescence of gas bubles in non-Newtonian polymer solutions. *J. Non-Newtonian Fluid Mech.* **1990**, *37*, 1.

(244) Blanco, A. Quelques aspects de l e'coulement autour d une bulle de'forma-ble: une approche par simulation directe. Ph.D. Thesis, **1995**, Inst. Nat. Polytech. Toulouse, Toulouse, France

(245) Takagi, S.; Matsumoto, Y. Three-dimensional calculation of a rising bubble. *Proc. Int. Conf. Multiphase Flow*, 2nd, Kyoto, Japan, **1995**, pp. PD2.9 16.

(246) Lunde, K.; Perkins, R. Observations on wakes behind spheroidal bubbles and par-ticles. *Proc. ASME Fluids Eng. Div*. Summer Meeting, Vancouver, **1997**, *97*, 3530.

(247) Adrian, R. J. Particle-Imaging Techniques For Experimental Fluid-Mechanics. *Annu. Rev. Fluid Mech.* **1991**, *23*, 261−304.

(248) Willert, C. E.; Gharib, M. Three-dimensional particle imaging with a single camera. *Exp. Fluids* **1992**, *12*, 353.

(249) Hsieh, C. C.; Wang, S. B.; Pan, C. Dynamic visualization of two-phase flow patterns in a natural circulation loop. *Int. J. Multiphase flow* **1997**, *23*(6), 1147.

(250) Lu, F. K.; Zhang, X. Visualization of a confined accelerated bubble. *Shock Waves* **1999**, *9*(5), 333−339.

(251) Takemura, F.; Magnaudet, J. The history force on a rapidly shrinking bubble rising at finite Reynolds number. *Phys. Fluids* **2004**, *16*(9), 3247−3255.

(252) Vokurka, K.; Beylich, A. E.; Kleine, H. Experimental study of gas bubble oscillations using a shock-tube. *Acustica* **1992**, *75*(4), 268−275.

(253) Vasconcelos, J. M. T.; Orvalho, S. P.; Alves, S. S. Gas−liquid mass transfer to single bubbles: Effect of surface contamination. *AIChE J*. **2002**, *48*(6), 1145−1154.

(254) Oakley, T. R.; Loth, E.; Adrian, R. J. A two-phase cinematic PIV method for bubbly flows. *J. Fluids Eng. Trans. ASME* **1997**, *119*(3), 707−712.

(255) Bui-Dinh, T.; Choi, T. S. Noninvasive measurements of instantaneous bubble rise velocity using digital image analysis. *Mech. Res. Commun.* **2001**, *28*(4), 471−475.

(256) Raffel, M.; Willert, C. E.; Kompenhans, J. Particle Image Velocimetry: A Practical Guide (Experimental Fluid Mechanics), Springer-Verlag 1998 ISBN: 3540636838.

(257) Murai, Y. (http://ring-me.eng.hokudai.ac.jp/murai/papers.html)

(258) Yamamoto, F. (http://mech.mech.fukui-u.ac.jp/~yamamoto/)

(259) Kulkarni, A. A.; Joshi, J. B.; Ravikumar V.; Kulkarni B. D. Simultaneous measurement of hold-up profiles and interfacial area using LDA in bubble column: predictions by time series analysis and comparison with experiments. *Chem. Eng. Sci.* **2001**, *56*(19), 6437.

(260) Terasaka, K.; Inoue, Y.; Kakizaki, M.; Niwa, M, Simultaneous measurement of 3-dimensional shape and behavior of single bubble in liquid using laser sensors. *J. Chem. Eng. Japan* **2004**, *37*(8), 921−926.

(261) Saberi, S.; Shakourzadeh, K.; Bastoul, D.; Militzer, J. Bubble size and velocity measurement in gas−liquid systems: Application of fibre optic technique to pilot plant scale. *Can. J. Chem. Eng*. **1995**, *73*, 253.

(262) Chabot, J.; Lee, S. L. P.; Soria, A.; Delasa, H. I. Interaction Between Bubbles and Fiber Optic Probes in a Bubble Column. *Can. J. Chem. Eng.* **1992**, *70*, 0 (1), 61−68.

(263) Steinemann, J.; Buchholz, R. Application of an Electrical Conductivity Microprobe for the Characterization of Bubble Behavior in Gas−Liquid Bubble Flow. *Part. Charact.* **1984**, *1*, 102.

(264) Kuramoto, K.; Hasegawa, T.; Tsutsumi, A. Microscopic flow structure around rising bubbles in a continuous single-bubble flow system. *Kagaku Kogaku Ronbunshu* **2001**, *27*(4), 466−469.

(265) Mishima, K.; Hibiki, T.; Saito, Y.; Tobita, Y.; Konishi, K.; Matsubayashi, M. Visualization and measurement of gas−liquid metal two-phase flow with large density difference using thermal neutrons as microscopic probes. *Nucl. Instrum. Methods Phys. Res. A* **1999**, *424*, 229−234.

(266) Hibiki, T.; Saito, Y.; Mishima, K.; Tobita, Y.; Konishi, K.; Matsubayashi, M. Study on flow characteristics in gas-molten metal mixture pool. *Nucl. Eng. Des.* **2000**, *196*, 233.

(267) Saito, Y.; Mishima, K.; Tobita, Y.; Suzuki, T.; Matsubayashi, M. Velocity field measurement in gas−liquid metal two-phase flow with use of PIV and neutron radiography techniques. *App. Rad. Isotopes* **2004**, *61*(4), 683−691.

(268) Seeger, A.; Affeld, K.; Goubergrits, L.; Kertzscher, U.; Wellnhofer, E.; Delfos, R. X-ray-based flow visualization and measurement—Application in multiphase flows. *Vis. Imag. in Transport Phenomena Ann. N.Y. Acad. Sci.* **2002**, *972,* 247−253.

(269) Heindel, T. J. Bubble size measurements in a quiescent fiber suspension. *J. Pulp Paper Sci.* **1999**, *25*(3), 104−110.

(270) Theofanous, T. G.; Angelini, S.; Chen, X.; Luo, R.; Yuen, W. W. Quantitative radiography for transient multidimensional, multiphase flows. *Nuc. Eng. Des.* **1998**, *184*(2−3), 163−181.

(271) Räbiger, N. *VDI−Forschungsheft* **1984**, No. 625.

Received for review September 9, 2004
Revised manuscript received February 9, 2005
Accepted February 11, 2005

IE049131P